

**Optical emission spectrometry with microwave induced plasmas
in structures based on microstrip technology for the
determination of Hg, As, Sb, Cl, Br and S with the aid of cold
vapour generation techniques**

Beim Department Chemie der Universität Hamburg

eingereichte

Dissertation

Zur Erlangung des Akademisches Grades

DOCTOR RERUM NATURALIUM

(Dr. Rer. Nat.)

vorgelegt

von M. Sc. Andrés Israel Humberto Jiménez Zapata

geboren am 14.09.1978 in Lima

Hamburg 2008

Sei du selbst die Veränderung,
die du dir wünscht für diese Welt.

Mahatma Gandhi

The present work was prepared between October 2005 to March 2008 under the supervision of Prof. Dr. José Broekaert in the Institute for Inorganic and Applied Chemistry at the University of Hamburg, Germany.

1. Gutachter: Prof. Dr. J.A.C. Broekaert
2. Gutachter: Prof. Dr. N.H. Bings
Disputation: 07.11.2008

I thank Prof. Dr. José Broekaert for giving me the opportunity to do my doctoral thesis under his supervision with a wonderful scientific group in Hamburg. I really enjoy my time in the Department of Chemistry.

I would like to thank to Dr. Pawel Pohl for his strong corporation during my doctoral work especially in the development of the different setups used in the present work and also Prof. Dr. Nicolas Bings for his support in building up the electrolytic cell and for his valuable discussions during the different stages of my work.

I also thank the people who were around me and contributed to my work as my colleague Martin Amberger for his extensive discussions and clever ideas and Torborg Krugmann for supplying all kind of lab materials. I cannot forget the glass shop and the mechanical workshop of the department for supplying me with glass material and giving me technical support.

I am deeply grateful to Prof. Dr. Jorge Angulo for his constant effort and precious work in San Marcos University in Lima, Perú. I cannot skip Prof. Dr. Lothar Beyer and his great interest in Perú for the really valuable cooperation in different aspects with my university.

I express my best wishes and extend a grateful appreciation to my wonderful family, my mother Ana Zapata who was a permanent and unconditional support in my life, my grandmother Haydeé Zapata for her lovely character and my wife Elizabeth Yamashiro and her understandings and permanent motivation to go further.

I am grateful to the Deutscher Akademischer Austauschdienst (DAAD) for the scholarship and financial support and to Frau Rosa Anna Nagel who assisted me in all questions and problems that I had.

At the end but not the least I am glad to name all my friends who made me have a wonderful time in Hamburg especially to Julio del Prado for his support and following all my steps and achievements in Germany, to Miguel C. Córdova for his visits, constant worries and very good mud in every moment of the life and to Alicia Jaime León and her encouragement along my work.

Summary

Optical emission spectrometry with microwave induced plasmas in structures based on microstrip technology for the determination of Hg, As, Sb, Cl, Br and S with the aid of cold vapour generation techniques

Andrés Israel Humberto Jiménez Zapata

University of Hamburg, Dissertation

144 P., 213 Ref., 47 Fig., 11 Tab.

The use of two types of microstrip plasmas (MSP) inside and exiting the sapphire wafer with Ar and He as working gases at a forward power of 40 W for the determination of metals and non-metals, such as Hg, As, Sb, Cl, Br, S and C in their volatile form using cold vapour generation techniques with SnCl₂ as reducing agent, chemical and electrochemical hydride generation as well as redox reactions coupled to optical emission spectrometry is investigated in the present work. The vapour generation systems were determined with a univariant procedure for the different parameters such as stabilizing reagent substances, reagent concentrations as well as reagent and gas flow rates for an efficient production and separation of the volatile analyte species to be introduced into the MSP source. The use of a miniaturized spectrometer (USB2000 Ocean Optics) is shown to be advantageous due to the affordance of the systems developed for micrototal analysis systems (μ -TAS), to portability, to lower working costs, to less use of reagents and to fast chemical analyses. Studies for the removal of the water vapours were performed. The use of a tank filled with H₂SO₄ was found to be the most reliable way to separate the analyte from the moisture due to its long-term life and effectiveness.

In the first part of the work, a comparison of excitation temperatures and electron number densities for the case of He and Ar as working gases and plasmas sustained fully inside the sapphire wafer is done when introducing Hg vapours generated with SnCl₂ as reducing agent. At a maximal forward power of 40 W, an Ar plasma was found to be the most appropriate for the determination of Hg with the cold vapour technique. Further investigations of an Ar-MSP sustained inside the wafer for the determination of As and Sb using chemical hydride generation were performed. The by-products of the reaction and especially the excess of H₂ influence the plasma features and lead to a deterioration of figures of merit like the limits of

detection. They are 18 and 31 ng ml⁻¹ for As and Sb, respectively, when the plasma contains 28 % of H₂.

In the second part of the work, a comparison of two different cold vapour generation techniques for the determination of Hg using an MSP exiting the wafer is investigated. An Ar-MSP exiting the wafer overcomes the geometry limitations of a plasma sustained inside the wafer and shows a higher resistance to H₂ (~50 %) as compared to the plasma sustained inside the wafer. The performance with SnCl₂ as reducing agent is better than when using NaBH₄. Indeed the limit of detection found for an MSP sustained inside the wafer for the case of Hg is 12 times lower when using SnCl₂. Due to its low amount of by-products, the electrochemical hydride generation with a miniaturized cell using a Nafion cation exchange membrane, a Pt rod as anode and a carbon fiber bundle as cathode for the determination of As and Sb was found to be better than chemical hydride generation for the case of an MSP exiting the wafer. The electrochemical hydride generation further allows it to reduce the use of expensive reagents as NaBH₄, which also can be a source of contamination and suffer from long term-stability problems. The figures of merit of the electrochemical hydride generation are better than those of the chemical hydride generation but unfortunately it presents disadvantages such as an irreversible pollution of the electrodes.

In the last part of the work, the determination of non-metals such as Cl, Br, S and C with a He-MSP was investigated. For the determination of Cl⁻ and Br⁻, KMnO₄ was used as oxidizing agent. The redox reaction is realized at high acidic conditions using H₂SO₄. For Cl⁻ and Br⁻ different acid conditions were found to be optimum. They are higher for an efficient generation of Br₂ than in the case of the oxidation of Cl⁻, which is due to the fact that Br₂ is heavier and less volatile than Cl₂. It was also found necessary to use a slightly higher gas flow rate to transport the Br₂ than in the case of Cl₂. For the determination of S²⁻, the sample solution can be mixed with HCl so as to generate H₂S. When introducing a solution of CO₃²⁻ molecular bands appear which stem from the species C₂⁺, CO₂, N₂⁺ and CN. The limits of detection for C are lower than those found when using gas chromatography.

The effects of NaCl concentrations similar to those in sea water for the Hg cold vapour generation technique were studied as well. For the determination of As and Sb using the chemical hydride generation, the effects of transition metals and volatile-hydride forming elements were studied. No especial trend could be found. For the case of the determination of

As and Sb using the electrochemical hydride generation technique, the effects of transition metals were found to be lower than those of volatile hydride-forming elements. The effects caused by a series of anions in the determination of Cl^- and Br^- were discussed as well.

To verify the accuracy of the procedures developed standard reference materials such as sewage sludge (NIST SRM 1633a and 2781) subsequent to sample dissolution, and water samples (drinking, river and lake water) were analyzed. The results were found to be in good agreement with the certified values. Finally, the procedures developed were used for the determination of the elements mentioned in water samples collected from different points of Hamburg, as well as in industrial process waters and sewage sludge.

Zusammenfassung

Optische Emissionspektrometrie mit mikrowelleninduzierten Plasmen in mikrostrukturierten Systemen für die Bestimmung von Hg, As, Sb, Cl, Br and S nach ihrer Überführung in flüchtige Verbindungen

Andrés Israel Humberto Jiménez Zapata

Universität Hamburg, Dissertation

144 S., 213 Ref., 47 Abb., 11 Tab.

Im Rahmen dieser Arbeit wurden zwei Arten von Microstrip-Plasmas (MSP) als Strahlungsquellen für die optische emissionsspektrometrie (OES) untersucht, die innerhalb und am Ausgang eines Saphirwafers mit Ar und He als Trägergas und einer Mikrowellenleistung von 40 W betrieben wurden. Sie wurden zur Bestimmung von Metallen und Nichtmetallen, wie Hg, As, Sb, Cl, Br, S und C in ihren flüchtigen Verbindungen verwendet, die mittels Kaltdampftechnik mit SnCl_2 als chemischem Reduktionsmittel, chemischer und elektrochemischer Hydrierzeugung, sowie durch Redoxreaktionen erzeugt wurden.

Die univariate Kaltdampftechnik hinsichtlich unterschiedlicher Betriebsparameter, wie Reagenzkonzentrationen, Reagenzien und Arbeitsgasfluss, für eine effiziente Produktion und Abtrennung des Analyten in der Gasphase und des MSP wird vorgestellt. Der Gebrauch des Minispektrometers USB2000 Ocean Optics ist vorteilhaft in Bezug auf die Mobilität des Systems, geringere Arbeitskosten und geringeren Reagenzienverbrauch, sowie schnellere chemische Analysen. Zur Trocknung des mit Analyt beladenen Trägergases erwies sich die Verwendung eines mit konzentrierter H_2SO_4 gefüllten Gefäßes zur Trennung des Analyten von der Feuchtigkeit aufgrund der langen Lebensdauer des Systems als zuverlässig.

In dem ersten Teil der Arbeit wurden die Anregungstemperaturen und die Elektronenanzahldichten in einem MSP innerhalb des Saphirwafers bei He und Ar als Arbeitsgasen bestimmt. Es wurde Hg eingeleitet, das durch Einsatz von SnCl_2 als Reduktionsmittel erzeugt wurde. Ein Ar Plasma mit einer Mikrowellenleistung von 40 W stellte sich für die Bestimmung von Hg(I)-Verbindungen mit der Kaltdampftechnik als optimal heraus. Bei weiteren Untersuchungen des Ar-MSP innerhalb des Wafers im Falle des

durch chemische Hydriderzeugung ins Plasma eingebrachten As und Sb wurde festgestellt, dass der erzeugte H_2 die Stabilität des Plasmas beeinträchtigen kann. Für As und Sb liegen die Nachweisgrenzen bei jeweils 18 und 31 $ng\ ml^{-1}$.

Im zweiten Teil der Arbeit wurde ein Vergleich zwischen zwei verschiedenen Kaltdampftechniken zur Bestimmung von Hg im Falle eines MSP, das aus dem Wafer austritt, durchgeführt. Ein solches Ar-MSP hat im Vergleich zu einem Plasma im Waferkanal keine geometrische Einschränkungen, und weist eine höhere Resistenz gegen H_2 (50 %) auf. Der Einsatz von $SnCl_2$ als Reduktionsmittel ist besser als der Einsatz von $NaBH_4$. Die Nachweisgrenze, die bei einem MSP im Waferkanal gefunden wurde, ist für Hg 12 mal niedriger, wenn $SnCl_2$ verwendet wird. Aufgrund der niedrigen Mengen an H_2 ist die elektrochemische Hydriderzeugung mit einer miniaturisierten Elektrolysezelle bei der Verwendung einer Nafion Membran, eines Pt-Stabs als Anode und eines Bündels aus Kohlenstofffasern als Kathode für die Bestimmung von As und Sb besser geeignet als die chemische Hydriderzeugung. Außerdem braucht die elektrochemische Hydriderzeugung keine teure Reagenzien wie $NaBH_4$, was übrigens auch eine Quelle von Blindwerten ist und eine geringe Wärmebeständigkeit aufweist. Die Güteziffern der elektrochemischen Hydriderzeugung sind besser als die der chemischen Hydriderzeugung, aber leider gibt es auch Nachteile, wie beispielsweise eine irreversible Kontaminierung der Elektroden.

Im letzten Teil der Arbeit wurde die Bestimmung von Nichtmetallen wie Cl, Br, S und C mit einem He-MSP untersucht. Zur Bestimmung von Cl^- und Br^- wurde $KMnO_4$ als Oxidationsmittel verwendet. Die Redoxreaktion wurde unter stark sauren Bedingungen unter der Verwendung von H_2SO_4 durchgeführt. Es wurde festgestellt, daß bei Cl^- und Br^- die optimalen Konzentrationen von $KMnO_4$ und H_2SO_4 unterschiedlich sind. Die optimale Säurekonzentration für eine effiziente Erzeugung von Br_2 ist höher als für die Oxidation von Cl^- . Dies liegt daran, dass Br_2 schwerer und weniger flüchtig als Cl_2 ist. Zur Bestimmung von S^{2-} kann die Probenlösung mit HCl gemischt werden, so dass H_2S erzeugt wird. Beim Einsatz einer CO_3^{2-} Lösung treten Molekülbanden auf, die aufgrund der Spezies C_2^+ , CO_2 , N_2^+ und CN entstehen. Die Nachweisgrenzen für C sind niedriger als die bei der Verwendung der Gaschromatographie gefundenen Nachweisgrenzen.

Auch der Einfluss von NaCl in Konzentrationen, wie sie in Meerwasser auftreten, wurde für die Hg Kaltdampftechnik untersucht. Bei der chemischen Hydriderzeugung wurden für die

Bestimmung von As und Sb die Einflüsse von Übergangsmetallen und der Hydridbildenden Elemente untersucht. Es konnte keinen besonderer Trend herausgefunden werden. Bei der Bestimmung von As und Sb mit Hilfe der elektrochemischen Hydrierzeugung waren die Einflüsse der Übergangsmetalle niedriger als die Einflüsse der Elemente, die flüchtige Hydride bilden. Bei der Bestimmung von Cl^- und Br^- wurden die Einflüsse von Anionen ebenfalls untersucht.

Zur Überprüfung der Richtigkeit der entwickelten Verfahren wurden Standardreferenzmaterialien analysiert. Die Ergebnisse stimmten mit den zertifizierten Werten gut überein, wie es für den Fall eines Klärschlamm (NIST SRM 1633a and 2781) und einer Wasserprobe (Trink-, Fluß- und Seewasser) gezeigt wurde. Abschließend wurden die entwickelten Verfahren für die Bestimmung der erwähnten Elemente in an verschiedenen Orten Hamburgs gesammelten Wasserproben, sowie für industrielle Prozessgewässer und Schlammproben nach Aufschluß eingesetzt.

Table of Content

A. Introduction	1
B. Theoretical Part	
1.1 Atomic emission spectrometry	4
1.2 Miniaturization	10
1.3 Plasma	11
1.3.1 Direct current plasma (DCP)	13
1.3.2 Inductively coupled plasma (ICP)	14
1.4 Microwave plasmas	16
1.4.1 Capacitively coupled microwave plasmas (CMP)	19
1.4.2 MIP cavity according to Beenakker (TM ₀₁₀ resonator)	20
1.4.3 Surfatron	21
1.4.4 Microwave plasma torch (MPT)	22
1.4.5 Microstrip plasma (MSP)	24
1.5 Sample introduction	25
1.5.1 Pneumatic nebulization	25
1.5.2 Ultrasonic nebulizers	29
1.6 Chemical hydride generation	30
1.7 Electrochemical hydride generation	32
1.8 Mercury cold vapour generation	34
1.9 Other volatile species generation techniques	34
1.10 Electrothermal vaporization (ETV)	35
1.11 Laser ablation (LA)	35
1.12 Spark ablation	36
1.13 Spectrometers	36
1.14 Detectors	39
1.14.1 Miniaturized spectrometers	40
1.15 Plasma mass spectrometry	42
C. Instrumentation	
2.1 Microstrip plasma	44
2.1.1 Plasma inside the wafer (type A)	44
2.1.2 Plasma exiting the wafer (type B)	44
2.2 Miniaturized spectrometer	46
2.3 Sample introduction systems	48
2.3.1 Efficiencies of different setups for water vapour removal	48
2.3.2 Continuous hydride generation system for the determination of As and Sb of Hg	50
2.3.4 Miniaturized chemical and electrochemical hydride generation for the determination of As and Sb	52
2.3.5 Continuous gaseous species introduction system for other non-metals	54
D. Practical Part	
3.1 Experimental conditions	56
3.1.1 Preparation of sample solutions	56
3.1.2 Water and galvanic bath solution samples	58
3.1.3 Microwave assisted digestion of standard reference materials	58

3.1.4 Measurement of the amount of H ₂ produced in the continuous CHG and ECHG	59
3.1.5 Determination of excitation temperatures and electron number densities	59
3.1.6 Measurement of the hydride generation efficiencies	60
3.2 Wavelength selection	60
3.3 Preliminary investigations with an MSP type A using He as working gas	62
3.3.1 Dry He and Ar plasma and plasma loaded with water vapours	62
3.3.2 Plasma loaded with Hg vapours generated by a gas flow passing over a drop of Hg	63
3.3.3 Introduction of Hg by the cold vapour technique	64
3.4 Evaluation and application of Ar and He microstrip plasma (type A) combined to the cold vapour technique for the determination of Hg by OES	65
3.4.1 Area of plasma stability	65
3.4.2 Effect of the microwave forward power and the working gas flow rate on the excitation temperature and the electron number density	66
3.4.3 Influence of the microwave forward power and the working gas flow rate on the relative net intensity of Hg I 253.6 nm and its SBR	68
3.4.4 Analytical performance	71
3.4.5 Interferences	71
3.4.6 Analysis of real samples and standard reference material 2781	72
3.5 Simultaneous determination of As and Sb by continuous flow chemical hydride generation and a miniaturized microwave microstrip argon plasma operated inside the capillary channel (type A)	73
3.5.1 Optimization	74
3.5.1.1 Influence of the NaBH ₄ concentration	74
3.5.1.2 Influence of the acid and its concentration	76
3.5.1.3 Influence of the Ar flow rate	78
3.5.1.4 Influence of the sample and reducing agent flow rates	79
3.5.1.5 Influence of the residual liquid volume in the gas-liquid phase separator	81
3.5.2 Chemical interferences caused by transition metal ions	81
3.5.3 Effect of masking agents	82
3.5.4 Figures of merit and analytical application	85
3.5.5 Analysis of real samples and NIST SRM 1663a	85
3.6 Comparison of the cold vapour generation using NaBH ₄ and SnCl ₂ as reducing agents for the determination of Hg with a microstrip microwave induced Ar plasma exiting from the wafer (type B)	86
3.6.1 Optimization	86
3.6.1.1 Influence of the concentrations of the reducing agents	86
3.6.1.2 Influence of the concentrations of substances stabilizing the reducing agent solutions	88
3.6.1.3 Influence of the concentration of HCl in the sample	89
3.6.1.4 Influence of the Ar flow rate	90
3.6.1.5 Influence of the flow rate of the reagents	92
3.6.1.6 Influence of the volume in the gas liquid separator	93
3.6.2 Areas of stability	93
3.6.3 Chemical interferences	94
3.6.4 Figures of merit and analytical application	97
3.6.5 Analysis of NIST SRM 2781	98

3.7 Comparison of chemical and electrochemical hydride generation for the optical emission spectrometric determination of As and Sb using a miniaturized microwave induced Ar plasma exiting the microstrip wafer	98
3.7.1 Optimization of the CHG	99
3.7.1.1 Influence of the NaBH ₄ concentration	99
3.7.1.2 Influence of the sample and the reducing agent flow rates	100
3.7.1.3 Influence of the concentration of HCl in the sample solution	101
3.7.1.4 Influence of the Ar flow rate	102
3.7.2 Optimization of ECHG	104
3.7.2.1 Influence of the electrolysis voltage	104
3.7.2.2 Influence of the electrolyte flow rates	105
3.7.2.3 Influence of the concentration of H ₂ SO ₄ in the anolyte and the catholyte	105
3.7.2.4 Influence of the carrier gas flow rate	106
3.7.3 Interferences from transition metal ions and other volatile hydride-forming elements in CHG and ECHG	106
3.7.3.1 Generation of AsH ₃	107
3.7.3.2 Generation of SbH ₃	108
3.7.4 Analytical performance	111
3.7.5 Analysis of real samples and NIST SRM 1663a	112
3.8 Determination of non-metals with the aid of an improved MSP exiting the wafer and optical emission spectrometry	112
3.8.1 Generation of Br ₂ and Cl ₂	112
3.8.2 Generation of H ₂ S	114
3.8.3 Analytical performance	115
3.8.4 Interferences	115
3.8.5 Application to the determination of Br, Cl and S in tap water samples	116
3.8.6 Emission characteristics of the He MSP	117
E. Conclusions and outlook	120
F. Instruments and chemicals	125
G. References	127
H. Lebenslauf	145

A. Introduction

In plasma spectrometry the use of different electrodeless microdischarges and discharges operated with electrodes, comprising the microwave-induced microstrip plasma, the capacitively coupled microplasma, the direct current glow discharge microplasma, the stabilized capacitive plasma and the microfabricated inductively coupled plasma have been found useful for the determination of different analytes in the gaseous phase.

The present work deals with a contribution on the use of microwave plasma focusing on two types of miniaturized plasma in wafers and microstrip technology (MSP). Here, the plasma once is fully sustained inside the wafer and in the other case it exits the wafer and the discharges are coupled to different types of volatile species generation for the determination of Hg, As, Sb, Cl, Br and S, respectively.

Optical emission spectrometry (OES) is a well-known analytical principle for the quantitative determination of the elements. For purposes of miniaturization of the whole analytical system, a USB2000 spectrometer of a small size equipped with a CCD-array detector is used. This miniature fiber optic spectrometer is plugged into the USB port of a PC and used for recording the spectra of the MSP, which eliminates the need of using external A/D converters.

In the last years, great progress in the instrumentation for atomic emission spectrometry was made. Innovations took place with respect to the emission sources, the spectrometric systems and the detector technologies. A growing interest is noticed in the miniaturization of the plasma discharge devices used for atomic spectrochemical analysis including their use as chromatographic detectors. Miniaturized plasma sources could also be used for the determination of the elements capable of forming vapours or volatile species through chemical vapour generation reactions performed in solution, however, in this field much less research has been performed.

The analytical features of a microwave-induced plasma sustained inside the wafer based on microstrip technology have been demonstrated by the determination of Hg in aqueous solutions through the cold vapour generation technique using SnCl_2 as reductant. Hence, investigations on the coupling of novel small-scale and chip-based analytical microplasma sources with different sample introduction techniques enabling an efficient loading of the

plasma with the volatile species of the elements prior to their excitation and subsequent detection by atomic emission spectrometry or mass spectrometry are of special importance for the development of miniaturized and portable measurement instrumentation. The influence of the low residence time of the analytes in the plasma channel of the microdischarges as well as the relatively low excitation temperatures in these sources in comparison with other plasma sources, however, must be investigated in detail. Ar and He plasmas, based on microstrip technology and combined on-line with continuous cold vapour generation were studied for the determination of Hg. For both Ar and He plasmas coupled with the CV technique, the effect of the forward power and the gas flow rate on the excitation temperature (Ar I, He I) and the electron number density was investigated. Further, their influence on the relative intensity of the Hg 253.6 nm line and the signal-to-background ratio (SBR) for that line was studied. It was also found that the MSP could tolerate the H₂ co-produced with the volatile hydrides in chemical hydride generation CHG at well selected conditions. Accordingly, a direct coupling of continuous flow-hydride generation (CF-HG) to the MIP under the use of different introduction samples systems has been realized with a special membrane-based separation of H₂ and water vapour, concentrated H₂SO₄ tanks, or water cooled condensers for a desiccation of the water vapour before entering the gases into the radiation sources. With all the techniques studied it has been found that the introduction of H₂ and water vapour into the MIP is critical for the MIP discharge and the analytical figures of merit of HG-MIP-OES. With the different types of the sample introduction systems used for CF-HG and microwave structures such as surfatrons, the Beenakker cavity and microwave plasma torches, the high amounts of H₂ originating from the reaction, which sometimes constitute up to 30 % of the working gas, made it necessary to operate the discharges at high power input. Despite this experience the coupling of continuous flow-chemical hydride generation (CF-CHG) performed in a small volume HG system to an MSP with a plasma sustained inside was found to be possible. The experimental conditions for the HG and the MSP features were investigated in detail. The analytical performance of the CF-HG-MSP-OES procedure was optimized for As and Sb.

An MSP in which the microstrip was located near to the open end of the gas channel was found to enable the plasma to exit from the wafer. Its analytical application in combination with gaseous analyte species generation is described. Preliminary experiments showed that this MSP exiting from the wafer can be coupled to the chemical Hg CV generation technique even when NaBH₄ is used as reductant and an excess of H₂ is produced. Although both NaBH₄ and SnCl₂ can be used for the reduction of Hg(II) in acidic solutions to its volatile

elemental form, NaBH_4 is very often preferred over SnCl_2 as the reduction of both inorganic and organic Hg is more effective and faster. Therefore, it has been decided to compare the analytical performance of the MSP exiting from the wafer for the determination of Hg by the CV generation technique when both SnCl_2 and NaBH_4 are used as reductants in detail.

To minimize the CF-CHG disadvantages, the reaction has to be carried out under carefully optimized conditions regarding the NaBH_4 concentration and the flow rates of a sample and a reducing agent, as they determine the amount of H_2 produced in the HG reaction. Instead of using CHG with NaBH_4 as a reducing agent for the formation of hydrides, electrochemical hydride generation (ECHG) performed in an electrolysis cell can also be used as an alternative. As it has been shown, that such an approach usually allows a better analytical performance in the case of the MIP, mostly because of a higher achievable plasma stability due to reduced volumes of co-generated H_2 compared with CHG. Both techniques were compared with respect to their figures of merit.

As a further topic of the work the microwave induced plasma (MIP) operated with He at atmospheric pressure was found to be of a particular significance for the optical emission spectrometric (OES) determination of the halogens and other non-metals. In this study, an atmospheric pressure He MSP exiting from the wafer was coupled to CF chemical generation of Br_2 , Cl_2 and H_2S and their determination investigated by OES. Optimal conditions for the generation of gaseous Br_2 , Cl_2 and H_2S were identified and the analytical characteristics of the He MSP-OES with gas-phase sample introduction for the determination of Br, Cl and S was evaluated and discussed.

It could be expected that changes in the chemical volatile species generation occur as a result of interferences by concomitants in the reactions used. Therefore, the influence of transition metals in cold vapour and hydride generation was studied. The use of masking elements was also considered for complexing the interferents and reducing interferences. Analyses of synthetic and real liquid samples as well as of standard reference materials subsequent to dissolution with the aid of microwave assisted digestion were performed for validation purposes.

B. Theoretical Part

1.1 Atomic emission spectrometry

First atomic line spectra were observed by von Fraunhofer, Brewster and Herschel in the 1820s. Bunsen and Kirchhoff demonstrated that the line spectra could be used for qualitative chemical analysis in 1859. Significant observations until 1860 were also made by Stokes, Stewart, Fox, Talbot and others. Bunsen and Kirchhoff showed like Swan (1850) that the yellow line which coincidences with the Fraunhofer dark D solar line stems from contaminations in the sodium salts. Further, Bunsen isolated Cs and also Rb and In were discovered on the basis of their atomic emission spectra. Crookes in 1861 detected the existence of Tl by using spectroscopy. Kirchhoff began the chemical analysis of the atmosphere, of the sun and of the stars using emission measurements and found that the dark Fraunhofer lines stem from the same elements, which caused atomic emission lines at the same wavelengths. In 1925 Gerlach introduced the principle of the use of an internal standard. Lundergarth sprayed a solution into a premixed air-acetylene flame and in 1928 he also constructed the first calibration graphs for quantitative analysis. This development can be considered the beginning of modern atomic spectrometry. In the forthcoming decennia, signal detection with the aid of photographic emulsions was replaced by photocells or photomultipliers and direct reading spectrometers providing for simultaneous multielement determinations at high speed became available. In the mid-1930s Siemens and Zeiss were the first manufacturers of emission spectrometers.

Nowadays flame emission spectrometry is still used for the determination of Na but since the beginning of the 1960s flames have been replaced by different sources, such as plasma discharges. During the 1970s the first commercial plasma emission spectrometer became available. The inductively coupled plasma (ICP) is still the most used source for routine work. Walsh gave a very important contribution to atomic spectrometry between 1944 and 1986 by the introduction of atomic absorption spectrometry. Atomic absorption became most prominent after its applicability to the analysis of real samples has been shown, e.g. in the direct determination of Pb in gasoline.

As a result of the interaction between electromagnetic radiation and matter, such as a crystal lattice, molecules or free atoms, absorption, emission and scattering of radiation occur. The

electromagnetic radiation can be used in spectroscopic methods for qualitative and quantitative analysis. Because of its relative simplicity, sensitivity and ability to provide qualitative information, the presence of absorbed, emitted or scattered radiation at element-specific wavelengths can be used as criterion for the presence of a chemical compound. For quantitative analysis, the intensities of the electromagnetic radiation at these element-specific wavelengths can be used.

Each atom has a nucleus, around which the electrons follow orbits. If energy is transferred to the atoms, as it is the case in flames, plasmas, electric arcs or sparks, they undergo excitation and the electrons move to higher orbits. Atoms will not remain in this state, especially if they are removed from the source of energy and return to their original state by the electrons falling back to lower orbits. This transition is accompanied by the emission of a quantum of radiation energy of which the magnitude depends on the energy at the orbit involved. The released energy is given by:

$$E = h \nu = h c / \lambda \quad (1)$$

h is Planck's constant, ν is the frequency, c is the velocity of the light and λ is the wavelength. Hence, the larger the light quantum, the shorter the wavelength.

Atomic emission spectrometry is based on the promotion of valence electrons to higher levels by energy taken up during collisions with other atoms and these atoms return to their more stable state of energy by emitting element-specific radiation, which can be measured with suitable detectors.

The improvement and development of the sources of radiation aim at a better performance of chemical analysis. For atomic emission spectrometry the source should have a robust geometry enabling the analyte to pass through highly energetic zones with a high excitation efficiency as a result of high electron temperatures. The electron number density is influenced by the analyte ionization and its value should be constant so as to keep matrix interferences low. The analyte dilution should be high enough so as to obtain narrow lines. Every line spectrum is specific for an element. A dispersive system is required to realize an adequate line selection and isolation of an element line to verify the presence of an element and to determine its concentration. An atomic emission instrument comprises a radiation source, a

sample introduction system, an optical dispersive system, a detector and electronics for data acquisition and processing. As radiation sources arcs, flames or plasmas can be used. Their radiation is spectrally resolved with the aid of diffraction gratings.

In atomic emission spectrometry the sample analyte must be adequately introduced into the radiation source (plasma, flames, arcs, etc). This step is called the sample introduction and involves physical and chemical transformations, which can be realized by a sample nebulization system or volatilization devices. They produce aerosols or bring the analyte into the gaseous phase, respectively. Both processes lead to an atomization of the sample. The effectiveness of the atomization process depends on various plasma properties such as the plasma temperatures describing the kinetic energy distributions and the number densities.

Molecular bands may severely interfere with atomic spectral lines in atomic emission spectrometry, which leads to systematic errors. Therefore, it is important to study the influence of molecular and also radical species that exist in high temperature plasmas.

Plasma sources can be considered to be in local thermal equilibrium when all their temperatures have the same value. Therefore, the statistical distributions for each of the species present in the plasma, such as molecules, radicals, ions, atoms and electrons at any energy level can be described by the Maxwell equation. For the respective species, the population of different energy levels is described by the Boltzmann equations. The ionization of the atoms, molecules and radicals is given by the Saha equation, with:

$$n_e n_{i,p}/n_{a,q} = (2 (2\pi m_e kT)^{3/2} / h^3) \cdot (g_{i,p}/g_{a,p}) \cdot e^{-(E_i + E_p - E_q)/kT} \quad (2)$$

$n_{a,q}$ is the atom number density for the state q and $n_{i,p}$ the ion number density of the state p, $g_{a,p}$ and $g_{i,p}$ are the statistical weights of these two states, E_q and E_p are the energies of the states p and q, respectively, n_e is the electron number density and m_e is the mass of the electron.

From processes in which molecules, radicals and their products, respectively, are involved, a temperature can be defined. The rotational temperature (T_{rot}) can be obtained from the intensity distribution for the rotational lines in the rotational-vibration spectra, depending on the kinetic energy of the molecules and radicals, of which signals are found in the spectra. The main molecular species stemming from the plasma are CN, NH, NO, OH and N_2 (or N_2^+).

For a series of rotational lines in a vibrational band, one can write:

$$\ln(I_{nm}/(J'+J''+1)) = \ln(16\pi^3 c N v_{nm}^4)/(3T(Z)) - hc B_0 J'(J'+1)/kT_{rot} \quad (3)$$

Here $hc B_0 J'(J'+1)$ is the rotational energy, J' and J'' are rotational quantum number of upper and lower states, B_0 is the rotational constant and I_{nm} is the intensity of the respectively rotational line.

When the population of the rotational energy levels is described by a Boltzmann function, a plot of $\ln(I_{nm}/(J'+J''+1))$ vs $J'(J'+1)$ yields a straight line and the slope of the line is equal to $-1/kT_{rot}$. In most cases the radical OH is used for measuring T_{rot} and the 306.4 nm band is used. The $N_2^+B \rightarrow X$ band at 391.4 nm can also be used for measuring T_{rot} . A determination of this parameter is important because the bands of molecules and radicals present in the plasma interfere with atomic lines giving errors in the analytical applications of atomic emission spectrometry.

The gas temperature (T_{gas}) describes the kinetic energy of radiating species such as neutral atoms, molecules and ions in the plasma. T_{gas} can be calculated from the half-width of the Doppler broadening (Δv_d) of the spectral line, which results from the movement of the emitting atoms and their velocity component in the observation direction. The line widths also are related to other broadening mechanism such as Stark broadening and Zeeman splitting.

$$\Delta v_d = (2 (\ln 2)^{1/2}/c) v_o ((2RT_g)/M)^{1/2} \quad (4)$$

c is the velocity of light, v_o is the frequency of the light maximum, R is the gas constant and M is the atomic mass.

Furtheron, Rayleigh scattering can also be used for measuring T_{gas} .

The population of the excited levels of atoms and ions determines the excitation temperature (T_{exc}). When assuming a Boltzmann distribution of the atomic energy levels of the working gas or of an introduced element, the line intensity I_{qp} of a transition from level q to level p can be written as follows:

$$I_{qp} = (hc/4\pi \lambda_{qp}) g_q A_{qp} n (Q(T)) \exp(-E_q/KT_{exc}) \quad (5)$$

T_{exc} is important to describe the analyte line intensity at various plasma conditions. Assuming a Boltzmann distribution T_{exc} can be determined by the line pair method using the relative line intensities.

$$T_{exc} = (E_q - E_s)/K \ln(I_{sr} g_s A_{sr} \lambda_{sr}/I_{qp} g_q A_{qp} \lambda_{qp}) \quad (6)$$

q and s are the two upper levels, p and r the two lower levels, I_{qp} is the intensity for the transition from level q to level p, A_{qp} is the transition probability for spontaneous emission, E_q is the energy of the level q, n is the total number density of atoms in question, $g_{q,s}$ is the statistical weight of the level q and s, respectively. Some disadvantages in this method are caused by the often large difference in excitation energy of two upper levels.

T_{exc} can also be determined from the slope of the plot of functions of various atomic line intensities versus their energies as $\ln(I_{qp}/(g_q A_{qp} \nu_{qp}))$ or $\ln(I_{qp}/(g_q A_{qp} \lambda_{qp}))$ versus $1/kT_{exc}$. The accuracy of the plot can be improved when the lines chosen cover a broad range of excitation levels and when they are as close to each other as possible, so as to avoid changes in the wavelength response of the detection system. Both methods require neither the measurement of absolute lines nor a knowledge of the concentrations of the analyte.

The ionization temperature (T_{ion}) describes all phenomena involving an equilibrium between analyte atoms, ions and free electrons in the plasma. When the number densities of the thermal species z and (z+1) stages are as given by the Saha equation and the system is in local thermal equilibrium, T_{ion} can be calculated from the intensity ratio of an ion and an atom line of the same element.

$$I_{ion}/I_{at} = 2(A_i g_i \lambda_i/A_{at} g_{at} \lambda_{at}) ((2\pi m K T_{ion})^{3/2} / (h^3) (1/n_e)) (T_{ion})^{3/2} \exp(-(E_{ion} - E_{ex,at} + E_{ex,ion} - \Delta E_i)/(K T_{ion})) \quad (7)$$

I_i is the ionization of the ion line, I_{at} is the intensity of the atom line, A_i, a_t are the probabilities of the ion and atom emission, g_i, a_t are the statistical weights of the ion and the atom levels, $\lambda_i,$

at ion and atom emission lines, n_e is the electron number density and ΔE_i is a correction for the ionization energy of the lowest level.

From the electron temperature (T_e), information on the energy distribution of the electrons can be obtained, which is important for a study of the excitation and ionization by collisions with electrons. The laser-based Thompson scattering method here can be used. Mostly higher values of T_e are found for He plasmas than for Ar plasmas.

The T_e is relevant for the spectral background intensity and depends on the interaction between free and free as well as between free and bound electrons as:

$$I(\nu) d\nu = K n_e n_r r^2 / (T_e)^{1/2} \exp(-h\nu/kT_e) d\nu \text{ (free-free)} + K' (1/j^3) n_e n_Z (Z^4) / T_e^{3/2} \exp(-(U_j - h\nu)/kT_e) \text{ (free-bound)} \quad (8)$$

K and K_0 are constants, n_e is the electron number density, n_r is the number density of the ions with a charge of r times the elementary charge, T_e is the electron temperature, ν is the frequency, h and k are the Planck and Boltzmann constants, respectively, U_j is the ionization energy of the term with quantum number j , n_Z is the number density of the atoms with atomic number Z .

A plasma is a partially ionized gas and the electron number density (n_e), as an important parameter of plasmas that indicates the grade of ionization and its values are given as the number of free electrons in a unit of volume. It can be calculated by different methods, such as Stark broadening, which represents the broadening by interaction between the emitted atoms and the local electric field generated by the surroundings ions and electrons. Thompson scattering and microwave interferometry can also be used for the determination of electron number densities.

The most common method for the measurement of n_e makes use of the Stark broadening of the H_β 486.4 nm line. n_e is namely a function of the half-width of the H_β line, which must be measured experimentally. $\Delta\lambda_H$ is proportional to $n_e^{2/3}$ according to the quasi-static theory. Other lines can also be used for a determination of n_e . Generally:

$$n_e = C_H(n_e, T) \Delta\lambda_H^{3/2} \quad (9)$$

The values of n_e are in the range 10^{14} - 10^{15} cm^{-3} for atmospheric pressure plasmas and microwave fields e.g. have little effect on their values. It was observed that the values of n_e for He plasmas are lower than for Ar plasmas. This can be understood from the higher ionization energy of He. Values of n_e determined by Thompson scattering for He and Ar plasmas often are three orders of magnitude lower than the one from the Saha equation considering local thermal equilibrium (LTE), e.g. in the case of microwave plasmas [1]. This difference can be attributed to the deviation from LTE in the case of He and Ar plasmas operated at atmospheric pressure.

1.2 Miniaturization

Miniaturization can be described as the action to realize systems on a very small scale. In the recent developments of analytical chemistry three trends can be shown up: simplification, automation and miniaturization. In the present work, the focus is on the miniaturization of the analytical system, which involves the entire analytical process and aims at micrototal analysis systems (μ -TAS) or part of it [2].

The way followed in miniaturization depends on the analytical target considering the sample complexity and the selectivity which can be realized with different analytical microsystems [3] One e.g. may aim at a direct measurement of one or few components with little or no sample preparation, at the determination of one component or of a few components with some treatment of the sample or at the analysis of more complex samples.

Total analysis systems (TAS) have also been developed to realize on-line and automated analysis. This field has still difficulties arising e.g. from sample introduction, from a slow sample transport and from the need to develop interfaces between the different components. Downsizing and integration of the analytical steps onto a single monolithic device are aimed at and one wants to enhance the analytical performance at a reduced size. Miniaturization not only includes a reduction of the size or scales, but it also has to deal with the relevance of other forces and phenomena [4-6]. As not only analytical tasks are pointed out but also other chemical functions as synthesis are considered, μ -TAS developed to a lab-on-a-chip concept [7].

Miniaturization has to deal with difficulties in all activities (calibration and validation) and steps (sampling and sample introduction, treatment, sample transport) involved in analytical

procedures. Also the level of miniaturization is to be taken into account (“mini” from mm to μm , “micro” from mm to μm and “nano” $< 1 \mu\text{m}$) because they affect the activities and the steps. Considering the level of miniaturization and its incidence in the whole analytical process some steps can be reduced or eliminated. Specifically in preliminary steps like sampling, sample introduction and treatment of the sample, and on the other hand in detection systems and signal transduction as well as in data acquisition and processing, a high degree of miniaturization nowadays has been achieved.

Whereas chemical analysis usually is performed by skilled personal using specialized instrumentation it is a recent trend to face customers with bulk samples and in-situ analysis. Here, the miniaturization must help to develop easy to handle, portable and reliable equipment, which eases automation and does not require technical personal.

The concept of miniaturization is related with the scaling-down of a system, but it must consider that all forces and processes change with the scale. An example is how in an analytical microsystem, where viscous forces dominate over inertial forces (laminar flow), the transport of molecules is done by diffusion. This process in analytical microsystems is relevant for the sample introduction especially for in-situ analysis and to perform direct sample introduction. Those points are essential aspects of $\mu\text{-TAS}$ and are important requirements in order to achieve success in the real world: features of microsystems should correspond with the needs of the clients asking for solutions to analytical problems in the real world. Another point in the field of miniaturization is the representativeness of the results and the development of a suitable method of analysis at all stages in industrial processes. Additional possibilities of miniaturization lie in a decrease of costs, through the use of less reagents and sample in chemical analysis. This is an important challenge for specialized laboratories in order to perform cheaper and faster analysis. Finally, miniaturized system must allow it to obtain reliable results with respect to calibration and validation.

1.3 Plasma

A plasma is a gas containing positive particles, neutral particles and free electrons which is electrically neutral. Its behaviour is dominated by the interaction between the different types of particles; this means that its properties depend on the degree of ionization so that it becomes a good electrical conductor.

For creating a plasma, the gas is seeded with a few electrons. In the magnetic field circular flow currents are induced in the gas. By the resistance to the circular current flow heat is produced so that the charged particles can reach the ionization temperature and a self-sustaining plasma is formed. The electrons respond much more rapidly to the electromagnetic fields than heavy ions and carry most of the current because of their smaller mass. The plasma remains electrically neutral because the electrons and ions are formed in pairs and have opposite charges. Desirable properties of the plasma include high temperatures and sufficient energy to excite and ionize atoms which are introduced for analysis purposes, producing emission of atom and ion lines. At temperatures over 5000 K, collisions between gas particles cause a cascade ionization of the gas [8].

A variety of gases such as Ar and He are particularly suitable to form plasmas because those gases are monoatomic and can be obtained in pure forms, they have high ionization energies and good characteristics for atomization, ionization and excitation of the analyte. Once formed Ar ions are capable of absorbing sufficient power from an external source.

The number of excited atoms and hence the intensity of emission increases when increasing the temperature and the number of excited atoms is larger when the energy required is low. Typical plasma temperatures can reach several thousands K and consequently there is a much higher ratio of excited to ground state atom densities and a much higher intensity of atom emission as compared to flames which have difficulties to excite atom lines as a result of their low temperatures (2200-3200 K). In contrast to the flames, plasmas need a supply of external electrical energy in order to ionize the gas and to sustain the plasma, where this energy is transferred to the sample to atomize and to excite it [9, 10]. At high plasma temperatures chemical matrix interferences can be overcome and refractory elements such as B, U and W can be determined with plasma emission spectrometry.

New plasma sources may present several advantages over classical arc, laser and spark emission methods with respect to precision but the need for extensive sample treatment can be considered a shortcoming. Indeed sample decomposition is needed and contamination can occur and accordingly, plasma spectrometric analysis becomes time consuming [11]. On the other hand, arc, laser and spark emission are known for their feasibility to introduce samples

directly as solids, which is an advantage for materials such as refractory minerals, ores, glasses and alloys, which are difficult to be brought into solution.

Plasmas can be classified according to the type of electrical field which is used to sustain the plasma. Direct current plasmas, (DCP), inductively coupled plasmas, (ICP) and microwave induced plasmas, (MIP) are well known.

1.3.1 Direct current plasma (DCP)

Developments of DCP were reported since the 1920s. Systematic studies of a three-electrode DCP were performed in the 1970s, when a commercial device was introduced into the market, which had enough features to compete with available flames and inductively coupled plasma devices [12].

The three-electrode DCP consists of two graphite anodes and a common shielded tungsten cathode. The electrodes are shielded with an Ar flow which also supports the plasma discharge. The plasma is ignited by a smooth contact of the cathode with the anodes. The solutions are nebulized and the aerosols are brought in the plasma area between the two Y arms. The DCP has temperatures of ca. 6000 K in the observation region and 10000 K in the arc core. Some advantages of the three-electrode DCP are its inexpensive instrumental costs and low Ar gas consumption. Figures of merit such as detection limits and precision are comparable to the values obtained with the ICP [13].

Samples containing high amounts of salts present difficulties when analyzed by DCP-OES, where significant chemical interferences, ionization problems and matrix effects are produced. The lifetime of the electrodes is a major disadvantage. Here contamination of the source can occur and the electrodes have to be replaced regularly.

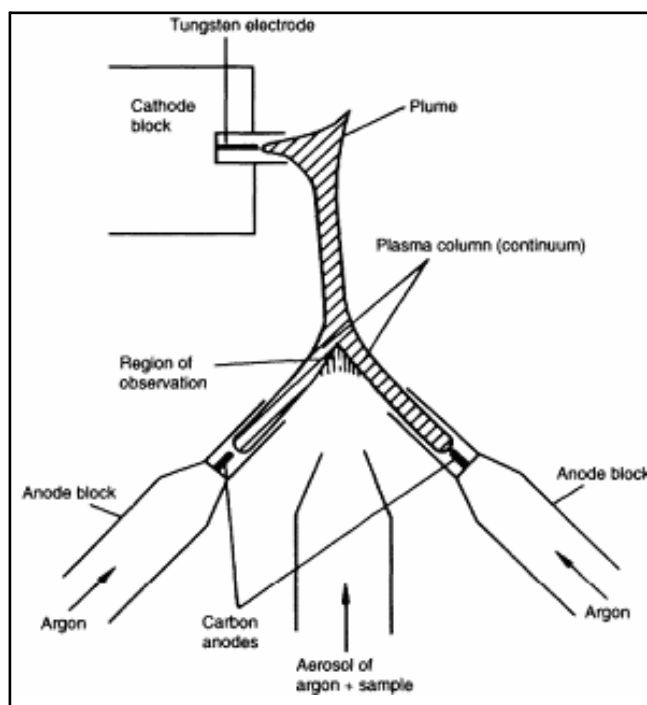


Fig. 1 The three-electrode DCP plasma jet [12].

1.3.2 Inductively coupled plasma (ICP)

In 1963 Reed [14] reported on the use of an ICP at atmospheric pressure for crystal growth experiments and in 1964 Greenfield [15] as well as Wendt and Fassel [16] studied the use of an ICP as an analytical emission source. The first commercially available ICP was introduced on the market in 1970. Many different plasma sources exist, but the most common by far is the inductively coupled plasma (ICP). The ICP is generated by coupling the energy from a radiofrequency generator into a suitable gas via a two- or three-turn, water-cooled copper coil. The radiofrequency energy is normally supplied at a frequency of 27 MHz, but other ICP frequencies too have been studied in the range of 1.6 to 148 MHz, where frequencies of 40-50 MHz are more frequently used [17]. The forward power required is between 500 and 2000 W. Two gas flows, usually Ar are used and the outer flow normally is tangentially introduced between the intermediate and the outer tubes of a concentric, three-tube quartz torch which is placed axially in the copper coil (Fig. 2). Because the outer gas flows tangentially (i.e. with a swirl around the torch axis), the plasma has a ring shape with a weak spot at the centre of its base, through which the internal gas flow loaded with the sample can be introduced. When the gas is seeded with electrons, usually by means of a tesla spark, they are accelerated in the electromagnetic field and reach energies, which are sufficient to ionize the gas atoms. By subsequent collisions with other atoms further ionization occurs and so the plasma becomes

self-sustaining. This occurs almost instantaneously. The field brings the ions and electrons to circular paths, thereby heating the neutral argon by exchange of collisional energy and a hot fireball is produced. The hottest part of the ICP may have a temperature between 8000 and 10000 K, though the analytically useful region is in the tail-flame, which has a temperature between 5000 and 6000 K.

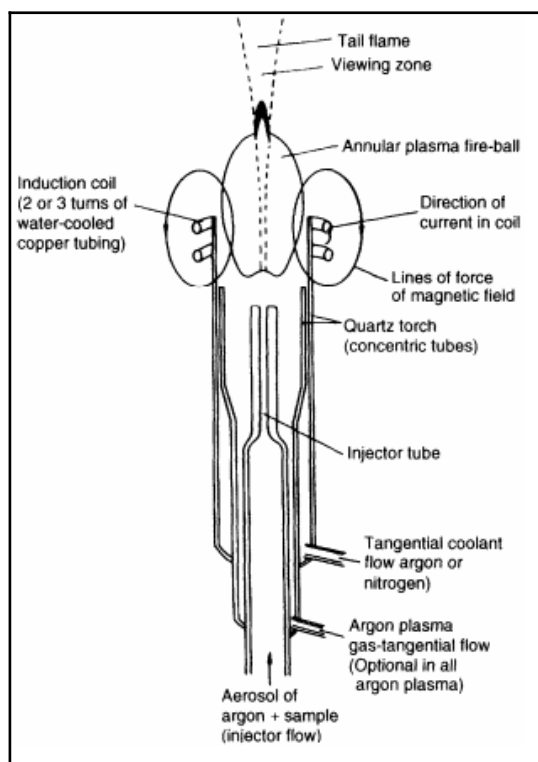


Fig. 2 Geometry of the inductively coupled plasma (ICP) [18].

In the absence of analyte atoms, water and sample matrix components, the predominant species in the plasma are Ar, Ar⁺ and e⁻; although others such as Ar metastables are important. The RF energy used to sustain the plasma is only coupled into the outer region of the plasma, where the above mentioned species are primarily formed and then diffuse to the centre. This is known as the skin effect. A consequence of the skin effect is that the ICP is much more energetic in the outer region, which facilitates the sample introduction. The plasma is optically rather thin, which means that the radiation emitted in the centre will not be re-absorbed by unexcited atoms in the outer regions, as it is the case with flames. This is responsible for the fact that in ICP-OES the linear dynamic range is large.

The various species present in the plasma will circulate between the skin and the central region. When the sample is introduced through the axial channel, the centre will be additionally cooled and the analyte species as well as the species from the sample matrix and water will be present here at a high concentration. The region between the central channel and the plasma is known as the boundary region. The ICP can be divided axially into a number of other regions. The region within the copper load coil is known as the initial radiation zone (IRZ). A further region is located between 10 and 20 mm above the load coil and is called the normal analytical zone (NAZ). The radiation emitted in this zone is normally observed in analytical determinations.

It is obvious that the ICP exhibits a large degree of spatial inhomogeneity. In addition, the ICP is not in thermal equilibrium (TE) because the various collisional processes which occur in the plasma such as ionization, recombination, excitation and de-excitation are not in equilibrium with each other. However, the ICP is near to thermal equilibrium. It is in local thermal equilibrium (LTE), which means that all the processes equilibrate with each other excepted for those involving electromagnetic radiation. Consequently, the ICP cannot be characterized by a single temperature and the ionization temperature (T_{ion}), gas temperature (T_{gas}), excitation temperature (T_{exc}) ≈ 6000 K [19] and rotational temperature (T_{rot}) ≈ 4000 K [20] all have different values. It may be confusing when one temperature is used. One cannot measure temperatures in the ICP with the insertion of probes but must rely on spectroscopic methods of temperature measurement. The temperatures measured then simply depend on the particular method that was used to measure it.

1.4 Microwave plasmas

In 1952 Cobine and Wilber [21] first developed a microwave plasma (MWP) operating at 2.45 GHz under the use of a cavity and a central electrode. Later this plasma was called a capacitively coupled microwave plasma (CMP). In 1959 Schmidt [22] focused his research on this type of plasma and especially on the improvement of the sample introduction system. The CMP was used for the analysis of solution samples by Mavrodineanu and Hughes [23] in 1963. Broida and Meyer [24] succeeded in the analysis of $\text{H}_2\text{-D}_2$ mixture, which can be considered as the first application of a microwave plasma for spectrochemical analysis. Later reports were published by Feuerbacher [25]. Tappe and Van Calker [26] did pioneering work on CMP-OES. After two decades of intensive research on microwave plasmas the first commercial equipments were produced, namely the Hitachi 300 UHF Plasma Scan and the

Applied Research Laboratories (ARL) model 31000, but they were found to be prone to severe memory effects and also matrix effects hampering routine use.

After work in coaxial cavities with He at reduced and atmospheric pressure and Ar at atmospheric pressure, Beenakker developed a TM_{010} cavity, used as GC element-specific detector [27, 28] and as an emission source for gases and solution aerosols. In the cavity He and Ar plasmas could be sustained at atmospheric pressure because of their improved transfer of electrical energy to the plasma. The TM_{010} cavity could also be coupled to SFC [29] and also MIP-MS [30] was described.

In 1975 Moisan [31, 32] developed a new microwave plasma source called surfatron, which also could be sustained in He and Ar at atmospheric pressure. Until 1984 studies were rather focusing on modelling. In the 1990s the surfatron was coupled to different chromatographic techniques such as GC [33] and SFC [34]. Also its use for AAS [35] and as an ion source for MS [36] was reported. In 1985 a microwave torch was developed by Jin [37] at Jilin University and it was substantially improved by Jin and Hieftje at Indiana University. This new plasma source is robust as compared to the previously mentioned devices, and it can work also with He and Ar gases at atmospheric pressure.

Mostly a magnetron is used for the generation of microwaves and the electromagnetic waves are transmitted at a fixed frequency through a coaxial cable to a waveguide (hollow metal pipe or box) and to the electrode at the receiver end or to a resonator. Transmission through coaxial cables is also common in microwave plasmas. Here two coaxial metal cylinders are used as inner and outer conductors separated by an insulating material. The current flows only on the metal surface due to the skin effect and the field is confined to space between the conductors. Microwaves can also be transmitted by microstrips with top and bottom planar conductors on an insulator material.

Microwave sources transmit energy through a transmission line consisting of coaxial cables, microstrip lines or waveguides to the discharge tube containing the working gas. The electrical field is at maximum at the point where the plasma is formed. So as to initiate the discharge the gas is seeded with electrons using a Tesla coil or by releasing electrons from the walls of the vessel because microwave heats the walls allowing self-ignition. The plasma is sustained by collisions of the electrons with the atoms of the working gas.

Microwave plasmas can be classified in two groups according to the type of microwave power transfer from the source to the plasma. A CMP uses a waveguide and an MIP uses a transfer of microwaves through coaxial cables.

MIPs are sources where deviations from local thermal equilibrium (LTE) occur as a result of collisions between electrons and atoms or ions in various states. These species have different energies as compared to each other, by which high electron temperatures and relatively low gas temperatures are found. Measurements of plasma temperatures are based on the assumption of local thermal equilibrium and the Boltzmann and Saha equations. The high power density of MIPs makes them a suitable source for the excitation of metals and non-metals [38]. The microwave plasma temperatures can be summarized as follows [25]:

$$T_e \gg T_{\text{ion}} \approx T_{\text{exc}} > T_{\text{rot}} \approx T_{\text{gas}} \quad (10)$$

In studies of the excitation mechanism and the deviation of the local thermodynamic equilibrium the MIP versus ICP were compared. Huang *et al.* [39] showed that the electron temperature T_e of the MIP is higher than in the ICP but that the electron number density is lower. This can be explained by the high concentration of free electrons and a gas temperature value which is one order lower than the electron temperature.

MIPs have some advantages over other sources like ICPs and their coupling to different techniques and systems for sample introduction were investigated. Especially the low operation costs and ease of handling are advantageous but they are also sources with low tolerance to aerosols and when introducing aerosols from water or organic solvents they are extinguished. So their use is practically limited to the analysis of gas samples.

Liquid chromatography (LC) has been difficult to couple to microwave plasmas as here wet aerosols must be introduced into the discharge resulting in spectral and excitation interferences and in extinguishing the plasma. Research in the field, however, led to modifications of the cavities in order to increase the plasma stability or to desolvation techniques, such as a rotating interface disc to evaporate solvent on a moving belt to transport an effluent while the mobile phase is removed by heating [40].

Gas chromatography (GC) has been recognized as a simple way to introduce gaseous species into the MIP discharge without altering its properties and it was developed to commercial application. With the development of the Hewlett Packard atomic emission detector (AED) HO5921A in 1989 a breakthrough point started for MIPs extending their application to elemental organic analysis [41, 42]. In GC the analyte must be brought into the gaseous phase, so that often a derivatization step for metal species is required to form stable gaseous compounds. An advantage of the MIP is that also He can be used to sustain an MIP discharge.

1.4.1 Capacitively coupled microwave plasmas (CMP)

The CMP was developed by Murayama *et al.* [43] at the Hitachi Central Research Center in 1968. The CMP is generated by transmitting microwaves from a magnetron through a rectangular waveguide to the tip of the electrode [44] (Fig. 3). The electrode is placed within a discharge tube and the plasma is formed around the tip of the electrode surrounded by the working gas. The CMP suffers from contamination by the electrode material, so that the electrode must be changed regularly.

The CMP offers robustness with respect to sample introduction, where mixtures of gases containing moisture and molecular species can be taken up. Indeed, the CMP has a very good performance at relatively high power input (200-1000 W). CMP-OES was also used for the direct analysis of solid samples. Ar, He, air [45, 46] and mixtures of gases, such as He and N₂ [47] were used as working gases. Typical carrier gas flow rates are in the range of 2-3 l min⁻¹ and the total gas flow is between 7-8 l min⁻¹.

Determinations of temperatures and electron number densities in the CMP were performed at different gas flows (< 6 L min⁻¹) and power input (< 700 W) for He [48, 49]. When using N₂ as working gas high temperatures and lower detection limits were obtained as compared to Ar and air.

The CMP has been coupled to several sample introduction techniques such as GC [50] for the determination of organic compounds, non-metals [51] and organotin compounds [52]. Liquid samples were also analyzed by CMP-OES and organic fluorine and chlorine determined [48]. Pb was determined in blood samples [53-55]. Non-metals were determined with a furnace

combined to a He-CMP [56]. After all the CMP suffers from high background emission from the metal electrode due to erosion and contamination.

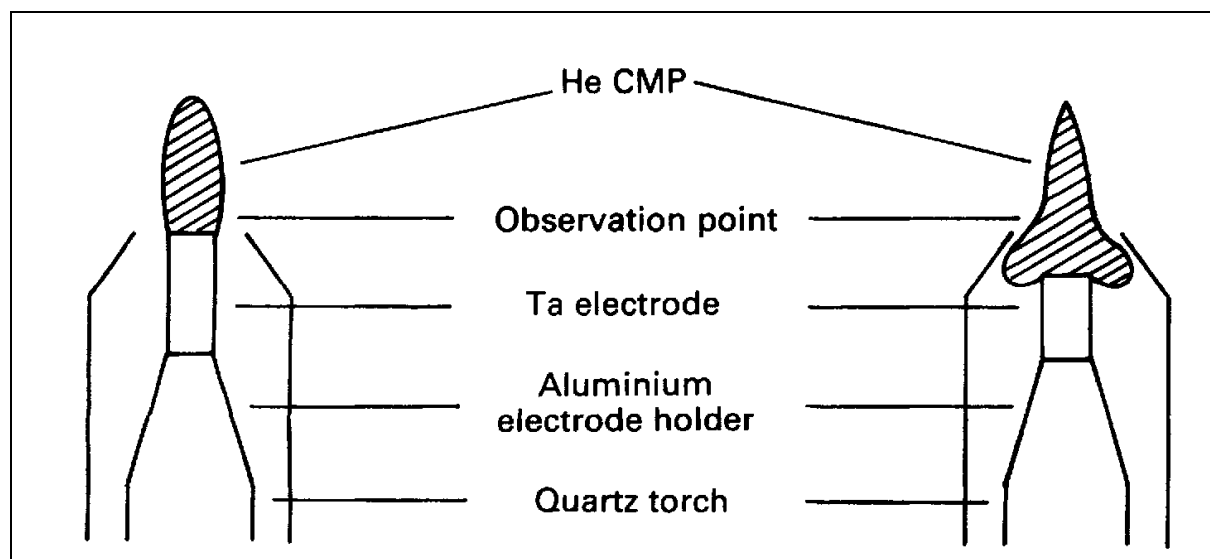


Fig. 3 Capacitively coupled microwave plasma [49].

1.4.2 MIP according to Beenakker (TM₀₁₀ resonator)

The use of a TM₀₁₀ resonator was reported by Beenakker in 1976 [27], who operated an MIP with He and Ar as working gases at atmospheric pressure and used it as an element-specific detector for GC. This MIP can be sustained at a gas flow rate $< 1 \text{ L min}^{-1}$ and a forward power below 100 W. A silica tube is centered in a cavity, which is constructed of Cu. The cavity volume is made as small as possible in the area of maximum electrical field strength to reach the highest energy density possible. The microwave power is transmitted with the aid of a coupling loop located perpendicularly to the plasma tube at 10 mm from the wall. The plasma is generated in a centrally located capillary. When increasing the power a toroidal plasma in Ar [57] or a diffuse He plasma [58] also can be formed. The advantage of observing the plasma in a TM₀₁₀ resonator axially into the capillary is an efficient collection of the emitted radiation. The cavity is cooled by an air stream. Because the system is easy to build and to operate, the MIP in a TM₀₁₀ resonator was coupled to a variety of sample introduction system [59, 60] as well as with GC. The devices were operated in combination with a computerized photodiode array (PDA) spectrometer [61]. Furthermore, the MIP in a TM₀₁₀ resonator was used as radiation source in the case of pneumatic nebulization [59, 62], electrothermal evaporation of aqueous solutions and in combination with hydride generation.

[63-65]. Finally, the MIP in a TM_{010} resonator was also used as ion source for mass spectrometry [66]. Rosenkranz [67] showed the importance to couple it with a cold vapour system producing dry analytes so as to increase the lifetime of the plasma and to reduce the peaks-widths, which on their turn increase the power of detection.

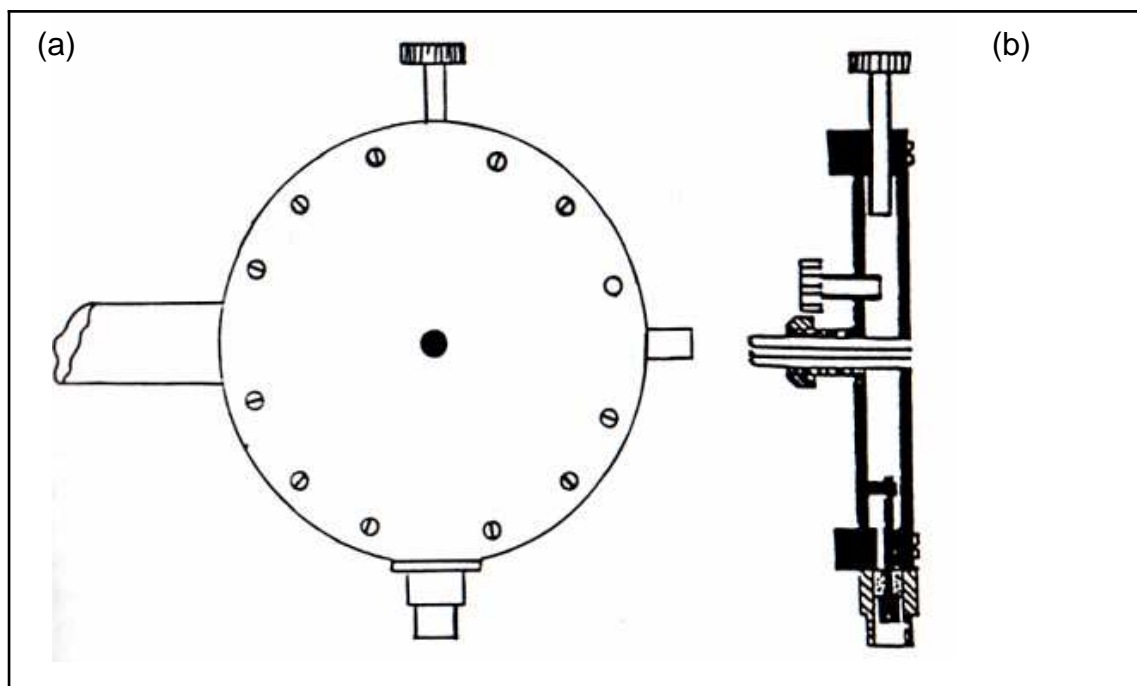


Fig. 4 MIP according to Beenakker cavity: front (a) and side view (b) [27].

1.4.3 Surfatron

The surfatron was proposed as analytical source by Hubert *et al.* [32] at the end of 1970s. An integrated surface wave propagation system was also described by Moisan *et al.* [31] in 1975. They operated the MIP at reduced and at atmospheric pressure with He and Ar as working gases. In a surfatron the microwave energy propagates through the plasma as electromagnetic waves with a maximum in the interface between the plasma and the discharge tube. The resonant structure has a varying depth and the microwaves are coupled through a side-on antenna near to the plasma capillary into the gases. The surfatron is easy to tune and to operate as compared to an MIP in a TM_{010} resonator. This makes it possible to sustain different plasma configurations with the same system [68]. Moisan *et al.* [69] focused part of their surfatron studies on the physical aspects of the resonant cavity. The instrumentation in the case of a surfatron also is inexpensive and versatile, so the surfatron MIP was well investigated and coupled to a variety of sampling systems such a supercritical fluid

chromatography (SFC) for the determination of S and GC, as described by Selby and Hieftje [70] and Luffer *et al.* [34], respectively. The use of a surfatron for the speciation of Hg and C was also reported when coupling it to a multicapillary GC [71]. For Hg the cold vapour technique was used and the surfatron gave better results than atmospheric pressure microwave plasmas. Costa-Fernandez *et al.* [72] showed that the coupling of HPLC to a surfatron operated at low pressure with Ar via continuous hydride generation could be used for As determinations.

Microwave structures using a TM_{010} resonator or a surfatron also present common disadvantages. They include microwave leakage. Also the low tolerance to wet aerosols is a common drawback for these sources. The annular shape of the discharges can be a cause of contamination of the plasma because of contacts with the tube that contains the plasma.

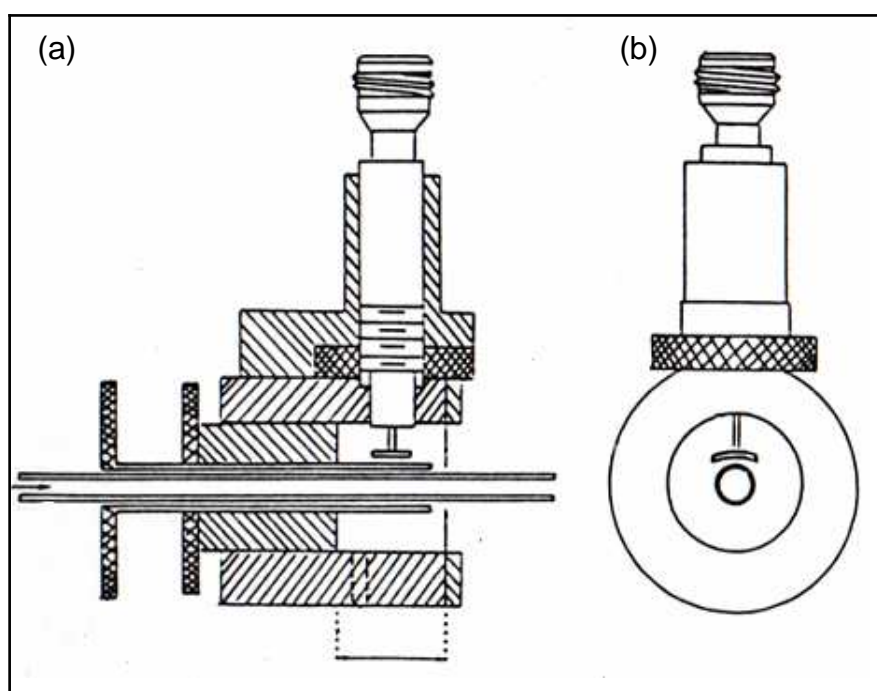


Fig. 5 MIP Surfatron: side (a) and front view (b) [32].

1.4.4 Microwave plasma torch (MPT)

Jin [37] first described the microwave plasma torch (MPT) in 1985. It consists of three concentric tubes made from brass and copper. The outer tube is only a protector of the cavity. Through the inner tube the aerosols and vapours are brought to the plasma and through the intermediate tube the working gas is entered. The microwave energy is optimally coupled into

the plasma by adjusting a cylindrical antenna to its optimum position L_1 and the plasma is tuned by changing the distance L_2 between the top of the torch and the short circuit. The plasma is formed between the tops of the intermediate and the central tube. It has an annular shape at a gas flow rate of 1 L min^{-1} and a power of 150 W for Ar and a cylindrical shape with a brilliant center at a gas flow of 2 L min^{-1} and more than 200 W for He.

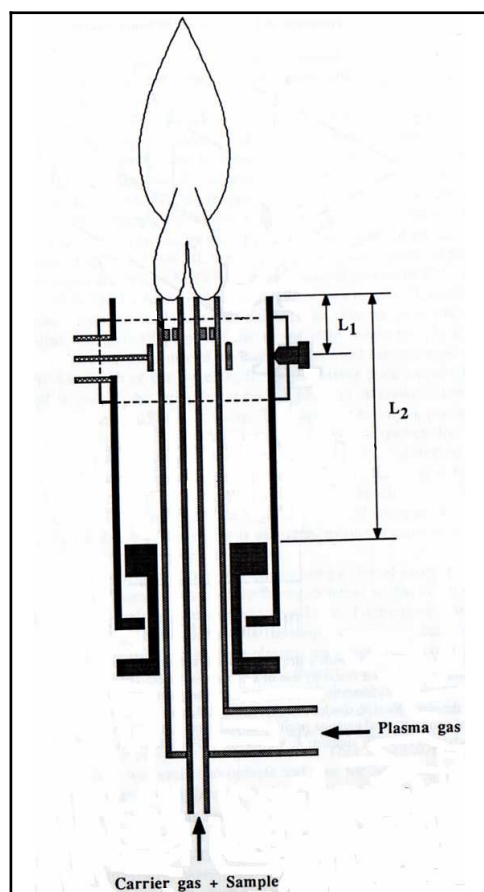


Fig. 6 MIP Microwave plasma torch MPT [37].

The MPT plasma has a structure similar to the ICP. Accordingly, it has a high tolerance to wet aerosols containing molecular species and sample matrix compounds. Flow injection using pneumatic nebulization with desolvation was coupled to the MPT and showed a good performance with low matrix effects and detection limits similar to ICP-OES [73]. ETV was also coupled to the MPT [74, 75]. With an MPT operated with He, non-metals and Hg could be determined and a coupling with GC and SFC was also described [76]. Real samples could also be analyzed by using the MPT and halogenated hydrocarbons could be determined with improved limits of detection between 160 and 330 pg for I, Br and Cl, as compared to the MIP in a TM_{010} cavity in the case of mass spectrometry [36]. Although the MPT has a high tolerance to wet aerosols, its performance was improved when using on-line pre-separation and

preconcentration techniques like solid phase extraction, physical and chemical adsorption and ion-exchange membranes and hydride generation [36, 37].

1.4.5 Microstrip Plasma (MSP)

Microstrip technology has been shown useful for the production of a microwave discharge in a small resonator. So the MIP could be fully integrated in a miniaturized system for element determinations consuming low power. Bilgic *et al.* [77] described a such structure and called it Microstrip Plasma. In its original version, it consisted of a groove made in two quartz plates with the aid of a commercial dicing-saw, which were glued together with water glass. The microwave power was brought to the plasma channel by connecting an SMA type microwave connector to the copper microstrip, deposited on the surface of the wafer (over the plasma channel). The microstrip was fabricated by sputtering and electroplating procedures. The bottom side of the wafer was connected to a copper block acting as ground connection and for cooling. The plasma was fully enclosed inside of the quartz wafer and did not suffer from contamination from the material of the device and from the surrounding air. The plasma was ignited with the piezoelectric discharge from a lighter. A microplasma was formed at a power input in the range of 10-40 W and an Ar flow of 50-1000 mL min⁻¹. Rotational and excitation temperatures were measured using OH bands and Fe, respectively, and values of 650 and 8000 K were found. Hg could be determined by FI-CV-MSP-OES with a limit of detection of 50 pg mL⁻¹ [78].

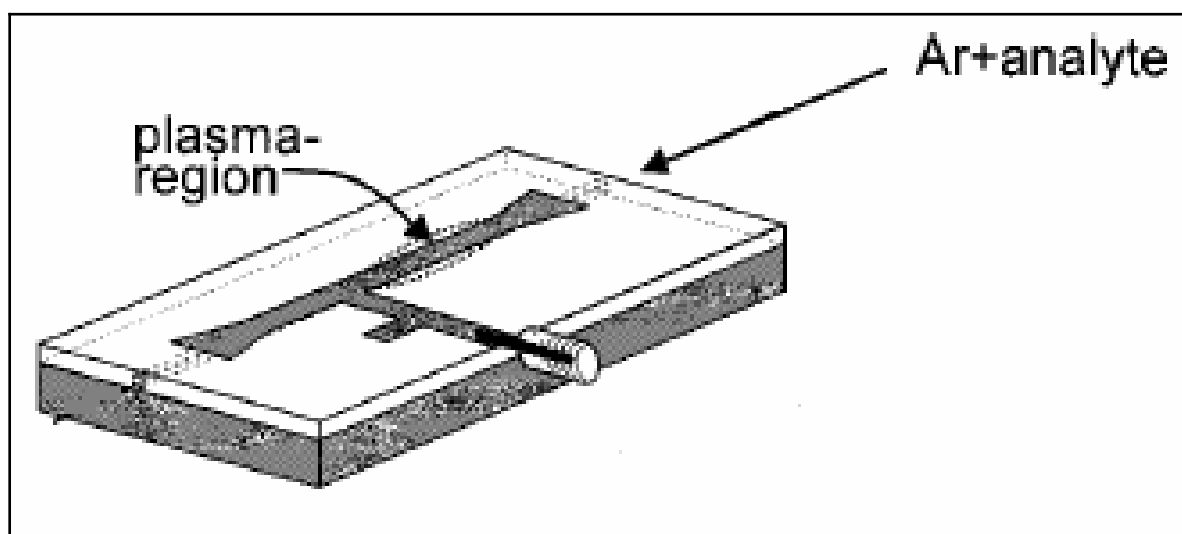


Fig. 7 Microstrip plasma (MSP) on quartz wafer [80].

A He microstrip plasma operating at atmospheric pressure sustained inside a sapphire wafer was also described by Bilgic *et al.* [78]. Sapphire material was chosen for this arrangement and a high electric field strength could be realized in the plasma channel. A microstrip plasma in this device could be operated at a microwave power of 5-30 W for He and 1-10 W for Ar and with a gas flow between 50-1000 mL min⁻¹. The He plasma was found to self-ignite at a microwave input power and a gas flow rate of 10 W and 100 ml min⁻¹, respectively. The gas and excitation temperatures in the case of He were found to be 600 and 4000 K, respectively. It was shown that in a He MSP at 15 W and 700 ml min⁻¹ organic molecules can be entered, atomized and the elements excited. When HCCl₃ vapours were introduced into the He gas stream emission signals of Cl at 912.11 nm can be measured. Accordingly, this MSP can be used for element specific detection. A modified structure of the MSP, where the plasma exits from the sapphire wafer channel was described by Schermer *et al.* [79]. This modified structure has the advantages that it can be used as spectrochemical radiation source without suffering from space angle limitations. The plasma can be operated at a power input range of 5-40 W and gas flow rates of 0.2-1 l h⁻¹ and the excitation temperature is 6000-7000 K. This MSP has been shown to be suitable for a determination of Hg by OES with detection limits of 10 ng L⁻¹.

1.5 Sample introduction

1.5.1 Pneumatic nebulization

In this way of aerosol production a high velocity gas stream passes over a liquid surface and small droplets of aerosol are produced. A such production of droplets takes place when a liquid passes through a capillary tube parallel or perpendicular to a gas stream carrying the droplets to the source. During the transport of the aerosol droplets built at the end of the capillary, a series of process can take place. These may include a desolvation of the droplets, a vaporization of the solid samples, a dissociation of the molecular species or an ionization of the analyte. All the processes need to be optimized to maximize the transport efficiency and to minimize matrix interferences. A series of nebulizer designs has been described to produce an optimum droplet size and to realize a highly efficiency transport. They include concentric glass nebulizers, cross-flow nebulizers, Babington nebulizers, fritted-disc nebulizers and ultrasonic nebulizers. To produce steady signals the nebulizer is usually placed in a spray

chamber to sort out the large droplets. Often a desolvation system is used but also direct injection nebulizers have been described.

Concentric Nebulizers

Gouy [80] was the first who reported the use of concentric nebulizers which are self-aspirating. Pt-Ir capillaries are very often used even for highly acid solutions. However, also quartz capillaries can be used, unless for HF acidified solutions. The use of concentric glass nebulizers is well-known in atomic emission spectrometry because of their long-term stability. However, their sensitivity is often affected by the presence of alkali and earth alkali elements [81]. Also saline samples affect this sort of nebulizers by clogging. A concentric micronebulizer with a reduced inner diameter and thinner walls of the capillary was developed [82] and with this arrangement higher sensitivities and lower limits of detection can be obtained.

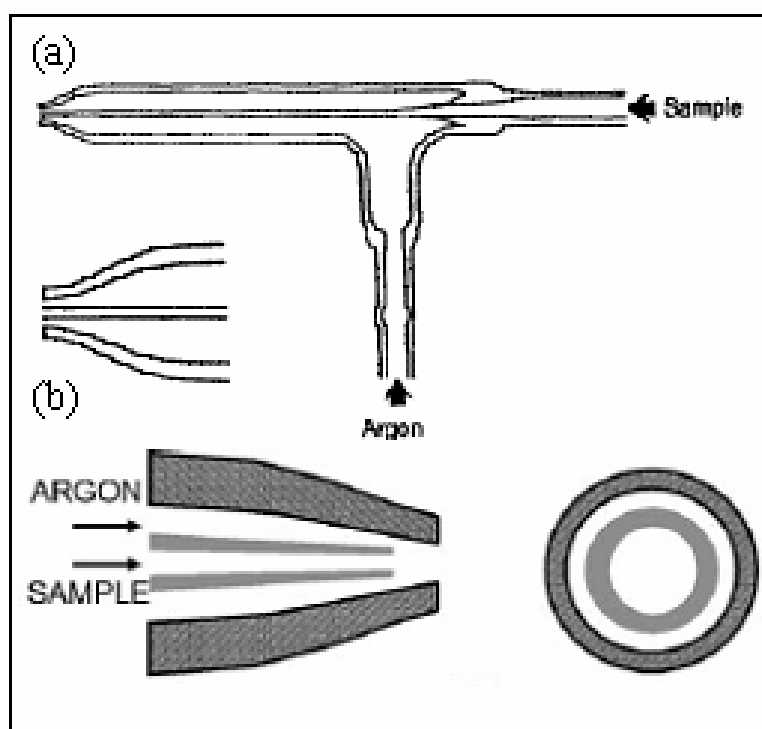


Fig. 8 Concentric nebulizer [81] (a) and concentric micronebulizer [82] (b).

Cross-flow nebulizers

In a cross-flow nebulizer two capillaries are positioned perpendicularly to each other and with the tips close to each other. One capillary is fed with sample solution with the aid of a peristaltic pump and in the other gas flows. Typical capillary diameters for ICP nebulizers are around 0.2 mm and the tip separation is 0.05-0.5 mm. When the capillaries are made of Ryton the device can tolerate acidified solutions containing HF [83]. Cross-flow micronebulizers [84] often are very useful to be coupled with capillary electrophoresis (CE) and ICP-MS. Here a narrower capillary is placed inside the sample capillary to reduce the exit cross sectional area.

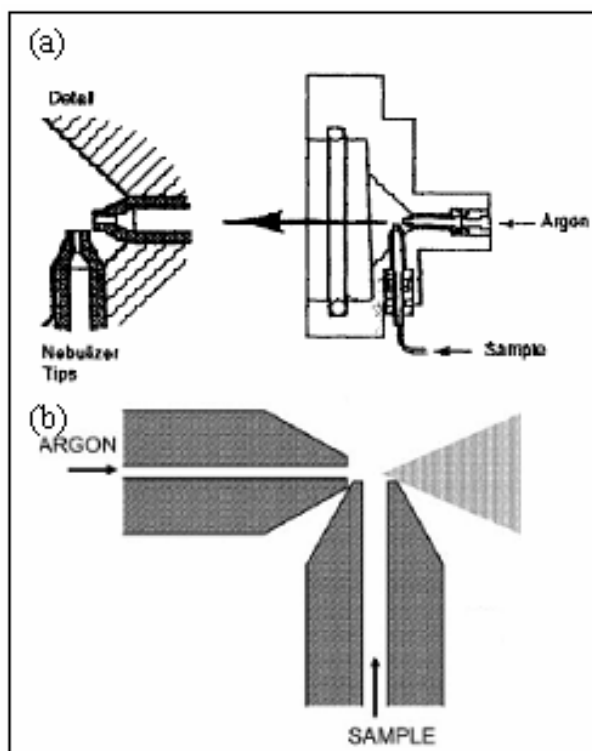


Fig. 9 Cross-flow nebulizer (a) and its operation (b) [84].

Babington nebulizers

In 1973 Babington [85] described a nebulizer where the sample solution flows through a wide tube into a groove. Here, the film of the off-running solution is nebulized by a perpendicularly entering gas flow. With this type of nebulizer solutions with high concentrations of salts can

be nebulized without risk of clogging and also slurry samples can be nebulized [86]. The sample capillary inner diameter is ~ 1 mm.

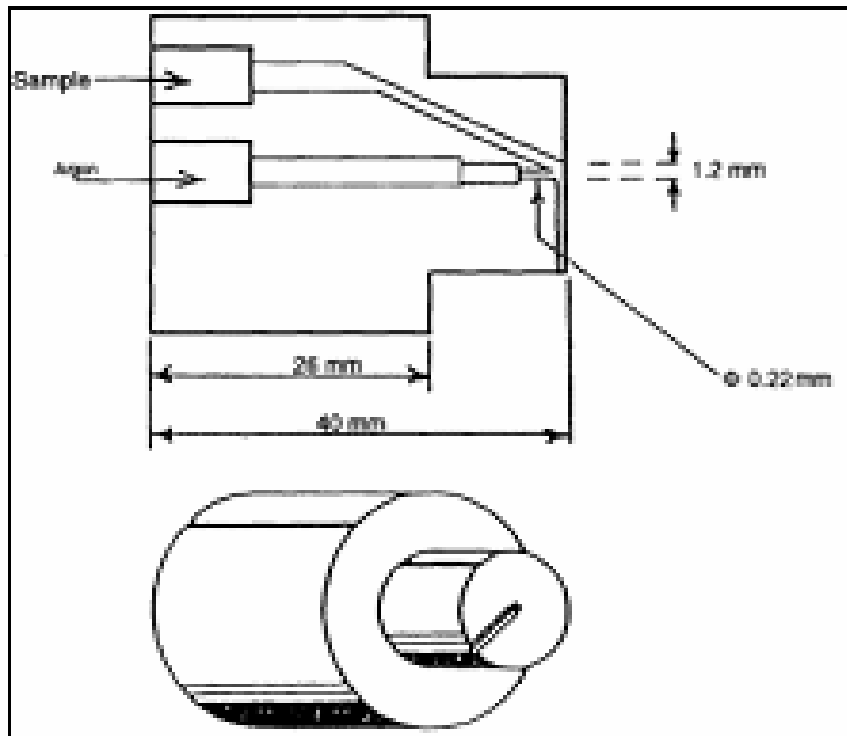


Fig. 10 V-groove or Babington-type nebulizer [18].

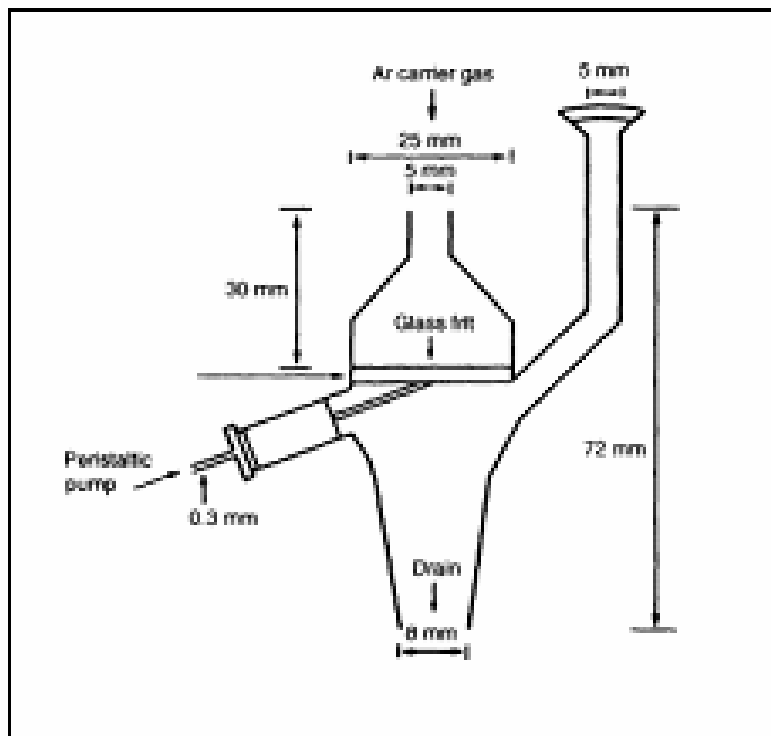


Fig. 11 Glass-frit nebulizer [18].

Fritted-disc nebulizers

At a low sample consumption, fritted-disc nebulizers have a very high nebulization efficiency. Fritted-disc nebulizers were shown to be useful for plasma spectrometry coupled to liquid chromatography, where solutions containing organic solvents need to be nebulized. Disadvantages of this type of nebulizer are the high memory effects as compared with other nebulizers. Here, the signal rising time seems to be long within the total time of analysis.

1.5.2 Ultrasonic nebulizers

Through the action of suitable acoustic energy waves at a certain frequency on the surface of a liquid an aerosol can be produced. Ultrasonic nebulization has several advantages over other nebulizers, such as the production of aerosol droplets with a lower diameter and narrow particles size. Therefore, the nebulization efficiency as compared to other nebulizers is high.

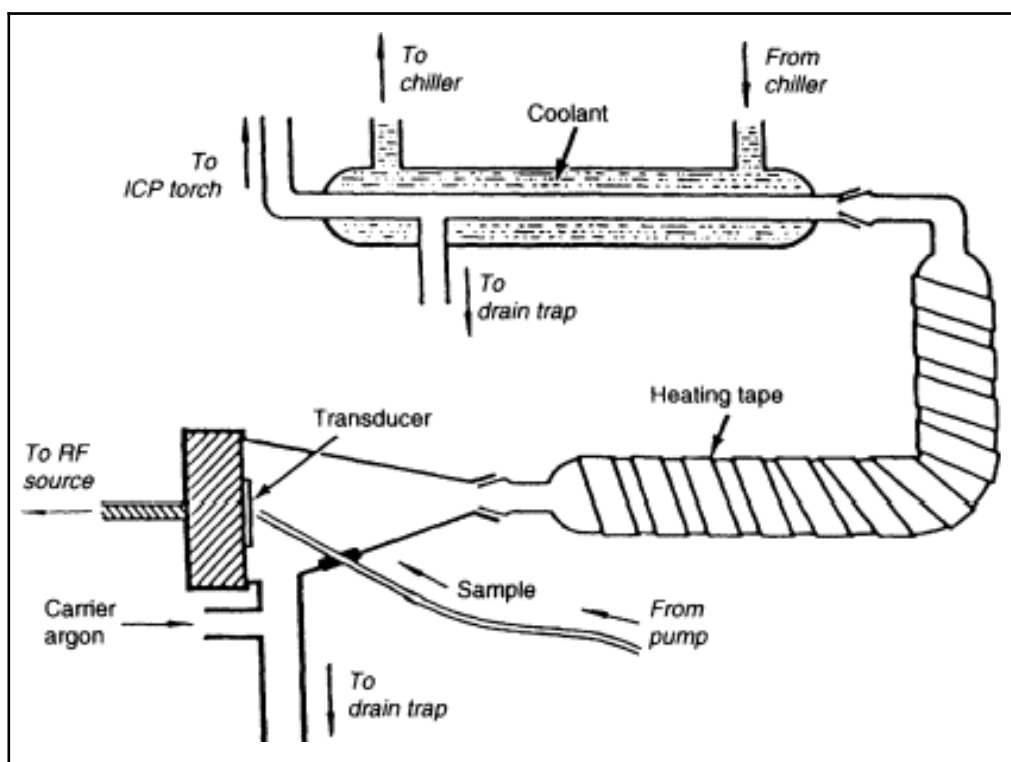


Fig. 12 Ultrasonic nebulizer used for ICP atomic spectrometry [18].

1.6 Chemical hydride generation

Volatile hydride generation as a first type of gaseous phase species generation has the advantage that for a number of analytes a high introduction efficiency in the plasma can be realized while leaving back interfering matrix constituents

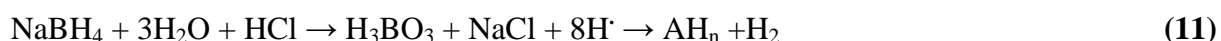
A first hydride generation technique was described by Holak *et al.* [87] to determine As while forming the AsH_3 volatile species which are introduced into a flame source. Madsen *et al.* [88] collected AsH_3 in a AgNO_3 solutions, which is aspirated into a flame source. Dalton and Malakonski [89] reported interesting limits of detection (0,1 μg) when entering the AsH_3 directly into the flame source. Fernandez *et al.* [90] improved the sensitivity by collecting the AsH_3 in a balloon as reservoir and subsequently introducing it in the flame. Pollock and West [91] extended hydride generation to Sb and Bi. In 1972 Braman *et al.* [92] reported the use of sodium tetrahydroborate (THB) as reducing agent to obtain hydrides. One year later Schmidt and Royer [93] reported the generation of arsine and selenine and then this was extended to stanane and telurine. Thompson and Tommerson [94] first mentioned the use of a heated quartz tube as atomizer in the case of As and Pb.

By the use of sodium tetrahydroborate the of HG technique could be extended to the generating of volatile species of other elements such as Cd, In, Tl, Cu, Ni, Zn, Au, Ag and Pt [95].

In atomic absorption spectrometry the production of volatile species for As, Bi, Ge, Pb, Sb, Sn and Te is widely used. Hydride generation follows some steps to obtain an optimum effect. First of all, a basic THB reagent solution is mixed at adequately acid conditions with the sample. Secondly, the volatile species are collected (optional) and third, they are transferred to the atomizer where a decomposition in the gas phase to the elemental form takes place. Many designs have been developed in the last decades with the aim to improve the sensitivity, the selectivity, the freedom of interferences and the detection limits in the case of a coupling to MIP sources at a variety of working parameters. The production of the volatile hydrides themselves bases on a reduction by hydrogen. The reaction of basic THB solutions with an acidified sample solution has been used both in AAS [96] as well as in ICP-OES [97, 98]. Here the produced hydride is separated from the solution and led into the source by a carrier gas flow. The production of an excess of hydrogen accompanying the HG can influence the

stability of the source, especially in the case of microwave sources with a low forward power. To avoid the introduction of an excess of H₂ in the sources a freezing trap or membranes can be used to isolate the hydrides before entering to the sources.

To avoid matrix interferences precautions should be taken to have the analyte elements in their inorganic state prior to hydride generation. The mechanism of the hydride production involves the reaction:



where the nascent hydrogen is produced.

However, the hydride generation also may be due to a non-nascent hydrogen mechanism.



Here, the hydride species are formed from the hydrogen bound to the boron intermediate species.

Dedina [99] concluded that for the generation of volatile hydrides neither of the two formation mechanisms has a convincing evidence. Supported by experiments on the acid decomposition of THB producing nascent hydrogen Robbins and Caruso [100] proposed a mathematical model for the pH dependence of the Hg cold vapour generation. They mentioned that the formation of elementary Hg could be improved by the generation of nascent hydrogen. Laborda *et al.* [101] objected against this assumption. They argued that considering the standard potential for H⁺/H, neither the reagents nor the reaction products would be able to reduce protons to the atomic state. Also D'Ulivo *et al.* [102] and Qiu *et al.* [103] performed experiments on the hydride generation mechanisms.

Many analyses of real samples with HG techniques were described. Water samples were analyzed after a treatment with acids [104] and interferences from Cu can act in a catalyzing

way as Welz and Melcher [105] reported. A removal of Fe by the use of masking agents, precipitation and/or complexing reactions before HG has been described as well.

1.7 Electrochemical hydride generation

Hydrides can also be generated electrochemically, which is known as electrochemical hydride generation (ECHG). Hereby the use of a reducing agent such as THB is avoided. The first report on ECHG stems from Sand and Hackford [106] for the case of As. It was in the 1960s that Tommlison [107] described the electrochemical formation of stibine. Rigin *et al.* [108-110] used a batch discontinuous mode for the production of the hydrides of As and Sn with a spiral cathode made of Pt or Pb. Lin *et al.* [111-114] constructed a flow-through cell and used a flow injection sample introduction to generate hydrides electrochemically. Vitreous carbon, Pt and amalgamated Ag foil were used as electrodes. Subsequently, several groups [115-119] reported studies of the influences of the parameters in a flow-through cell, as did Winefordner and Sima [120], who used several types of gas-liquid separators.

Electrochemical hydride generation is performed on the surface of the cathode and consists of three steps: deposition of the hydride forming element on the surface and its reduction, a formation of the hydride and its desorption. The reduction of the analyte is the result of a charge transfer reaction and it must be realized in an acid solution. The reduction depends on the attainable negative potential. The reduction can also be achieved at a cathode with a high overpotential for H₂ and at low current densities. The hydride formation at the cathode may involve an adsorption of hydrogen atoms at a surface with low overvoltages for hydrogen. The hydrogen then can combine with the reduced hydride forming element and the product can be desorbed in the catholyte flow. The final reaction can be summarized as:



(X: hydride-forming element; Me: surface of the cathode).

ECHG is an alternative to wet chemical hydride generation and has several advantages over it. First, the use of THB required in chemical hydride generation is avoided. THB solutions are a source of contamination and also are instable. They should be daily prepared in alkaline solution. Secondly, the consumption of expensive acids like H₂SO₄ is reduced. Finally, the

production of hydrogen can be controlled better or minimized to obtain optimum conditions with respect to the analyte excitation in the plasma.

For an optimum hydride generation in ECHG the cathodes must be properly selected so as to obtain the best figures of merits. Firstly, it can be said that the optimum cathode surface depends on the form of the cathode (planar, fibrous, etc) and its material (carbon, noble metals, etc). When these parameters are optimized a high reproducibility is obtained even when the sample is changed or when the cathode must be removed. By the presence of concomitants the analytical signal can be influenced positively or negatively, as deposition on the cathode surface can occur and the hydrogen overpotential can change. Finally, the hydride generation efficiency strongly depends on the analyte compound that is introduced in the cell as it is the case in chemical hydride generation.

The cathode material should be inert and should not take part in the electrochemical reaction on its surface. For that purpose several materials have been tested, such as Pd wire [121], as well as Pt foils, wires and shields [116, 122], Pt covered with Ag wool [123], Ag wool and wire [121, 123], amalgamated Ag foil [112], Cu foil and powder [123], polished vitreous carbon [111, 117], fibrous carbon, pyrolytic graphite [117, 118, 121], Pb covered fibrous carbon [123], Pb sheet [124, 125] and Pb wire [121]. Normal noble metals are chosen as cathode material. Especially Pt, Au and Ag are suitable because they adsorb hydrogen on their surface and they do not change by passing a current. In the noble metals the overpotential is lower than in the case of the amalgams. Pb and carbon can also be well used as cathode material due to their inertness to sample and reagent solutions, their high reducing properties, their low electrical resistance and the ease to form electrodes inexpensively. However, they have some drawbacks, such as the high susceptibility to interferences. Glassy carbon and pyrolytic graphite are often used as cathode material because of their porosity, by which the amount of active areas to produce hydrides is high.

The choice of anode materials is limited to conductive materials of which the corrosion is low as is the contamination of the anode solution when a large positive voltage is applied. Generally Pt is chosen as anode material due to inertness against the oxygen formed in the anode compartment.

1.8 Mercury cold vapour generation

Mercury is a liquid metal with low vapour pressure, which easily can be formed by a reduction with appropriate reagents. Accordingly, it can easily be released from a liquid and as elemental vapour be transported to a plasma source. A specific reaction to form elementary Hg is the reduction with a solution of SnCl₂. This reaction has the advantage that no H₂ is produced and the Hg can be released as a vapour from the solution with the aid of a gas flow. Before being introduced to the plasma source, it can be dried by conducting the loaded gas over HClO₄ or H₂SO₄. This procedure is known as cold vapour generation technique. The Hg can be preconcentrated by using Au to form an amalgam prior to releasing the Hg by resistance heating and sweeping the vapours into the discharge with the aid of a carrier gas. Also other metals like Cu, Ag, Au and Pt can be used to form the amalgam. Hg unlike most hydride forming elements is reduced to its metallic form Hg⁰:



1.9 Other volatile species generation techniques

Further reactions producing volatile species or elements in the gaseous state can be coupled to a plasma as radiation source for analytical atomic spectrometry. Elementary iodine can be generated by an oxidation with K₂Cr₂O₇ and brought with the aid of a carrier gas into the plasma. Sulfur vapour can be released from liquid samples as H₂S through acidification with HCl. Sulfur can also be oxidized with KMnO₄ to form SO₂. Both species easily can be released to plasma sources.

Of a particular interest for the generation of volatile element species and particularly for hydride generation is the treatment with UV irradiation. This technique has been worked out for non-metals (I, S) and noble metals (Ag, Au, Rh and Pd). The irradiation with UV light can also be used to produce radicals, which act as oxidizing or reducing agent to produce volatile species. A typical example is the reduction to elementary Hg by photochemical reactions with free radicals produced by UV irradiation of solutions [126-139].

1.10 Electrothermal vaporization (ETV)

ETV can be used to volatilize microquantities of solution from a carrier made of graphite or refractory metal, such as W, Tl or Rh. The atomizer may have different shapes such as a cup, a platform, a boat, a tube or a filament. The evaporation cell is connected by tubing to the injector in the plasma. The solution sample is aliquoted onto the heating device with the aid of a micropipette. The different steps of the procedure are the drying step to remove the solvent, the ashing step to remove the sample matrix and the volatilization step to bring the analytes into the carrier gas.

Different ETV systems have been developed for chemical analysis. The first is a carbon rod enclosed in a quartz cell, through which Ar flows to transport the analyte. The Ar flow can be introduced tangentially to minimize condensation on the walls. Further a W coil enclosed in a cylindrical quartz chamber can be used. A third system makes use of a graphite furnace where the atom cloud is kept inside the tube and transported into the plasma. In all three systems the three essential steps are drying, ashing and volatilization.

Chemical modifiers can be used to avoid the formation of carbide species and to facilitate the removal of the matrix. For this aim mixtures of $\text{Pd}(\text{NO}_3)_2$ are used as well as nickel salts, ascorbic acid and freon. ETV offers some advantages like work with low sample volumes (5-50 μL), the ability to remove the solvent and high efficiency sample introduction. Matrix substances and contamination from the heating material can cause condensation and losses during the sample transport. The introduction of samples by ETV produces transient signals and its operating parameters include the Ar carrier gas flow, the furnace temperature and the duration as well as of the rate of drying, ashing and vaporization. Furthermore, the signals of the more volatile elements in the sample can appear earlier than the ones of the less volatile elements. With spectrometers using CCD detectors transient signals for several elements can be recorded simultaneously.

1.11 Laser Ablation (LA)

Laser ablation makes use of a very short laser pulse that delivers a burst of energy to the surface of the sample. A small amount of material is ablated and the aerosol formed is transported with a carrier gas into a plasma discharge. The amount of material that is analysed

in the case of LA is small as compared to which is needed for ETV and LA can be considered to be nearly a non-destructive technique. The use of a laser system produces spots of very small size and accordingly spatially resolved information of the sample in the lateral as well as in the in-depth dimension can be obtained.

A drawback of this technique is that it is not possible to separate the analytes from the matrix. All the material is simultaneously brought into the source, so more matrix effects can be expected and calibration with aqueous standards is difficult to realize. Three ways for calibration can be used in LA.

- *Calibration with matrix-matched solid standards:* Here, the pure sample matrix should be mixed with increasing amounts of analytes to obtain a set of calibration samples.
- *Calibration with non-matrix-matched solids standards:* Here, an internal standard should allow it to correct for the difference in ablation rate from sample to sample.
- *Calibration using aqueous standards:* This is realized by mixing the aerosol produced during the ablation of the solid sample with the aerosol generated through nebulization of a standard solution.

1.12 Spark ablation

Spark/arc ablation makes use of the erosion of a sample by an electrical spark or arc and has been used for the direct analysis of solid samples since many years. For generating the spark a high voltage is applied between two electrodes in an Ar atmosphere, one of them being the sample. During the break-through a train of unidirectional electrical discharges is produced, which ablate material from a conductive solid sample. In the spark the atoms released from the sample surface are excited and ionized and the corresponding emission can be observed, which is used in spark-OES. The eroded material in spark ablation is transported in a radiation source (e.g. an ICP or an MIP).

1.13 Spectrometers

In OES the optical emission from the radiation source is focused onto the entrance slit of a spectrometer. Through convex lenses or concave mirrors, the radiation is led to a dispersive element and after spectral resolution the atomic emission line intensities are measured with a

detector. A monochromator is an instrument that can isolate a narrow wavelength band (e.g. 1-0.01 nm) within a comparatively wide spectral range (for atomic absorption or emission spectrometry typically 190-900 nm). Most of the instruments use a diffraction grating, which is a mirror having a certain number of lines per millimeter. Most often reflection gratings are used, which are manufactured by depositing a layer of aluminium on the blank grating and then ruling with a diamond tool. From a such master grating replica can be produced.

Radiation incident on the surface of the grating is diffracted to a larger or lesser degree depending on its wavelength. Hence, a spatial separation of lines of different wavelengths is achieved. The diffracted radiation is collimated and focused through a mirror on an exit slit. By rotating the diffraction grating radiation of different wavelengths can be focused onto the slit. The diffraction by a grating is described by the Bragg equation:

$$\sin \Theta_m = \sin \Theta_i + m\lambda/d \quad (16)$$

θ_i and θ_m are the angles between the incident as well as the diffracted light beams and the normal of the grating surface, λ is the wavelength, d is the grating constant and m the order of diffraction (integer value, $m = 0, \pm 1, \pm 2, \dots$). This equation is valid for reflexion gratings, of which the grooves are perpendicular to the plane of incidence. Gratings in spectrometers are most often used in the reflection mode. The equation shows that for $m \neq 0$ the radiation of different wavelengths will be spectrally dispersed angularly. Lines of different wavelengths are diffracted into different discrete angles according to the order m . Spectrometers usually use the dispersed light of one order. Influences of other orders and the non-dispersed zeroth order have to be suppressed.

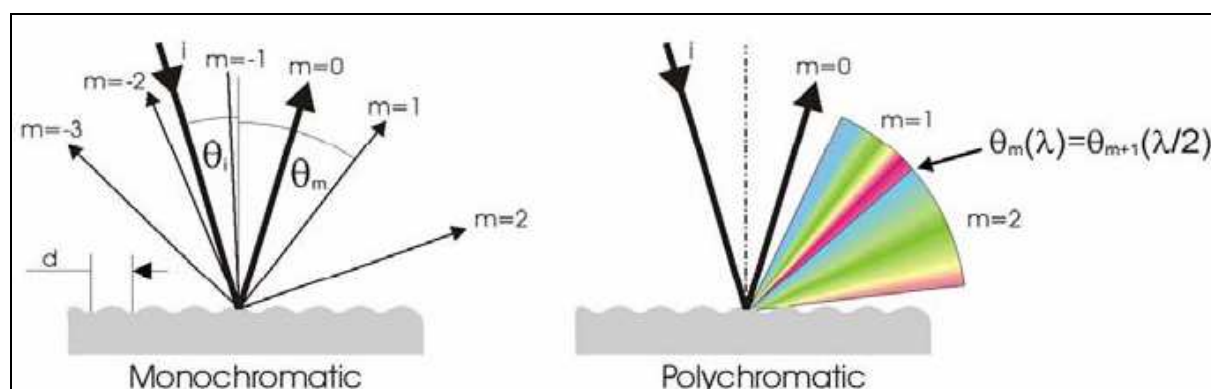


Fig. 13 Diffraction of monochromatic (a) and polychromatic radiation (b).

A grating can be mounted in a monochromator in several ways. In the Ebert mounting a large spherical mirror is used to collimate and to focus the beam. Czerny and Turner replaced the large, expensive Ebert mirror by two small, spherical mirrors allowing corrections for coma.

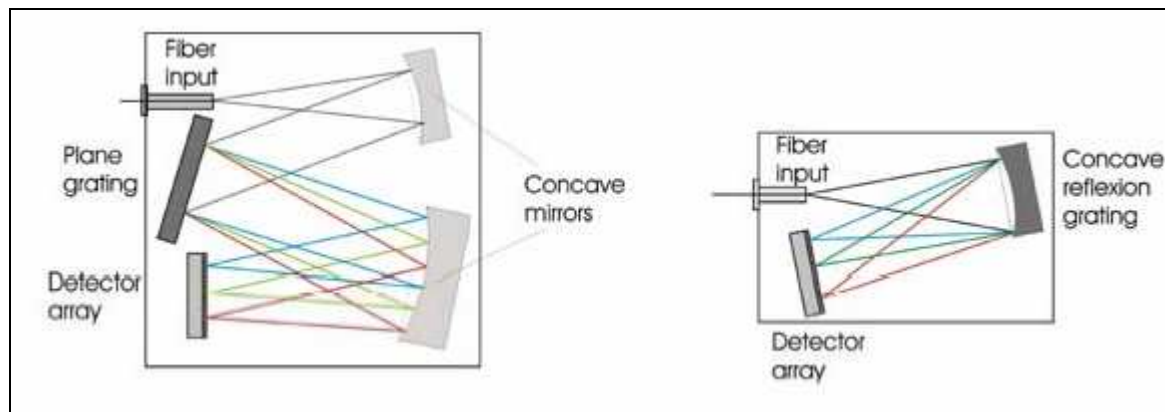


Fig. 14 Czerny-Turner (a) and flat field concave grating spectrograph (b).

A higher resolution can be achieved by using echelle monochromators. They contain a so-called Echelle grating, which has a grating constant of about $1/100$ nm and is used at higher orders (> 50) together with a prism as order sorter often in crossed dispersion. This setup, where the prism or another dispersing element, is used as an order sorter, results in a two-dimensional spectrum in which the blaze wavelength corresponding to each of the different orders can be used. Also Fourier transform spectrometers have been developed for the UV-visible region of the spectrum. Such spectrometers make use of a Michelson interferometer. They have excellent resolution and an electronic recording of the whole spectrum at extremely fast scanning speed (a few seconds) is possible. However, a main disadvantage of this technique arises from the fact that the whole spectrum is collected. Accordingly, very intense emission lines contribute to the noise in all regions of the spectrum, thereby degrading the signal-to-noise ratio for less intense lines. Other desirable features of a monochromator are stability and multi-element capability. Initially, direct reading spectrometers, based on a polychromator with a high number of photomultipliers behind exit slits, were used for simultaneous multi-element analysis. They were expensive, bulky and limited to the installed elemental lines. The development of rapid-scanning monochromators under computer control which sequentially select the analytical wavelengths, greatly increased the flexibility of analysis. More recently, high resolution echelle monochromators in conjunction with array detectors have been used, with which lines over the whole spectrum can be accessed

simultaneously. This can also be achieved with Paschen-Runge spectrometers where the focal plane is provided with a high number of CCD detectors arranged side by side.

1.14 Detectors

Charge injection devices (CID) and charge-coupled device (CCD) detectors can be used to monitor large portions of the spectrum by taking an electronic photograph. They are analogous to photographic plates, which were used in the earliest spectrometers. A typical array detector consists of 1024 linear photodetector arrays on a silicon chip with a surface area of 13 x 18 mm. Up to three array segments (pixels) can be used to measure an analytical line of high sensitivity and large dynamic range and relatively free from spectral interferences. The wavelengths of the emission lines are fixed by means of their location on the chip and lines can be measured simultaneously. The detector can then be electronically cleaned and a next spectrum record made. The advantages of such detectors are that they often can make as many as ten lines per element available, so that lines which suffer from interferences can be identified and eliminated. Compared with PMTs an array detector offers also a high quantum efficiency and a low dark current.

Currently, there are three different types of array detectors, which are used in spectrographs: CCDs, photodiodes and CMOS arrays. They differ in their distinct production technologies and their parameters. CCDs are array detectors with metal-oxide capacitors (photogates). During the illumination by the spectrally resolved radiation a charge (electron-hole pair) is produced under the gate. A potential well is created by applying a voltage to the gate electrode. The charge is confined in the well associated with each pixel by the surrounding zones of higher potential. The read out of the array is preceded by a charge transfer by means of varying gate potentials according to special clock schemes. The charges of the pixels are transferred simultaneously to the shift register(s), followed by a sequential transfer to the output section, where the charge is converted into a proportional voltage. The node doing this is first set to a reference level (clamp level) and afterwards to the signal level. The difference is used as the final signal. This technique is called Correlated Double Sampling (CDS) and allows a significant reduction of the system noise. There exists a wide variety of CCD arrays from several producers. The Sony ILX series is often applied in spectroscopy. Other types are the TCD 1201D of Toshiba and the S 703x series of Hamamatsu. The latter has not only one pixel line but 122. It can be used in the so-called line-binning mode. The signals of each pixel

row in the direction perpendicular to the spectrum are additionally combined to create a greater pixel height.

Photodiode arrays (PDA) consist of several photodiodes arranged in a line. The radiant energy impinging on a diode generates a photocurrent, which is integrated by an integration circuitry associated with this pixel. During a sampling period the sampling capacitor connects to the output of the integrator through an analog switch. PDAs like the S 39xx and S 838x series of Hamamatsu as well as the MLX 90255 of Melexis and LF2C of IC Haus are produced.

CMOS arrays also use MOS structures as pixels like the CCD arrays. The basic difference is that the charge-to-voltage conversion takes place directly in the pixel cell. This conversion consists again of two steps, the photon electron and the charge (electron) voltage conversion. This difference in read out technique has significant implications for the sensor architecture, capabilities and limitations. The S 837x series of Hamamatsu and the L series of Reticon are examples for CMOS detectors.

The optical resolution in a spectrum is reflected by the Full Width at Half Maximum (FWHM). It depends on the groove density (mm^{-1}) of the grating, the diameter of the entrance optics (optical fiber or slit) and the optical length of the spectrometer. It should be mentioned that the resolution increases with the groove density of the grating, but at the expense of spectral range and signal intensity.

1.14.1 Miniaturized spectrometers

Traditional laboratory optical spectrometers are table top-sized instruments that deliver very high performance. Currently used industrial spectroscopic analyzers are largely based on this laboratory technology. They are typically contained in a temperature controlled housing, eventually with fiber-optic connections to the respective source. The installation costs for this equipment are high, without even taking into account the cost of maintenance, and they are too expensive to be used as spectroscopic sensors e.g. in the environment. Herefor, currently available diode-array and other miniature spectrometers may be a better alternative, also because miniature detectors now have a high dynamic range, a fair resolution, high signal-to-noise ratios, and a good performance.

Analytical emission spectrometers also require a means to transport the radiation from the source to the spectrometer. This may make use of lenses and/or of optical fibers, where the opening angle of the spectrometer is to be taken into account.

Traditional laboratory optical spectrometers are typically bulky. The key challenge in constructing a miniature spectrometer is how to shrink the size of the device without compromising resolution and signal-to-noise ratio. A number of prototype miniature spectrometers using different techniques have also been constructed or proposed, including Fourier transform spectrometers.

Miniaturized spectrometers mostly use a detector array instead of many single-channel detectors and only need fixed components. Meanwhile, they are available as PC coupled, stand-alone as well as hand-held devices and begin to find their applications also for online process measurements.

Mostly diffraction gratings are used as the dispersive element, because they have a higher dispersion and lower production costs than prisms and their dispersion over the whole spectral range is nearly constant.

Array spectrometers consist of an input slit, a grating and possibly other optical imaging elements. One can distinguish between plane grating setups and concave grating spectrometers. The latter type combines diffraction and imaging in one optical element.

Array spectrometers show some disadvantages, too: they often suffer from high stray light, compared with monochromators. Furthermore, the sensitivity is lower than that of a conventional monochromator, which easily can be fitted with a photomultiplier. The precision and resolution is normally less than that of laboratory instruments with a turnable dispersive element.

The array detectors have a number of individually readable sensitive areas, so-called pixels (picture elements), arranged in one straight line. They are devices transforming a spatial light distribution into a signal voltage or current often changing with time (see Ref.[140]).

1.15 Plasma mass spectrometry

In plasma mass spectrometry, ions are physically extracted from the plasma into a mass spectrometer, which requires a low pressure (10^{-5} mbar), so that a suitable sampling interface must be used. The problem of extracting ions from a hot plasma at atmospheric pressure into a mass spectrometer at ca 10^{-9} atm now is overcome by making use of at least two differentially pumped vacuum chambers held at different low pressures. The plasma normally is aligned so that the central channel is directed to the tip of a water-cooled sampling cone, made of Ni or Cu, which has an orifice of approximately 1 mm in diameter. The pressure behind the sampling cone normally is at the order of some 0.1 mbar. So the plasma gases, together with the analyte ions, expand through the sampling orifice and form a shockwave. This expansion is isentropic (i.e. there is no change in the total entropy) and adiabatic (i.e. there is no transfer of energy as heat), resulting in a supersonic expansion and a fall in temperature. This supersonic expansion takes the form of a cone with a shockwave structure at its base called a Mach disc. The region within the expansion cone is called the zone of silence, which is representative of the ion species to be found in the plasma, i.e. the ionization conditions have been frozen. Behind the sampler there is a skimmer cone, of which the orifice at the tip protrudes into the zone of silence, and which axially is in-line with the sampling orifice. The ions from the zone of silence pass through the orifice of the skimmer into the vacuum chamber as an ion beam. The ion beam can then be focused by means of ion lenses, which deflect the ions along a narrow path and focus them onto the entrance to the mass analyser.

In the mass analyzer the ions of different mass-to-charge ratio (m/z) are separated. Since the ions of interest are almost exclusively singly charged, m/z is equivalent to mass for practical purposes. There are two types of mass analyzers commonly employed for elemental mass spectrometry, namely the quadrupole and the magnetic sector (see Becker [141]).

Quadrupoles comprise four metal rods, ideally of hyperbolic cross section. Through a combination of radiofrequency (RF) and direct current (DC) voltages, which are applied to each pair of rods, an electric field is created within the region bounded by the rods. Depending on the RF/DC ratio, the electric field between the rods will allow ions of a narrow m/z range to pass. Hence, by changing the RF/DC ratio in a controlled manner, the quadrupole can scan through the mass range allowing ions of increasing m/z to pass through, while the other ions strike the quadrupole rods. In practice, the quadrupole is rapidly scanned

in small steps, i.e. a typical mass scan from 2 to 260 m/z takes less than 100 ms. Alternatively, the RF/DC voltage may be adjusted to allow ions of any chosen m/z to pass, rather than performing a sequential scan, thereby allowing so-called peak hopping between widely separated m/z . Quadrupole mass analysers are nowadays cheap, reliable and compact. They have nearly single mass resolution, which is sufficient for many applications, and therefore it is the most commonly used mass analyser. However, when higher resolution or truly simultaneous mass analysis is required, magnetic sector instruments are more powerful.

Magnetic sector mass analysers make use of the fact that ions are deflected by a magnetic field, with ions of higher mass or charge being deflected to a greater extent. The electric sector can be placed either before or after the magnetic sector, denoted respectively as normal and reversed geometry. In a typical instrument the ions are accelerated after they are skimmed from the plasma and, then they travel through the electric sector, which acts as an energy filter. The ions then are deflected in a single plane by the magnetic field, with the degree of deflection increasing with increasing m/z . A mass spectrum can be generated by scanning the magnetic field, allowing the ions of increasing m/z to pass through a slit. Alternatively, the magnetic and electric field strengths can be held constant and several detectors can be provided in the plane, thereby allowing truly simultaneous mass analysis. Magnetic sector mass analysers are more expensive and more complex to operate than quadrupoles, and they cannot be scanned as rapidly as quadrupoles.

Apart from quadrupole and sector field mass spectrometers also time-of-flight systems now are important in plasma mass spectrometry [142].

C. Instrumentation

2.1 Microstrip plasma

The atmospheric pressure, low-power microwave plasmas based on the microstrip technology (MSP) were generated with the aid of a transistor microwave generator. Herewith microwaves of a frequency of 2.45 GHz with a maximal microwave power output of 40 W were produced.

2.1.1 Plasma inside the wafer (type A)

A first type of plasma was sustained fully inside a straight grown-in cylindrical channel (0.9-mm inner diameter) in a square sapphire wafer (30 mm long \times 30 mm wide \times 1.5 mm high), which has a relatively high anisotropic relative permittivity and was ignited with a spark [77, 79]. A 100-nm Ti adhesion layer covered both sides of the sapphire plate. On one side of the wafer, a 2- μ m Cu layer was provided by sputtering and served as a ground electrode. The other side was provided with the microstrip lines (width of 0.8 mm), as it is schematically shown in Fig. 15a. The microwave power was introduced to the microstrip structure by a coaxial cable with the aid of a sub-miniature version A (SMA) connector and propagated along the inner side of the sapphire substrate between the microstrip line and the ground electrode. The microstrip technology made it possible to use only a small wafer area. A compensated edge in the microstrip was provided so as to allow an effective propagation of the microwave field along the electrode. The ground electrode was connected to a copper socket provided with an active air cooler (25 mm long \times 25 mm wide). For controlling the gas flow rates, a mass flow meter was used. Ar and He were introduced into the analyte channel of the MSP structure by means of a 0.55-mm outer diameter polyethylene tube, after being loaded with the analyte, and serve as discharge gases.

2.1.2 Plasma exiting the wafer (Type B)

Also this type of microstrip plasma (MSP) was operated in a square sapphire wafer with a length of 30 mm and a height of 1.5 mm, in which a straight cylindrical channel (0.64 mm in diameter) for the introduction of the Ar and He working gas was grown-in. The microstrip structure in comparison with the previously described MSP structure was modified in so far that the microstrip (0.8 mm in width) on the wafer extends to the edge of the wafer, by which

the plasma exits from the gas channel by about 2-3 mm (Fig. 15b). The positions of a compensated edge and a matching element in this new design were also modified so as to keep the reflected power low. As in the former type a copper layer sputtered on the backside of the wafer was connected to a copper base cooled by a fan and served as ground electrode.

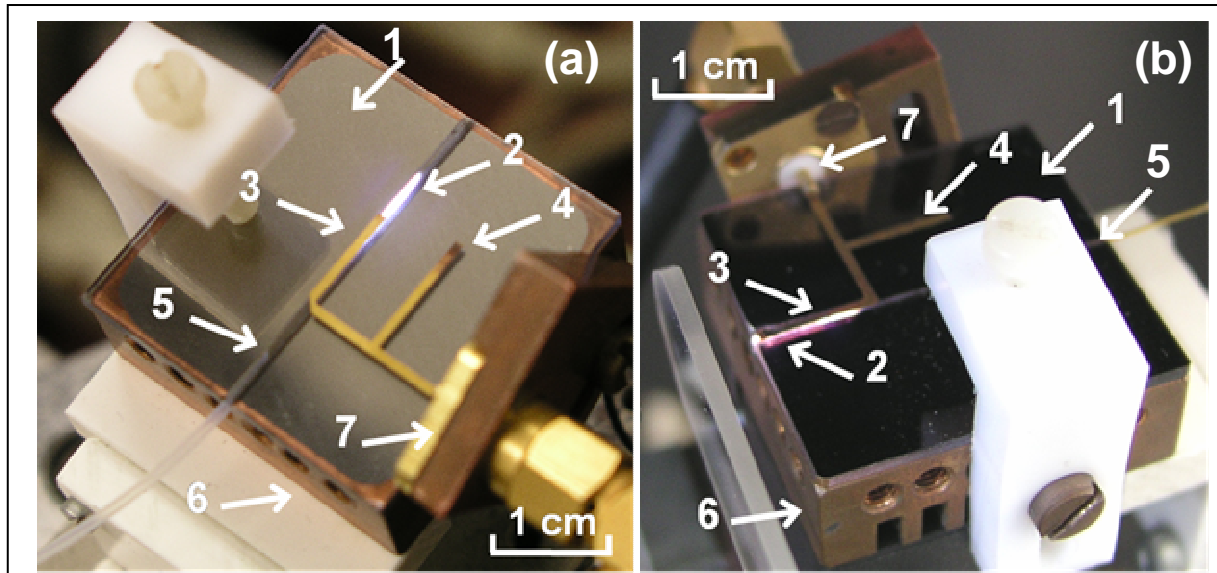


Fig. 15 Microplasma structure inside the wafer (a) and exiting the wafer (b). Sapphire wafer (1), Ar MSP (2), microstrip (3), matching element (4), gas/sample channel (5), Cu base with fan (6), coaxial connector (7).

Both types of microplasmas have several advantages over other devices described in the literature:

1. They can be generated at atmospheric pressure without need for a vacuum pump.
2. They are electrodeless discharges, reducing the plasma source contamination by sputtering of the electrodes.
3. Microstrip technology and a small microwave generator permit low power operation and portability of the microplasma system.
4. MSPs are very economical in gas and power consumption.
5. MSPs can be directly coupled to microwave generators by SMA connectors avoiding radiation losses.
6. A matching of the impedance can be done with the aid of simple components such as antennas.

2.2 Miniaturized spectrometer

For the acquisition of the spectra and the data recording, a miniaturized USB 2000 spectrometer (Ocean Optics, USA) coupled to a personal computer was employed. The spectrometer has an asymmetric crossed Czerny–Turner design.

The radiation is collected from the MSP using a 6-mm diameter quartz lens (focal length of 8.7 mm) and transmitted by a 2-m-optical fiber with 600 μm diameter to the spectrometer. To protect the lens from the gases released by the MSP, a quartz plate was placed between the plasma source and the lens. The collected radiation enters the optical bench through a suitable connector. Before entering the optical bench, the radiation passes through a filter that restricts the optical radiation to a pre-determined wavelength region. Then, the radiation is reflected by the collimating mirrors onto the gratings which diffract the light. This on its turn strikes the CCD detector, which converts the optical signal to a digital signal (Fig. 16).

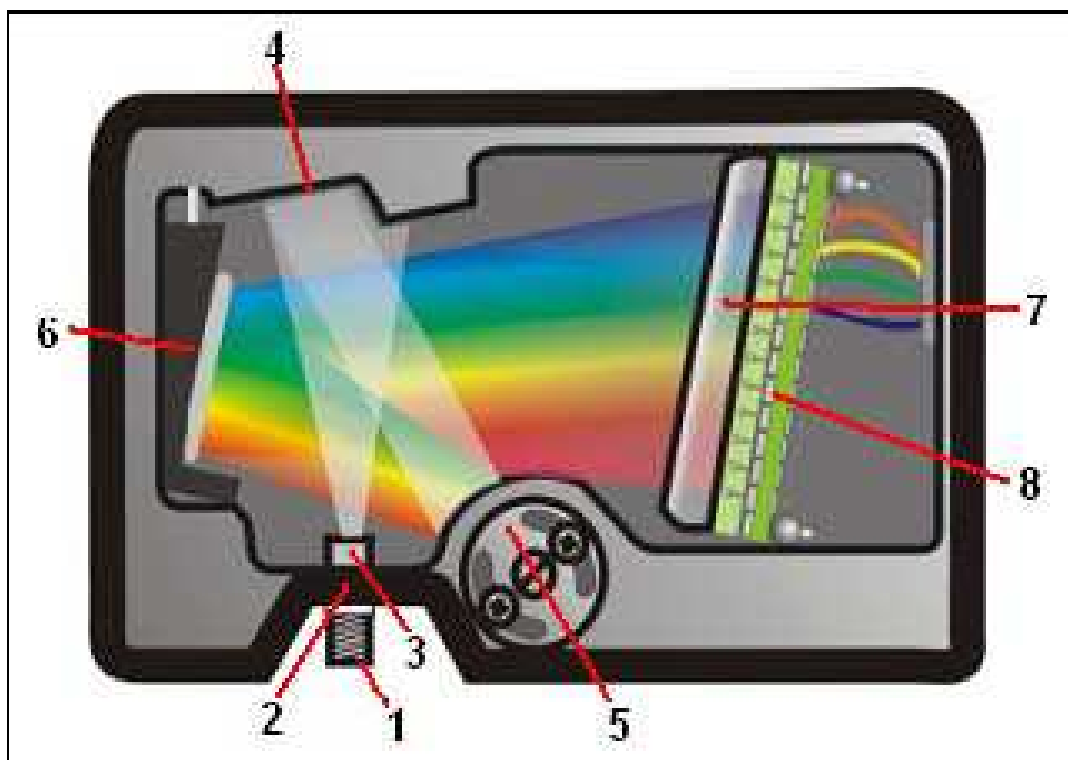


Fig. 16 USB 2000 miniaturized spectrometer. SMA connector (1), slit (2), filter (3), collimating mirror (4), gratings (5), focusing mirror (6), collection lens (7), CCD detector (8).

The specifications of the CCD detector used in the USB2000 miniaturized spectrometer and those of the USB2000 spectrometer itself are listed in Table 1 and 2, respectively.

Table 1. Features of the CCD detector

Type	Sony ILX511 linear silicon CCD array
Number of elements	2048 pixels
Pixel size	14 μm x 200 μm
Pixel well depth	62,500 electrons
Signal-to-noise ratio	250:1 (at full signal)
A/D resolution	12 bit
Dark noise	2.5 RMS counts
Corrected linearity	>99.8%

Table 2. Specifications of the USB2000 spectrometer

Dimensions	89.1 mm x 63.3 mm x 34.4 mm
Weight	190 g
Power consumption	90 mA, 5 V DC
Wavelength range	200-500 nm
Detector	2048-element linear silicon CCD array
Gratings	UV through Shortwave NIR, 600 and 1200 lines mm^{-1}
Entrance aperture	5, 10, 25, 50, 100 or 200 mm wide slits or fiber (no slit)
Order-sorting filters	Installed longpass and bandpass filters
Focal length	f/4, 42 mm (input); 68 mm (output)
Optical resolution	~0.3-10.0 nm FWHM (depending on grating and size of entrance aperture)
Dynamic range	2 x 10 ⁸ (system); 2000:1 for a single scan
Stray light	<0.05% at 600 nm; <0.10% at 435 nm; <0.10% at 250 nm
Sensitivity	400 nm – 90 photons/count; 600 nm – 41 photons/count; 800 nm – 203 photons/count
Data transfer rate	Full scans into memory every 13 milliseconds

Integration time	3 milliseconds to 65 seconds
Operating systems	Windows 98/Me/2000/XP when using the USB interface on a desktop or notebook PC. Any 32-bit Windows operating system when using the serial port on desktop or notebook PC. Windows CE 2.11 and above when using the serial port on palm-sized PC

2.3 Sample introduction systems

2.3.1 Efficiencies of different setups for water vapour removal

The generation of a vapour containing the analyte or one of its volatile species through chemical reactions is accompanied by the introduction of water vapour into the gas mixture which has been recognized to influence the stability and the excitation properties of sources like the microwave plasmas. Normally, the use of a desolvation trap is required so as to remove these residual water vapours before entering the analyte vapour cloud into the plasma sources [68, 143].

For a such purpose, different setups for drying the analyte vapours subsequent to the gas-liquid phase separation and before their entrance into Ar and He MSPs were examined and their effectiveness studied through a comparison of the analyte signals, as done with the Hg cold vapour technique (see Fig. 17). It was found that the setup with the $\text{Mg}(\text{ClO}_4)_2$ filled tube and the flask with concentrated H_2SO_4 with and without an additional cooler (to 4°C) produced the highest relative intensities of the Hg line for the case of both MSPs. The application of the water vapour cooler only was found to be less effective. A disadvantage of the setup with the drying tube, however, was the relatively fast exhaustion of the absorption capacity of $\text{Mg}(\text{ClO}_4)_2$ for H_2O , which then led to an absorption of the analyte and a deterioration of the detection limit for Hg. Therefore, the use of a flask containing concentrated H_2SO_4 was chosen for the desolvation of the analyte vapour because it was easy to install and it can be used for a relatively long time as well.

The Hg CV generation and the separation of the analyte species from the reaction liquid were performed in a continuous-flow mode. The principle of the CV system used is given in Fig. 18. Here the Hg containing sample solution, which is acidified with HCl, and the reducing

agent being a solution of SnCl_2 acidified with HCl were pumped in parallel with the sample to a T-piece, where both flows were mixed. Then, the reaction mixture was pumped into a cylindrical gas-liquid separator (15-mm inner diameter, 100 mm long) for separation of the Hg cold vapour from the sample solution with the aid of the gas flow. The Hg vapour and the accompanying solvent vapours were passed through a flask containing concentrated H_2SO_4 for desolvation, and were finally introduced into the MSP. The reaction liquid was removed from the separator by a peristaltic pump with a flow rate which was selected so that always a constant solution level was maintained inside the gas-liquid separator.

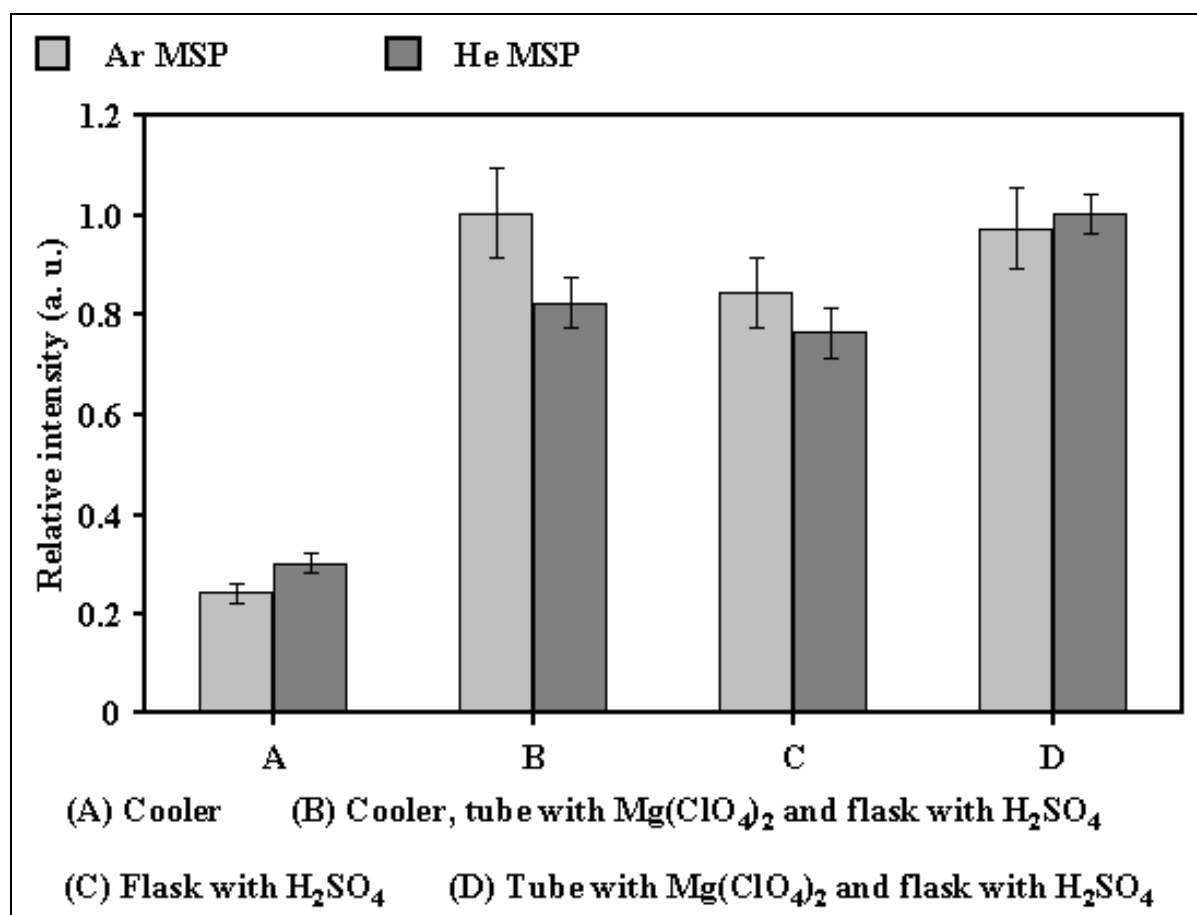


Fig. 17 Evaluation of water vapour removal systems for the Hg cold vapour technique combined to MSP-OES. Hg I 253.6 nm line.

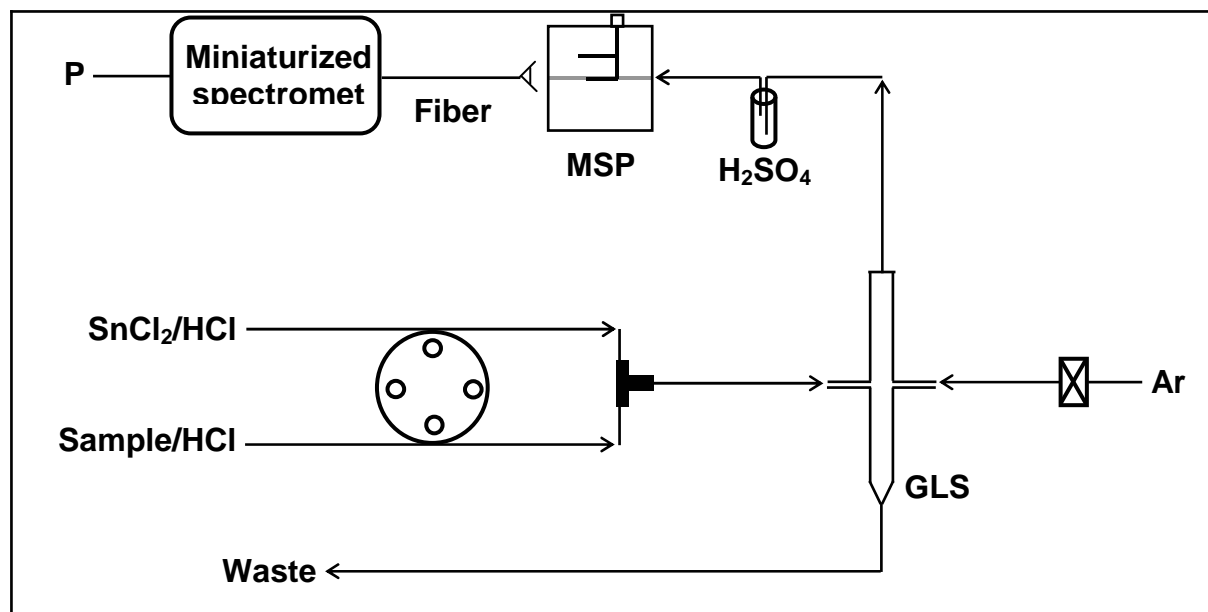


Fig. 18 Continuous cold vapour generation system for the determination of Hg using SnCl₂ as reductant to be combined with MSP-OES

2.3.2 Continuous hydride generation system for the determination of As and Sb

In the continuous flow-hydride generation (CF-HG) manifold, we used for the determination of AsH₃ and SbH₃, a small concentric gas-liquid phase separator (GLS), (65 mm in length and 14 mm in width). As compared to commonly used classic U-tube separators, the relatively small dead volume of this GLS decreases the dilution of the generated hydrides, which prevents a deterioration of the signals and their reproducibility [144]. In addition, a GLS without drain and a peristaltic pump were used, which makes it easier to maintain a constant filling level inside the GLS. This prevented from pressure fluctuations in the system and allows it to keep the dead volume of the GLS constant. For the generation of As and Sb hydrides, an acidified sample solution with HCl and a NaBH₄ solution containing NaOH were delivered at a constant flow rate with the aid of a two-channel peristaltic pump to a first T-piece. There, the reagents are mixed and the reaction starts. Then, the mixture was brought to the second T-piece where it is merged with an Ar flow. Finally, the generated gases and the residual reaction solution were passed to the GLS.

The volatile hydrides and the excess of H₂ were led into the plasma by the Ar flow after it has passed through concentrated H₂SO₄ in a flask to eliminate the moisture. The residual reaction

solution was pumped away with a further peristaltic pump maintaining a constant liquid volume inside the GLS.

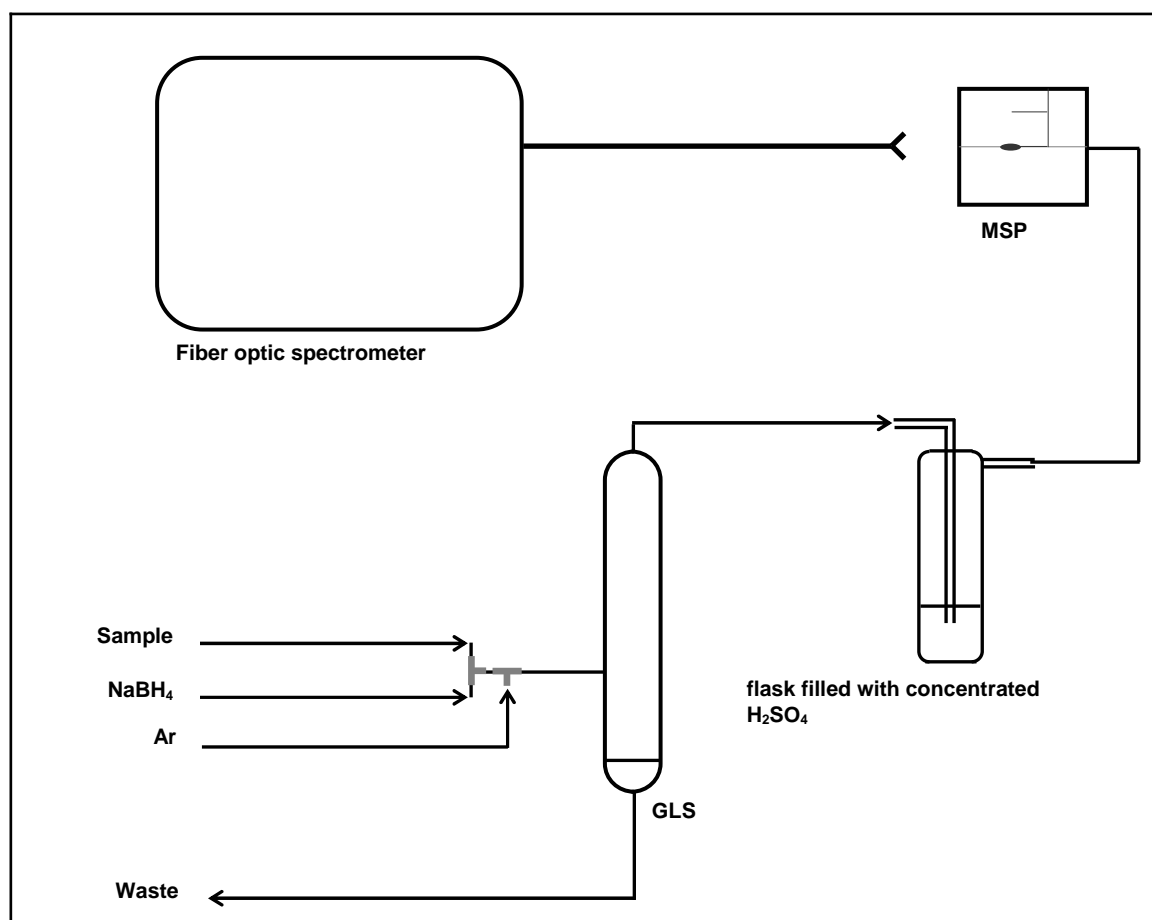


Fig. 19 Continuous hydride generation system for As and Sb combined to CF-HG-MSP-OES.

2.3.3 Cold vapour generation using SnCl₂ and NaBH₄ as reductands for the determination of Hg

For the continuous flow cold vapour generation of Hg, reducing agent solutions containing either NaBH₄ in NaOH or SnCl₂·2H₂O in HCl can be used, and in both cases the analyte solutions containing HCl and the reagents were pumped in parallel by a two-channel peristaltic pump. The solutions were mixed in the T-piece where the reaction starts and then provided with an Ar flow in a second T-piece. The resulting reaction mixture was brought into a small 10 mL cylindrical gas-liquid phase separator (GLS). For an optimum separation of the gases and the reaction liquid residue, the Ar flow is mixed with the reaction mixture before its introduction into the GLS. Before entering the MSP, the released vapours of Hg and

other reaction by-products in Ar were dried by passing them through a vessel containing concentrated H_2SO_4 . The whole experimental setup for the cold vapour generation system is shown in Fig. 20.

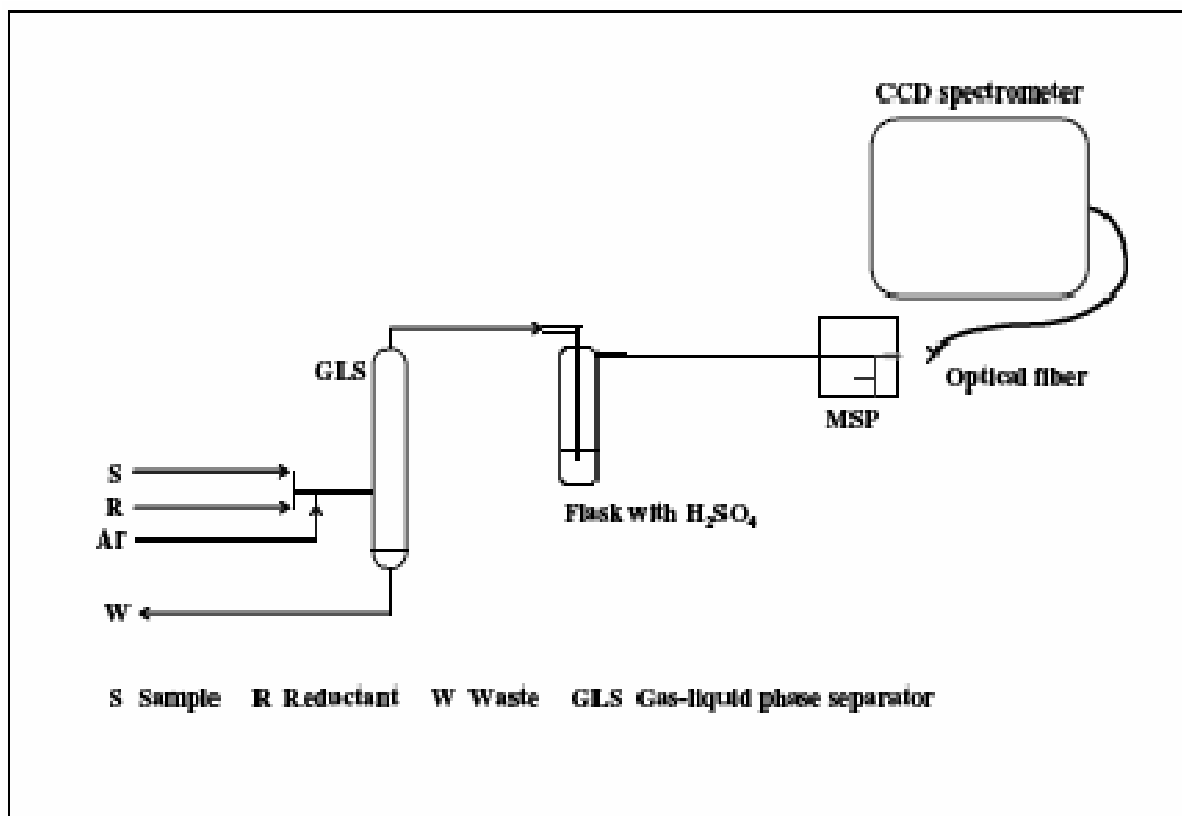


Fig. 20 Hg cold vapour generation system using SnCl_2 and NaBH_4 as reductands, to be coupled with MSP-OES.

2.3.4 Miniaturized chemical and electrochemical hydride generation system for the determination of As and Sb

In a miniaturized chemical hydride generation manifold an alkaline solution of NaBH_4 and a solution containing As and Sb acidified with HCl were delivered by means of a two-channel peristaltic pump to a T-piece where the HG reaction was initiated. The reaction mixture was then passed to a 6-ml gas-liquid phase separator (GLS) to separate the gaseous products of the HG reaction from the solution and to sweep the hydrides and H_2 by an Ar stream introduced at the bottom of the GLS out of the solution. Before entering the MSP, the Ar flow loaded with the volatile hydrides and the co-generated H_2 was passed through a 10-ml flask filled with concentrated H_2SO_4 to remove accompanying water moisture. The reaction residual

solution was instantly pumped away from the GLS by means of a second peristaltic pump (Fig. 21).

For ECHG a miniaturized electrolysis cell comparable to that formerly described by Bings *et al.* [145] was used. The internal volume of the anode and the cathode compartments in the cell used in the present study, however, was smaller (each about 0.2 ml). The compartments were separated by a Nafion cation exchange membrane. A Pt rod (45 mm of length and 1.5 mm in diameter) served as anode, while a carbon fiber bundle was used as cathode. For the HG an anolyte solution of H_2SO_4 and a catholyte solution containing in addition As and Sb were delivered to the respective compartments by means of a two-channel peristaltic pump. When applying a constant voltage to the electrodes the hydrides and H_2 were formed in the cathode compartment while in the anode compartment O_2 was produced. The catholyte reaction mixture containing H_2SO_4 , the hydrides and H_2 were introduced from the cathode compartment to the GLS. The separated gaseous reaction products were then carried with a flow of Ar to the MSP as in the case of CHG (Fig. 21).

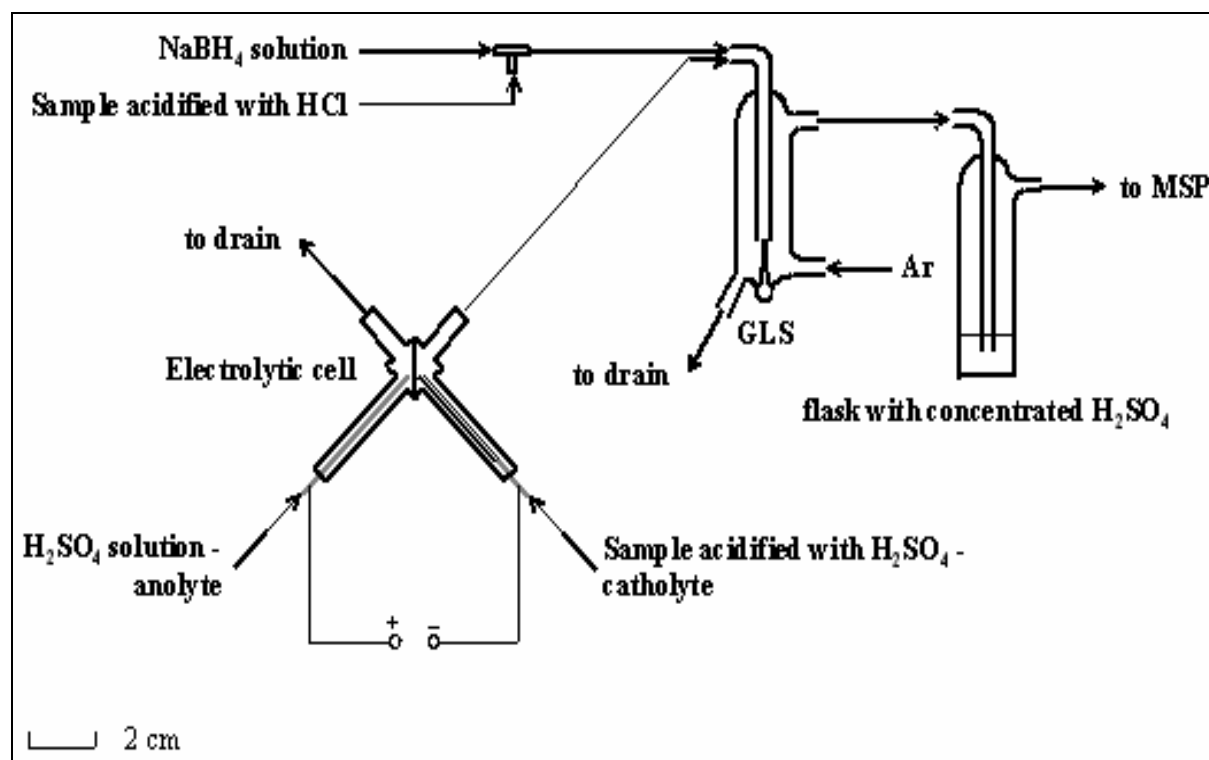


Fig. 21 Miniaturized CHG and ECHG systems for the determination of As and Sb by MSP-OES.

2.3.5 Continuous gaseous species introduction system for other non-metals

For the continuous flow generation of Br_2 and Cl_2 , a sample solution acidified with H_2SO_4 and containing Br^- or Cl^- was brought together with a solution of KMnO_4 at the same flow rate with the aid of a two-channel peristaltic pump. In a T-piece, the flows are mixed and the reaction takes place. The resulting reaction mixture is then passed through a 2.5-ml reaction coil and pumped into a frit-based gas-liquid phase separator (GLS). For an optimum separation efficiency of the gaseous halogens from the solution, the GLS was filled with glass beads and a He flow was introduced into the GLS *via* the glass frit so that it bubbles through the solution and smoothly sweeps the Br_2 and Cl_2 released in the oxidation reaction out of the solution. The reaction solution waste was removed from the GLS by another peristaltic pump. Before entering the MSP, the flow of He loaded with halogens was passed through a flask containing concentrated H_2SO_4 in order to remove the water moisture. The gas-phase sample introduction system is schematically shown in Fig. 22. The same device was also used for the CF generation of H_2S . Here, the gaseous H_2S was produced by acidification of a sample solution containing S^{2-} with HCl .

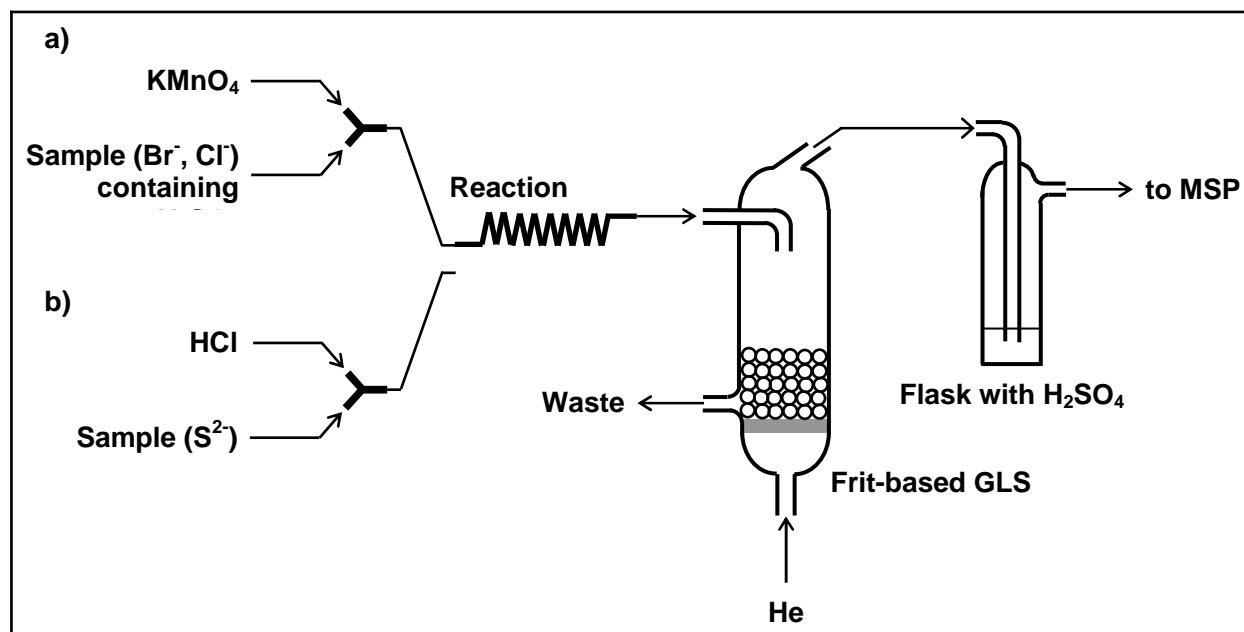


Fig. 22 Continuous flow system for the generation of non-metals (Cl , Br) (a) and non-metal volatile species (S) (b).

D. Practical Part

The present work focuses on the determination of Hg, As, Sb and non-metals like Cl, Br and S by a continuous flow vapour generation by reduction and oxidation reactions, respectively, coupled to optical emission spectrometry with two miniaturized microstrip plasma sources (MSP-OES) using a miniaturized spectrometer. One of the main aims of this research was to improve the cost/performance ratio and to offer solutions to challenging tasks in the environmental and the life sciences. Here, miniaturization of plasma discharge devices for elemental spectrochemical analysis has been a main goal so as to provide their use as element detectors. In this work, microstrip microwave plasmas are used because of their chance to be portable enabling in-situ analysis as well as less use of expensive reagents and a low consumption of working gas. Cold vapour generation techniques using SnCl_2 and NaBH_4 as reductant are considered for the determination of Hg, in combination with both MSP-OES systems. As and Sb have been determined under the use of chemical and electrochemical hydride generation in the present work, because of better figures of merit and the possibility to avoid the use of expensive reagents. Also the determination of non-metals using He plasmas has been studied.

In the first part of the present work a comparative study of the properties and the influence of plasma parameters like gas flow rate and microwave forward power on the excitation temperature, on the electron number density, on the background corrected signals for the Hg I 253.6 nm line and on the signal-to-background ratio (SBR) in the case of He and Ar as working gases for the MSP has been performed. Also an optimization of the analytical parameters in the determination of Hg using the cold vapour technique was done. Further, the use of hydride generation for the determination of As and Sb and the influence of the excess of H_2 on the plasma properties has been investigated. Here, the concentrations of the reagents as well as the flow rates of gas and reagent for an optimal production, transport and introduction of the hydrides into the MSP source were studied.

In the second part of the work, a comparative study of the use of SnCl_2 and NaBH_4 in the determination of Hg by the cold vapour technique was carried out. Here, an optimization of the concentrations of stabilizing substances as well as of the reducing agent and of the acidity of the sample and of the Ar and reagent flow rates were done. Also, a comparison of the possibilities of chemical and ECHG for the determination of As and Sb was included. This

necessitated on optimization of the parameters and a detailed determination of their respective figures of merit as well as a study of the interferences by transition metals and hydride forming elements in chemical and electrochemical hydride generation. For validation purposes NIST standard reference materials (domestic sludge and coal fly ash) were dissolved with the aid of microwave-assisted digestion and together with real samples analyzed.

As a last part of the work the determination of non-metals such as S, Cl, and Br through the use of oxidizing reagents at very strong acidic conditions was studied.

3.1 Experimental conditions

3.1.1 Preparation of stock sample solutions

Fresh stock and calibration solutions were daily prepared for the respective analyses. Stock solutions of Hg(II) for cold vapour generation were prepared with HCl, HNO₃ and H₂SO₄. Bidistilled water was used throughout to dilute the stock solutions. HCl was found to be the optimal stabilizing acid for the case of Hg cold vapour generation. The solution of SnCl₂ was prepared by dissolution of SnCl₂·H₂O in concentrated HCl and diluting with water according to Ref. [146]. In order to study interferences in the case of the cold vapour generation technique, synthetic sample solutions of Hg containing different concentrations of NaCl were prepared by the dissolution of suitable amounts of NaCl in water. These solutions were spiked with Hg and acidified with concentrated HCl and finally diluted with water. In a similar way, a multi-element matrix ICP standard IV solution containing Ag, Al, B, Ba, Bi, Ca, Cd, Co, Cr, Cu, Fe, Ga, In, K, Li, Mg, Mn, Na, Ni, Pb, Sr, Tl and Zn, spiked with Hg was also prepared.

For hydride generation, sample preparation was performed in the same way with bidistilled water. The NaBH₄ solution was prepared daily by dissolving NaBH₄ powder in a solution of NaOH for stabilization. Standard solutions containing both As(V) and Sb(III) were prepared by diluting the respective single-element stock standard solutions. The resulting solutions were acidified with concentrated HCl, HNO₃ or H₂SO₄. HCl was found to be the optimal acid for sample preparation. In order to evaluate the interferences of different elements, standard solutions of the individual elements Cd(II), Co(II), Cr(III), Cu(II), Fe(III), Mn(II), Ni(II), Pb(II) and Zn(II) were added to the solutions of As and Sb and the resulting solutions were acidified with HCl. A synthetic sample solution containing 2 µg ml⁻¹ of As and Sb and the

metals Cr^{3+} ($1 \mu\text{g ml}^{-1}$), Cu^{2+} ($0.6 \mu\text{g ml}^{-1}$), Fe^{3+} ($56 \mu\text{g ml}^{-1}$), Mn^{2+} ($0.9 \mu\text{g ml}^{-1}$), Ni^{2+} ($0.6 \mu\text{g ml}^{-1}$), Pb^{2+} ($0.4 \mu\text{g ml}^{-1}$) and Zn^{2+} ($1 \mu\text{g ml}^{-1}$) was prepared. The concentrations mentioned for the heavy metals corresponded to the composition of the sample solution obtained from 1 g NIST coal fly ash standard reference material (SRM 1633a), when dissolved in 200 ml. Solutions of NaI, KCN and L-ascorbic acid as well as L-cysteine were prepared from the respective solids to mask the interfering metal ions. These solutions were added to the sample solutions or to the NaBH_4 solution.

Samples of Hg acidified with HCl were also prepared for the cold vapour technique using SnCl_2 and NaBH_4 as described before. In order to study the chemical interferences in the cold vapour generation procedure, solutions of Hg containing Cd(II), Co(II), Cu(II), Fe(III), Ni(II), Zn(II), or the hydride forming elements As(V), Bi(III), Sb(III) or Se(IV) individually were prepared, acidified with HCl and then diluted with bidistilled water.

For ECHG standard solutions with As and Sb were prepared by diluting stock solutions of As(III) and Sb(III) with a solution of H_2SO_4 . HCl was not used, as it generates Cl_2 when passing through the cell, which can reach the plasma and change its properties with respect to the determination of As and Sb. HNO_3 was avoided because it causes depolarization of the cell. To study the interferences caused by Bi(III), Cd(II), Co(II), Cr(III), Cu(II), Fe(III), Hg(II), Ni(II), Pb(II), Se(IV), Te(IV) and Zn(II), with ECHG of As and Sb different amounts of individual standard solutions of these elements were added to stock solutions of As and Sb and diluted to the appropriate concentrations with a solution of H_2SO_4 in de-ionized water. All stock and calibration solutions were prepared on a daily basis.

For the determination of the non-metals, He was used as working gas. Stock solutions of Br^- , Cl^- and S^{2-} were prepared by dissolving NaBr, NaCl and Na_2S , respectively, in bidistilled water. Working standard solutions of Br^- and Cl^- were obtained by diluting the Br^- and Cl^- stock solutions with solutions of H_2SO_4 of the suitable concentrations. Working standard solutions of S^{2-} were prepared by diluting the S^{2-} stock solution in bidistilled water. For continuous flow oxidation of Br^- and Cl^- a solution of KMnO_4 in acid was used. H_2S was generated by mixing the S^{2-} solution with HCl.

3.1.2 Water and galvanic bath solution samples

As domestic water, tap water was taken from different points in the city of Hamburg. Furtheron, natural waters from the Elbe River and the Alster Lake were collected with 0.5 L pre-cleaned polyethylene bottles. After sampling, these water samples were acidified with concentrated HCl to a pH value of 2 and spiked with Hg. Prior to analysis 50-mL portions of the spiked water samples were acidified with concentrated HCl and their volumes brought up to 100 mL with bidistilled water.

A galvanic bath solution containing NaH_2PO_2 , carbonates and NiSO_4 at concentrations below 2.5 % (m/v) made available through Atotech (Berlin, Germany) was also analyzed. Prior to analysis, this solution was diluted 25 times and HCl was added until its concentration amounted to 3 mol l^{-1} . Sb was expected to be present in the galvanic bath sample as inorganic Sb(III). As originally was not present in this sample. We spiked it with As(V) up to a concentration of $45 \mu\text{g ml}^{-1}$. To minimize interferences from the components of the sample in the determination of Sb and As calibration by standard addition with solutions containing Sb(III) and As(V), respectively, was applied.

3.1.3 Microwave-assisted digestion of standard reference materials

To verify the accuracy of the developed procedures for the determination of Hg, As and Sb NIST SRMs were analyzed.

For the determination of Hg a domestic sludge standard reference material (NIST SRM 2781) was analyzed. It was decomposed under the use of microwave assisted digestion as described in Ref. [147]. Therefore, a portion of the material was dried for 2 h in an oven at $110 \text{ }^\circ\text{C}$. Then, 0.25 g samples were weighted into the decomposition vessels and 5.0 mL of suprapure concentrated HNO_3 as well as 5.0 mL of suprapure concentrated H_2SO_4 were added. A two stage microwave assisted digestion was applied: the 1st stage has a duration of 5 min at a power of 300 W (35 bar, $40 \text{ }^\circ\text{C}$) and the 2nd stage has a duration of 40 min at a power of 300 W (35 bar, $190 \text{ }^\circ\text{C}$). After completion of the digestion, the nitrogen oxide fumes were removed by heating the vessels for about 20 min on a hot plate. After cooling the contents of the vessels were quantitatively transferred to 50 mL calibrated flasks and latter filled up with water. In the solutions of the digested reference material Hg was determined with the aid of

the cold vapour generation technique using SnCl_2 and NaBH_4 as reducing agents and applying three standard additions.

Further, As and Sb were determined in a NIST coal fly ash standard reference material (SRM 1633a) after digestion in the microwave system MARS 5 (CEM Corporation, USA) equipped with a set of high pressure HP-500 Plus PTFE vessels. The digestion procedure applied was as previously described. Prior to analysis the digestion solutions were filtered through Whatman 42 paper filters and As was determined by hydride generation under the use of 2 standard additions.

3.1.4. Measurement of the amount of H_2 produced in the continuous CHG and ECHG

The amount of H_2 produced during CHG and ECHG, respectively, was measured under the assumption the predominant constituent of the gaseous mixture formed is H_2 . For that purpose, the exit tube of the GLS was inserted in a volumetric cylinder filled with water. The cylinder was placed upside down in a large beaker filled with water. The CHG and ECHG were performed without entering Ar into the system and its inlet was closed. In this way H_2 pressed the water out of the cylinder and it was possible to measure the volume of H_2 generated during a certain time and under selected experimental conditions. The amount of H_2 liberated per minute was measured 3 times and the results given are the mean values and the standard deviation.

3.1.5. Determination of excitation temperatures and electron number densities

The excitation temperature (T_{exc}) was determined with the aid of Ar and He atom lines (Ar I, He I) assuming a Boltzmann distribution of the population of the excited atomic levels. The temperature was calculated from the slope of the $\log(I \lambda/A)$ versus E plot using the least-squares method. The uncertainty of the determination of T_{exc} was estimated to be 15 to 20% and calculated from the error of the slope. Seven atom lines for Ar (425.1, 425.9, 426.6, 427.2, 430.1, 433.4, and 434.5 nm) and five atom lines for He (402.6, 447.2, 471.3, 492.2, and 501.6 nm) were used to obtain the Boltzmann plots [148, 149]. The values of the upper-state energies and the transition probabilities for the Ar and He lines were taken from the literature [150, 151].

For the determination of the electron number density (n_e) the H_β 486.1 nm line was used. Its broadening was accepted to be mainly due to Stark broadening, from which n_e was calculated with the aid of the equations given by Griem [152]. The precision of the determinations of n_e for the case of three replicate measurements could be expected to be 3–5%.

3.1.6. Measurement of the hydride generation efficiencies

The efficiencies of the continuous flow chemical and electrochemical hydride generation for the case of As and Sb were measured by determining the concentrations of As and Sb in the waste solution of the reaction with the aid of ICP-OES using pneumatic nebulization. The calibration was done with matrix matched standard solutions of As and Sb. Graphite furnace AAS was also used for the determination of the hydride generation efficiency in the case of the respective elements. The analyses made use of two standard additions and Pd–Mg(NO₃)₂ was used as matrix modifier. The efficiencies are given as percentages from the added analyte concentration and calculated from the difference between the concentration added to the sample and the one found in waste solution.

3.2 Wavelength selection

Within the wavelength range of the miniaturized USB2000 Ocean Optics spectrometer (200–500 nm) the most sensitive lines for Hg, As, Sb, Cl, Br, S and C were selected and used throughout the work.

For cold vapour generation using SnCl₂ and NaBH₄ the analytical line Hg I 253.6 nm [74] was found to be the most sensitive one. Also other lines of Hg were observed such as Hg I 365.02 nm and Hg I 404.65 nm. However, they were much less intensive than the Hg I 253.65 nm line (0.036 and 0.02 versus 1.0 a. u. in the case of an Ar MSP and cold vapour generation).

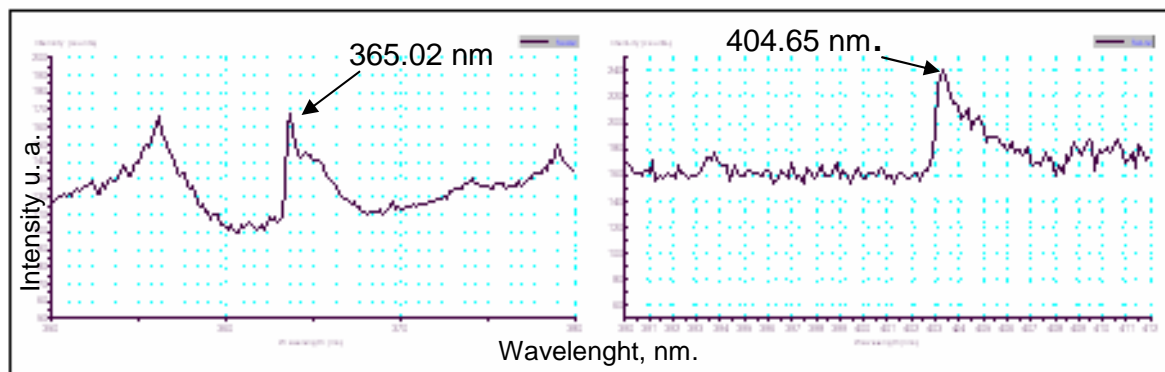


Fig. 23 Signals for the Hg I 365.02 and 404.65 nm lines for a solution containing 500 ng mL⁻¹ of Hg in 2 % HCl.

In the case of CHG and ECHG and both MSP discharges, the As I 228.8 nm and Sb I 252.8 nm lines have been found to be the most intensive ones. For the determination of non-metals, the most intensive analytical lines of the elements studied were Br II 478.5 nm, Cl I 439.0 nm and S I 469.4 nm.

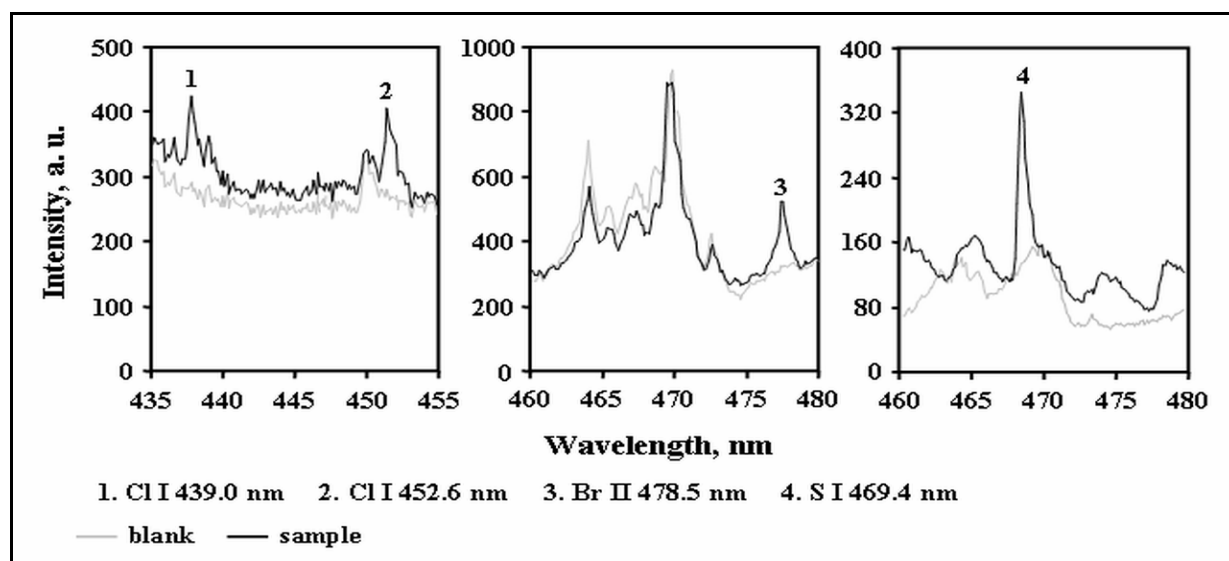


Fig. 24 Analytical lines for the determination of non-metals.

3.3 Preliminary investigations with an MSP type A using He as working gas

3.3.1 Dry He and Ar plasma and plasma loaded with water vapours

Dry He and Ar plasmas could be operated at a power between 35 and 40 W and with flow rates in the range of 5.7 to 450 ml min⁻¹. Under these conditions intensive discharges were observed inside the wafer.

Some experiments were done so as to critically evaluate the influence of some parameters on the properties of the He plasma. It was noticed that the introduction of water vapours to the He microstrip plasma resulted in a considerable decrease of the intensities of He I lines as compared to those observed when a “dry” plasma was used. The intensities of the He atom lines at 388.9, 447.1 and 501.6 nm for the plasma loaded with water vapours were 74, 75 and 70 %, respectively, of those for the “dry” He plasma (Fig. 25).

In addition, the influence of the gas flow rate on the intensities of the atom lines of the discharge gas spectra in the range of 15 to 450 ml min⁻¹ was investigated. Here, the plasma was loaded with water vapour by introducing water into the Hg cold vapour generator instead of the reagents. It was found that the strongest decrease of the intensities of the He lines occurred at gas flows of 15 to 110 ml min⁻¹ (from 15 % for the He I 501.6 nm line to almost 44 % for the He I 388.9 nm line). The intensities of the mentioned lines steadily decreased to a flow rate of 250 ml min⁻¹, and then they again increase and had a local maximum at 300-350 ml min⁻¹, after which they again decreased. Such a behavior indicates that an increase of the plasma gas flow rate leads to a cooling of the discharge as a result of the relatively small dimensions of the plasma channel as well as of the microstrip plasma itself. On the other hand, for flow rates lower than 15 ml min⁻¹, the discharge was found to be unstable. A flow rate of 15 ml min⁻¹ finally was regarded as optimal.

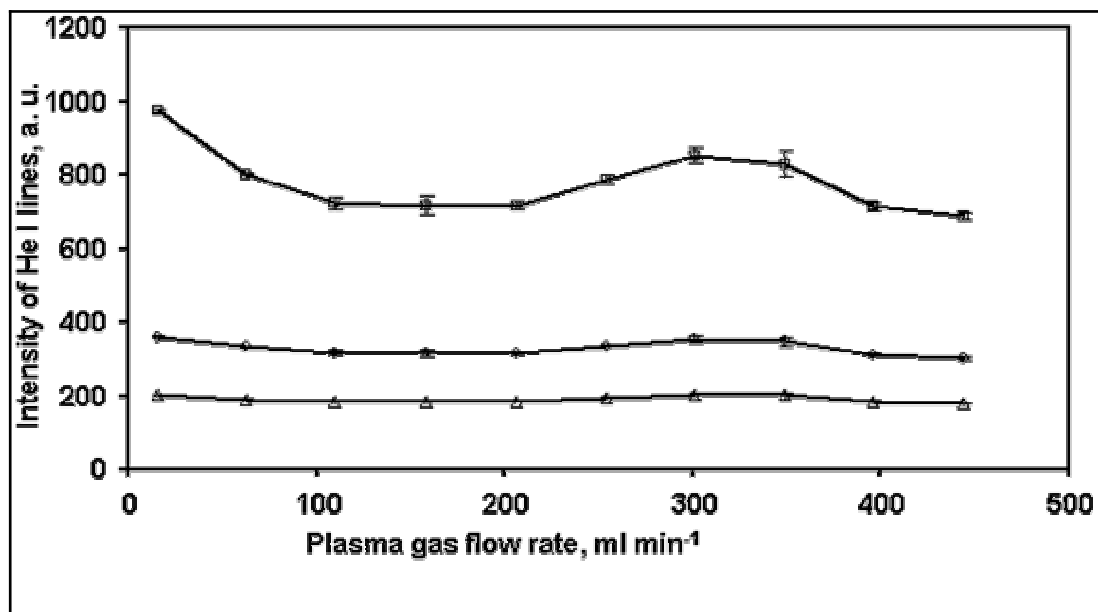


Fig. 25 Influence of the plasma gas flow rate on the intensities of the He I lines at 388.9 nm (□), 447.1 nm (○) and 501.6 nm (Δ) during the introduction of water vapours through the cold vapour generator at a power of 40 W.

3.3.2 Plasma loaded with Hg vapours generated by a gas flow passing over a drop of Hg

The Hg vapours were produced by conducting the working gas through a 10-ml flask containing a small drop of Hg with a weight of 0.3 g. The flow rate of the dry working gas was varied from 15 to 450 ml min⁻¹ and the intensities of the Hg I 253.7 nm line and the mentioned atom lines of the He were measured.

It was found that the highest response for Hg was obtained at the very low gas flow rate of 15 ml min⁻¹ or even lower, at 5.7 ml min⁻¹. When increasing the flow rate of the working gas from 15 to 300 ml min⁻¹, the suppression of the response for Hg was considerable and the intensity achieved at a flow rate of 300 ml min⁻¹ was respectively 3.4 or 2.8 times lower than at flow rates of 5.7 and 15 ml min⁻¹. At a gas flow rate of 300 to 450 ml min⁻¹, the intensity of the Hg line reached a plateau.

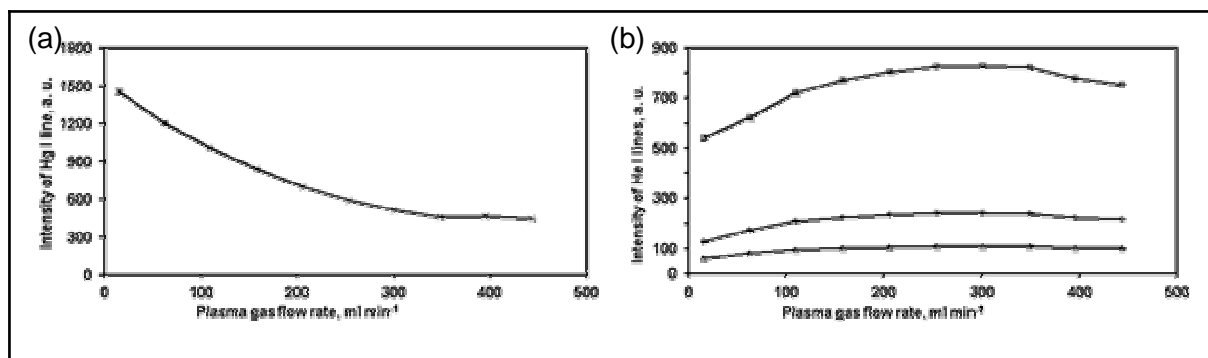


Fig. 26 Influence of the working gas flow rate on the intensity of the Hg I 253.7 nm line at 40 W during the introduction of Hg vapours obtained by conducting the gas through a flask containing a mercury drop (a) and of the working gas flow rate on the intensities of the He I lines at 388.9 nm (□), 447.1 nm (○) and 501.6 nm (Δ) (b).

3.3.3 Introduction of Hg by the cold vapour technique

The influence of the working gas flow rate during the introduction of Hg released by the cold vapour technique on the intensity of the Hg I 253.7 nm line and the He atom lines (He I 388.9 nm, He I 447.1 nm, He I 501.6 nm) was investigated with the following measurement conditions: forward power: 40 W, sample and reductant uptake rates: 1.0 ml min⁻¹ using the system described in Fig. 18, and the He working gas flow rate was varied in the range from 15 to 300 ml min⁻¹.

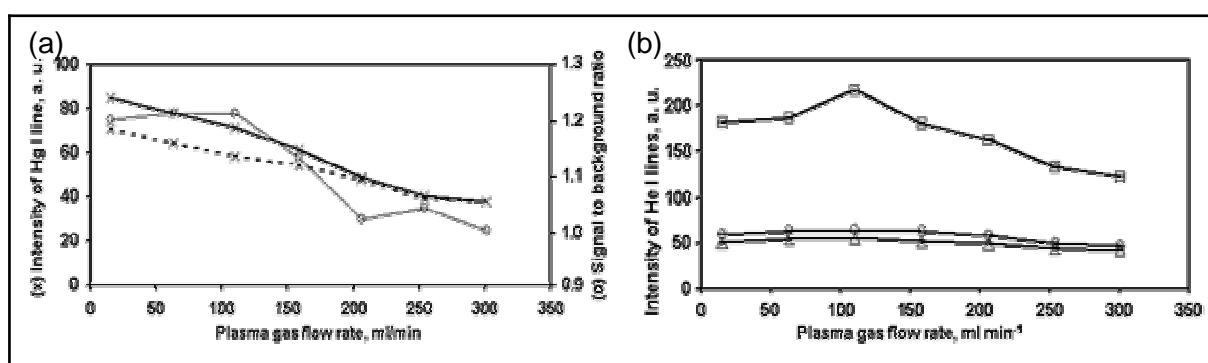


Fig. 27 Influence of the working gas flow rate on the intensity of the Hg I 253.7 nm line (—), on the intensity of the spectral background (---) and on the signal-to-background ratio (—) (a) and influence of the working gas flow rate on the intensities of the He I lines: 388.9 nm (□), 447.1 nm (○) and 501.6 nm (Δ) (b).

It could be observed that the maximum response for the Hg released by the cold vapour technique as shown by the Hg line intensity and the signal-to-background ratio was achieved at a working gas flow rate of 15 ml min^{-1} . For higher flow rates of the working gas, the analytical signals were much lower, probably due to the short residence time of the analyte in the plasma channel and to the cooling of the plasma under these conditions.

The intensities of the most intensive He atom lines observed were increasing with the He gas flow rate up to 110 ml min^{-1} , and then a gradual decrease of the He line intensities was noticed.

3.4 Evaluation and application of Ar and He microstrip plasma (type A) combined to the cold vapour technique for the determination of Hg by OES

An optimization was based on the previous studies, which showed that it was possible to introduce Hg vapours generated by the cold vapour technique using SnCl_2 as reductant in an MSP system as described in Fig. 18. A comparative evaluation of the properties of the Ar and the He MSP for the excitation of Hg when the vapour produced by the cold vapour generation technique is introduced into the discharge was made as well. Further, the effect of the microwave forward power and the Ar/He flow rate on the T_{exc} as determined with Ar I and He I lines and the n_e was measured. In addition, the influence of the power and the gas flow on the background corrected net intensity for Hg I 253.6 nm and the SBR was studied. Therefore, the net analyte signals obtained under different conditions were measured and divided by the highest value in the measurement series to obtain the relative intensities. As it was determined previously, the optimum gas flow rate was 15 mL min^{-1} . The analytical figures of merit for He and Ar plasmas were compared in terms of the limits of detection, the linearity ranges and the precision of the measurements. Furthermore, as analytical applications of the CV Ar MSP the determination of Hg in domestic and natural water samples as well as in a domestic sludge sample will be presented.

3.4.1 Area of plasma stability

The stability areas for the Ar and the He plasmas loaded with Hg vapour were determined in terms of the forward microwave power and the flow rates of the discharge gases. Both the Ar

and the He plasmas sustained inside the microstrip structure were found to be highly stable and reproducible. The Ar MSP was found to be stable at relatively low microwave power values as compared to the plasma generated in the same structure with He as discharge gas, especially at low gas flow rates. Also the minimum power required to ignite the Ar MSP plasma was found to be up to 20% (31.5 W) lower than the minimum power required to ignite the He MSP (38.5 W) at the respective gas flow rate (Ar and He: 15 ml min⁻¹). Such a difference could be explained and attributed to the differences in the thermal conductivity and in the specific heat of both gases [153]. Furthermore, it also could be expected that as a result of the higher thermal conductivity of He, the He MSP would consume more energy than the respective Ar MSP and therefore would require a relatively high forward power as compared to the Ar MSP. A similar effect was formerly observed with different microwave plasma structures coupled to chemical vapour generation techniques [68, 74, 153]. Also in the configuration of the discharges differences were observed. At an optimum gas flow rate of 15 mL min⁻¹ the Ar MSP was found to have the shape of a filament with a length between 3 and 9 mm depending on the forward power. At a forward power of 40 W, the filament was found to extend about 5 mm out of the microstrip line, while the remaining part of the plasma filament (about 4 mm) was under the strip line. When increasing the gas flow rate to 110 mL min⁻¹ a partial shift of the whole discharge into the gas channel was found to occur, and at a further increase of the Ar flow rate, an increase of the plasma size occurred [39]. When using He as the working gas, a so-called suspended type of microplasma was observed, which was located near the end of the strip line, similar as described in [77]. At a gas flow rate of 15 mL min⁻¹, the plasma length was found to be between 3 and 4 mm depending on the microwave power.

3.4.2 Effect of the microwave forward power and the working gas flow rate on the excitation temperature and the electron number density

Considering the stability areas of both MSPs, the effect of the microwave forward power on the T_{exc} , the n_e , the relative intensities of the Hg 253.6 nm line and the SBRs was investigated at a forward power of 35 to 40 W for Ar and of 38.5 to 40 W for He, respectively. Both plasmas were operated at a gas flow rate of 15 mL min⁻¹ and continuously fed with Hg released in the Hg cold vapour system (Fig. 18) in the case of a concentration of 40 ng mL⁻¹ of Hg in the solutions. The influence of the gas flow rate on the T_{exc} determined with Ar I and He I lines, on the n_e as well as on the relative intensities and the SBRs for the Hg I 253.6 nm

line was investigated between 15 and 400 mL min⁻¹ and for the same concentration of Hg. Both for Ar and He the MSPs were operated at the maximal forward power of 40 W.

Within the measurement error, the T_{exc} determined with Ar I lines was found to be constant (on average 5500 K) in the range of power investigated. This indicates that in the case of the Ar MSP most of the microwave power was consumed by an expansion of the plasma size [74] rather than by an increase of the excitation temperature. The power was found to have no remarkable effect on the n_e of the Ar MSP as the values of n_e measured when varying the power from 35 to 40 W remained within the range $1.4 \cdot 10^{14}$ to $1.6 \cdot 10^{14}$ cm⁻³ (see Fig. 29). For the He MSP, it could be observed that the T_{exc} measured with the He I lines changed with the forward power from 3200 K for 38.5 W to 4200 K for 40 W. Such a behavior shows that a relatively high part of the microwave power is consumed for the excitation of He atoms [72, 153]. The n_e in the He MSP, however, was found to remain practically unaffected by the microwave forward power and its value was found to be $1.1 \cdot 10^{14}$ - $1.2 \cdot 10^{14}$ cm⁻³ over the range of power investigated (from 38.5 to 40 W).

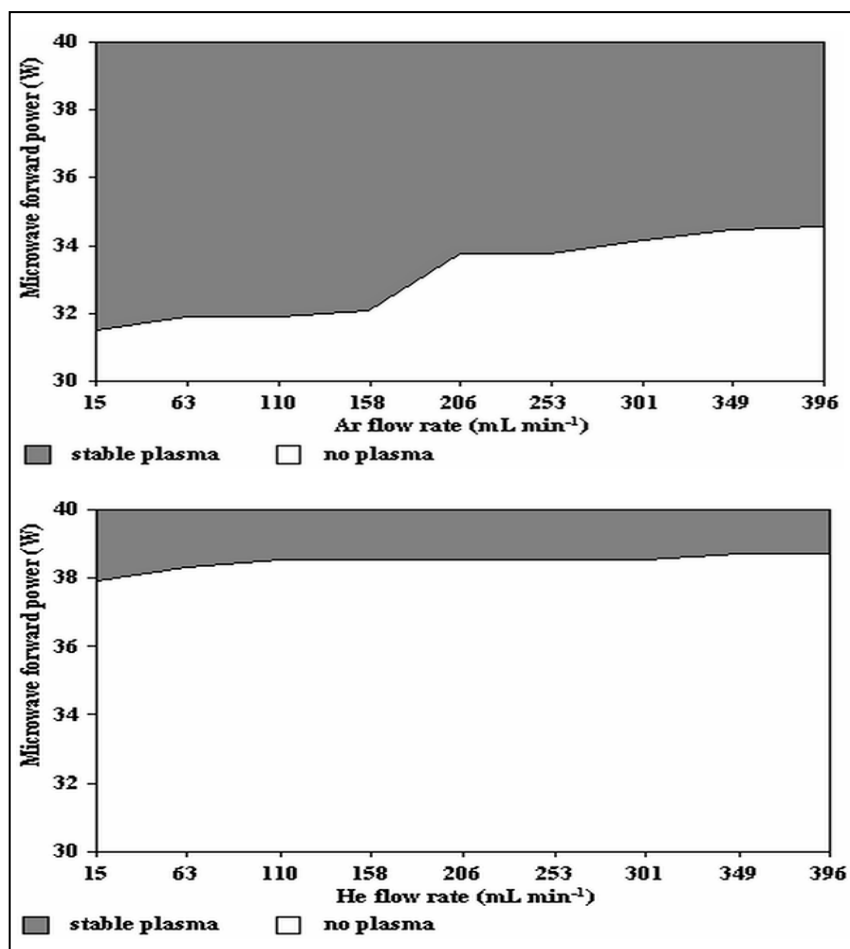


Fig. 28 Areas of stability for Ar and He MSP plasmas.

Within the errors of the temperature measurements, the flow rate of the working gas was found to have practically no effect on the T_{exc} in the Ar MSP. The average value of the T_{exc} as measured with Ar I lines in the investigated range of the gas flow rate was close to 5600 K (see Fig. 29). The intensities of the Ar atom lines at 415.5, 419.8, 433.5 nm first decrease with the gas flow. At a flow of 160 mL min^{-1} they were about 8 % on average lower than the intensities obtained at a gas flow rate of 15 mL min^{-1} . Then, they were found to steadily increase with the gas flow rate and at 400 mL min^{-1} they were about 15 to 30 % higher than at a flow rate of 15 mL min^{-1} . The values of the n_e were found to oscillate around a mean value of $1.5 \cdot 10^{14} \text{ cm}^{-3}$.

For the He MSP, an increase of the gas flow rate was found to result in a significant decrease of the T_{exc} as measured with He I lines and of the n_e . Indeed, changes from 4700 K and $1.2 \cdot 10^{14} \text{ cm}^{-3}$ for a He flow rate of 15 mL min^{-1} to 3300 K and $0.8 \cdot 10^{14} \text{ cm}^{-3}$ for a He flow rate of 400 mL min^{-1} could be observed. This behavior is in agreement with findings reported for other microwave helium plasmas [74, 154, 155] and presumably is the result of a de-activation of the excited He atoms by collisions with He ground-state atoms. Changes of T_{exc} and n_e found for the He MSP seem to correspond with those of the intensities of the atom lines of He.

3.4.3 Influence of the microwave forward power and the working gas flow rate on the relative net intensity of Hg I 253.6 nm and its SBR

For both MSPs investigated the relative intensities of the Hg I 253.6 nm line were found to increase with the forward power (see Fig. 29). In the case of the He MSP, this increase was found to be somewhat higher than the one found for the Ar MSP in the corresponding range of the power. The SBR determined in the case of the Ar MSP remained practically at 1.6. This is in compliance with the value of the T_{exc} determined with Ar I lines and the n_e at a varying forward power. It might be pointed out that the electron excitation might be balanced by the collisional excitation and recombination reactions [39]. Consequently, the increase of the intensity of the Hg line with the forward power will be compensated by the increase of the background emission intensity, as it was found to be the case.

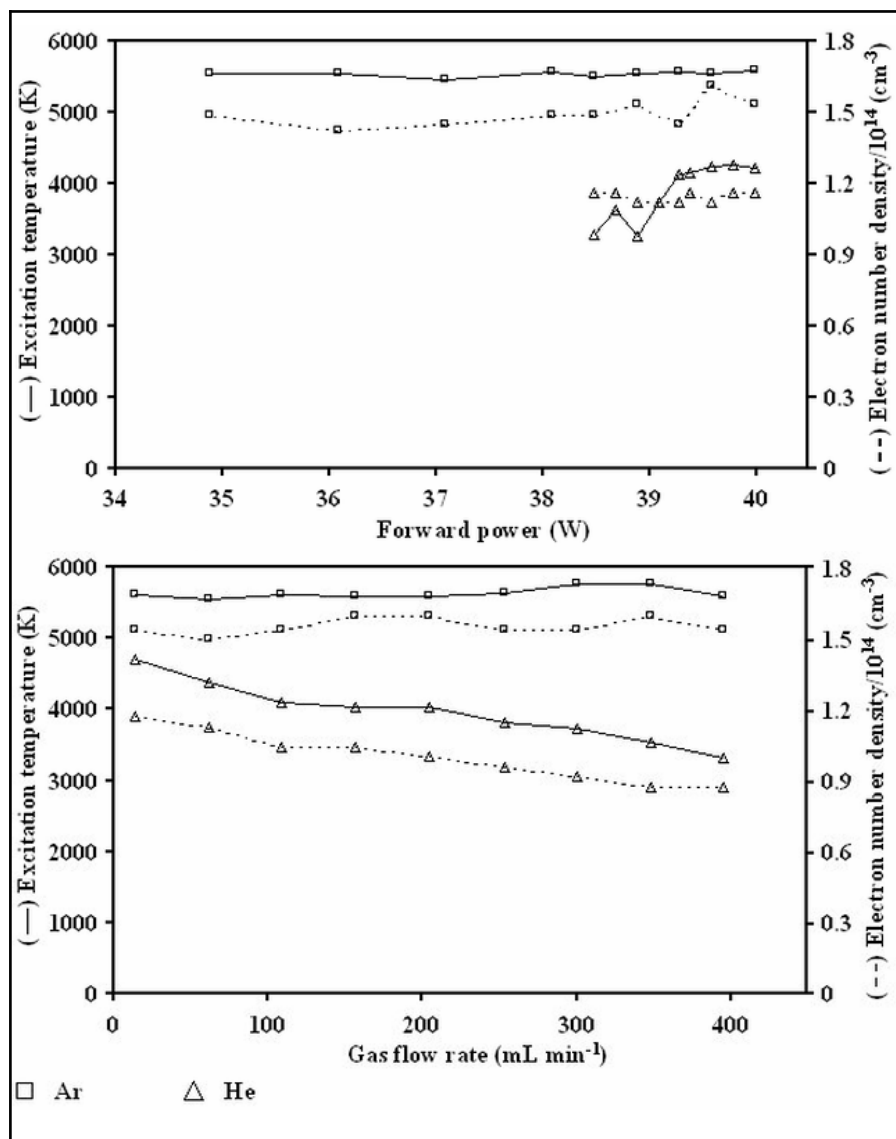


Fig. 29 Influence of the microwave forward power and the working gas flow rate on T_{exc} and n_e in Ar and He MSPs.

For a He MSP the SBR for the Hg I 253.6 nm line at increasing power was found to decrease. Referring to the increase of the T_{exc} as determined with He I lines with increasing power and an almost unchanged level of the n_e in the examined range of power, it was assumed that in this MSP, excitation by electrons and collisions with excited He atoms and/or metastable He species formed in the discharge might play a role in the excitation of Hg. It was difficult to elucidate, however, which of the mentioned processes is more significant under the conditions investigated [38, 139, 154, 156]. In view of the relatively low forward power used, it could be expected that an increase of the power probably results in a domination of the collisional excitation and an intensification of the recombination processes, leading to a higher increase of the spectral background.

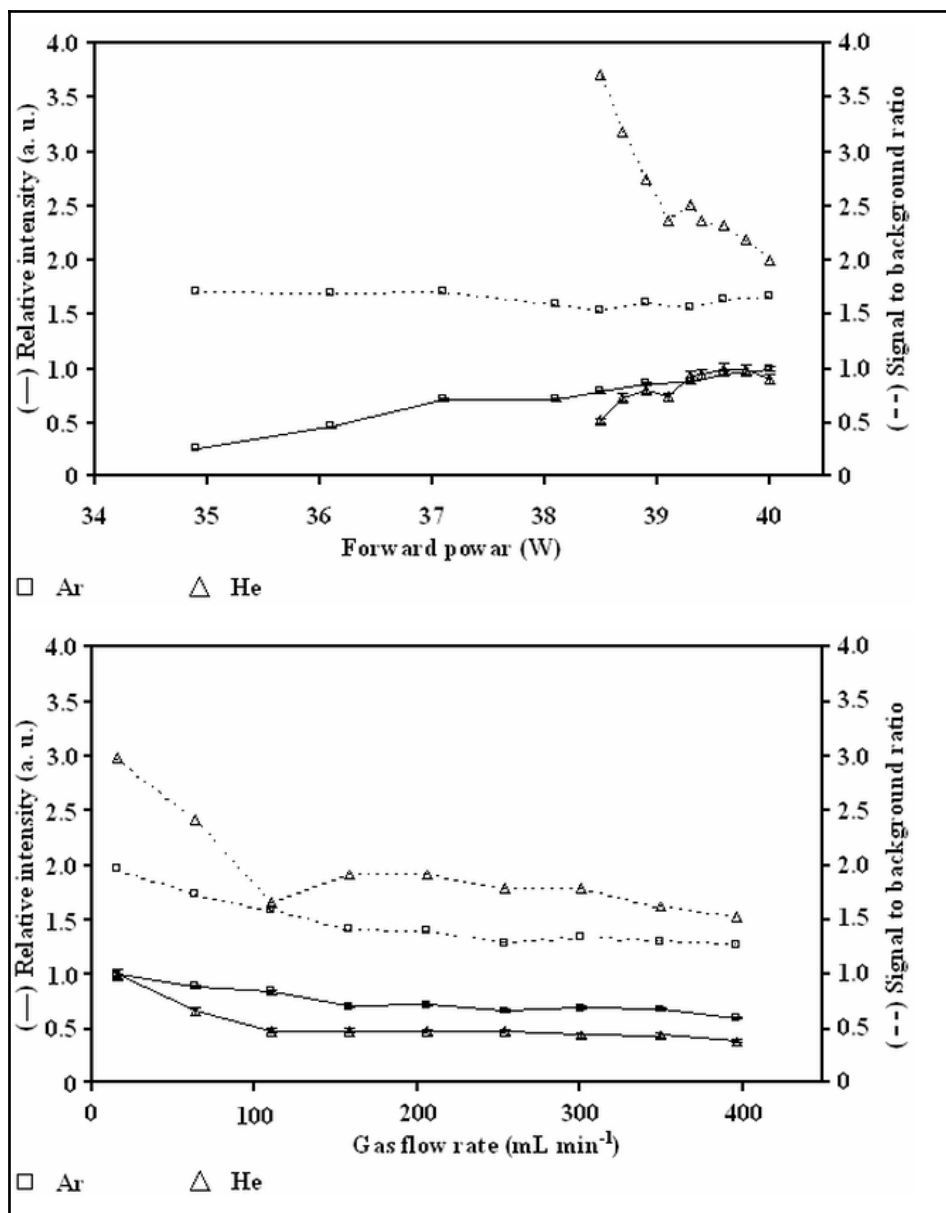


Fig. 30 Influence of the microwave forward power and the gas flow rate on the Hg I 253.6 nm line intensities and its SBR.

For both MSPs studied, a decrease of the relative intensities and the SBRs with the working gas flow rate was found to occur (see Fig. 30). Considering the dependence of the T_{exc} as measured with Ar I lines and the n_e on the gas flow rate for the case of the Ar MSP, it was suspected that the decrease of the intensity of the Hg line by about 40 % on the whole was associated with the short residence time of the analyte in the plasma.

The decrease of the Hg line intensity with the working gas flow rate for the case of the He MSP was found to be considerably higher, namely 60 % on average, than that observed for the case of the Ar MSP. It could be possible that apart from the decrease of the residence time

of the analyte in the small-volume He MSP the “cooling” of the plasma by the de-excitation process has an additional effect on the excitation of Hg and consequently on the analytical response for that element. The results for the SBRs well corresponded with those for the relative intensities of the Hg line, which also decreased at an increase of the working gas flow rate for both MSPs.

3.4.4 Analytical performance

Under the optimum conditions, namely a working gas flow rate of 15 mL min^{-1} and a forward power of 40 W, the sensitivity, the detection limit and the measurement precision at different concentrations of Hg were assessed as analytical figures of merit for the Ar and He MSPs coupled with the CV generation technique. For the determination of Hg by the cold vapour generation technique a linear calibration curve was obtained with a correlation coefficient of 0.9988 for standard solutions with concentrations between 2.5 and 300 ng mL^{-1} . The detection limit based on the $3\sigma_{\text{blank}}$ criterion was found to be 0.64 ng mL^{-1} and is comparable to that reported lately for the CV MIP-OES using a microwave plasma torch [74]. It is some higher than the value of 0.05 ng mL^{-1} , reported by Engel *et al.* [78]. This may be due to the poorer resolution of the spectrometer used for our measurements. The measurement precision, expressed by the relative standard deviation (RSD) for 3 replicates, at low concentrations of Hg, i.e. from 5 to 20 ng mL^{-1} , varied from 3 to 9 %. For the higher analyte concentrations, i.e., from 40 to 300 ng mL^{-1} , the RSD values were between 2 and 0.7 %. Due to the higher microwave power required for the analyte excitation in the He MSP, this plasma showed a lower analytical performance for the determination of Hg. The linear dynamic range extended only to 100 ng mL^{-1} and a poorer limit of detection 1.1 ng mL^{-1} was found. For that reason, the Ar MSP was used for the determination of Hg in the further measurements.

3.4.5 Interferences

A series of artificial water samples containing Hg and different amounts of NaCl were analyzed using a calibration with pure aqueous solutions containing only Hg so as to establish the influence of major sea, saline and waste water concomitants on the determination of Hg [144]. In addition, the solutions containing the multielement matrix were also analyzed with the Ar MSP (see Table 3). None of the interfering ions present in those samples obviously reached the plasma. Therefore, the interferences found must occur during the Hg CV

generation and the separation process. In the case of the higher concentration of Hg, it could be observed that the presence of NaCl at a concentration of 1, 2, 4 and 6 % (m/v), respectively, could be tolerated as the recoveries for Hg found were still between 92 and 104 %. For a lower concentration of Hg, the recoveries in the presence of a high content of NaCl in the solution were found to decrease. Also, it was found that the presence of the elements Ag, Al, B, Ba, Bi, Ca, Cd, Co, Cr, Cu, Fe, Ga, In, K, Li, Mg, Mn, Na, Ni, Pb, Sr, Tl and Zn of the multielement solution ICP Standard IV at a concentration higher than 50 ng mL⁻¹ has a negative effect on the recovery in the determination of Hg.

Table 3. NaCl and multielement matrix

Sample	Added (ng mL ⁻¹)	Found (ng mL ⁻¹)	Recovery (%)
Water containing NaCl matrix			
1 % (m/v)	100	91.6±2.2	91.6±2.2
2 % (m/v)	100	94.7±1.5	94.7±1.5
4 % (m/v)	100	106±4	106±4
6 % (m/v)	100	94.7±1.8	94.7±1.8
1 % (m/v)	50.0	54.6±4.5	109±9
2 % (m/v)	50.0	47.2±4.3	94.3±8.5
4 % (m/v)	50.0	40.0±3.1	80.0±6.2
6 % (m/v)	50.0	31.2±3.1	62.3±6.3
Water containing multi-element matrix^a			
50 ng mL ⁻¹	25.0	25.0±1.8	100±1
100 ng mL ⁻¹	25.0	22.7±0.8	90.8±3.4
250 ng mL ⁻¹	25.0	19.2±2.2	76.9±8.9

Results are mean values ($n=3$) and numbers behind \pm are the standard deviations

^a Multi-element ICP Standard IV

3.4.6 Analysis of real samples and standard reference material 2781

As application of the cold vapour generation coupled to MSP-OES the analysis of real samples and NIST SRM 2781 was carried out. Due to the absence of Hg in the samples of domestic and natural waters, the latter were spiked with different concentrations of Hg. The domestic sludge standard reference material was decomposed according to the procedure described in the section 3.1.3 using the microwave-assisted digestion technique and Hg was

determined in the solutions under the use of the cold vapour generation technique with SnCl_2 as reductant. Three standard additions were made and very good recoveries were obtained, which testifies the reliability and the accuracy of the method developed (Table 4).

Table 4. Real sample and standard reference material.

Sample	Added (ng mL^{-1})	Found (ng mL^{-1})	Recovery (%)
Domestic water 1	100	101±1	101±1
Domestic water 2	30.0	30.3±3.0	101±10
Alster lake 1	50.0	48.3±2.0	96.6±4.0
Alster lake 2	20.0	19.1±1.0	95.5±5.0
NIST SRM 2781	3.64±0.25 ^a	3.80±0.15 ^b	104±4

Results are mean values ($n=3$) and figures behind \pm are the standard deviations

^a Certified value (in $\mu\text{g g}^{-1}$)

^b In $\mu\text{g g}^{-1}$

3.5 Simultaneous determination of As and Sb by continuous flow chemical hydride generation and a miniaturized microwave microstrip argon plasma operated inside a capillary channel (type A)

A continuous flow-hydride generation reaction was coupled to an MSP type A, and the mixing of the reagents, the separation of the by-products and the transport of the analytes to the microplasma source optimized. The role of the following experimental conditions for the system described in Fig. 19 was investigated: the concentration of NaBH_4 , the sample acidity resulting from the addition of HCl , HNO_3 or H_2SO_4 , the Ar working gas flow rate, and the flow rate of the sample/reductant solutions. Their influence on the background corrected net line intensities and the signal-to-background intensity ratios (SBR) for As I 228.8 nm and Sb I 252.8 nm was examined under the use of a univariant approach and the results expressed as the relative net intensities by referring to the highest value in a given measurement series. The results referred to as the relative net intensities and the SBRs were the average values obtained from 3 replicate measurements with the precision expressed by the standard deviation calculated according to the law of error propagation. The influence of the NaBH_4 concentration and the Ar flow rate on the excitation temperature (T_{exc}), as measured with Ar atom lines, and the electron number density (n_e) were evaluated. The figures of merit of the HG-MSP system were also investigated and compared with those of other microplasma sources. The individual interferences of the transition metals were also studied. A metal

solution with element concentrations similar to NIST 1663a under the use of masking agent was analyzed with the aim to study the interferences connected with real sample matrices. A galvanic bath sample and a NIST SRM 1633a coal fly ash were analyzed with the procedure developed.

3.5.1 Optimization

3.5.1.1 Influence of the NaBH₄ concentration

The concentration of NaBH₄ has been recognized as one of the most critical variables in HG. It has an influence on the reaction efficiency in the liquid phase and through the amount of H₂ produced and entered into the plasma on the spectroscopic parameters of the MIP discharge. Typically, the optimum concentrations of NaBH₄ with respect to the analytical performance for volatile hydride-forming elements are close to 1 % [157-159]. Lower and higher values, from 0.5 to 5 % [160], however, also have been used depending on the respective HG manifold and the types of MIP discharge [161-165].

Considering the formerly reported features of the Ar MSP [78, 79], variations of the NaBH₄ concentrations in the range from 0.1 to 0.5 % (m/v) could be studied. It was found that the relative net intensity of the As line increases with the NaBH₄ concentration and reaches the highest values at concentrations of the reducing agent of 0.4 % to 0.5 % (Fig.31). It was also found that the SBRs for the As line under these conditions increased from 1.1 at 0.1 % NaBH₄ to 1.3 at 0.4 as well as at 0.5 % concentrations of NaBH₄. A quite different tendency was observed for Sb. Here we found that with an increase of the NaBH₄ concentration from 0.1 to 0.5 %, the relative net intensities for the Sb line decreased by about 50 % and the SBR values for the Sb line from 3.5 to 2.0.

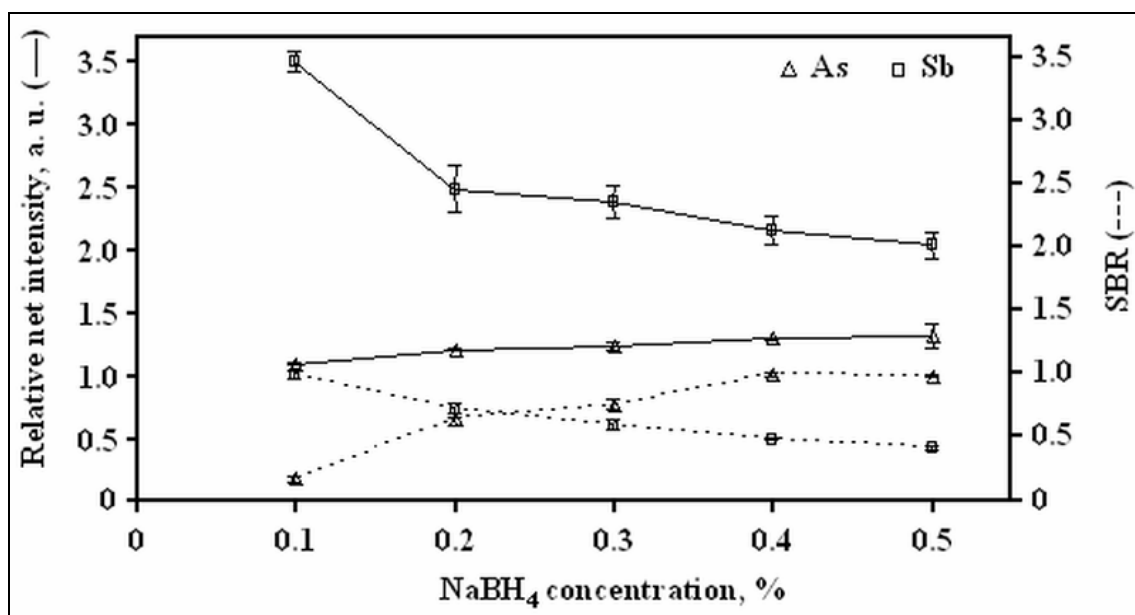


Fig. 31 Influence of NaBH₄ on the intensities of As I 228.8 nm and Sb I 252.8 nm and their SBRs.

The trend reported for the dependence of the analytical signals on the NaBH₄ concentration in the literature on HG coupled with different plasma sources normally is rather similar for different volatile hydride-forming elements studied with the same HG system [72, 116, 157-159, 162, 165, 166]. For a better understanding of the discrepancies observed, we determined the generation efficiency for the As and Sb hydrides at different NaBH₄ concentrations by analyzing the contents of As and Sb in the reaction solutions at the exit of the GLS placed after the HG reaction cell (Fig. 19). In addition, the T_{exc} as determined from the intensities Ar I lines and the n_e values were measured under the studied conditions as well as the amounts of H₂ formed. It could indeed be shown that the HG for As and Sb behaves different. The efficiency of the hydride generation for As was found to grow logarithmically from $23 \pm 1\%$ at a concentration of NaBH₄ of 0.1% to almost $95 \pm 1\%$ when using a 0.5% NaBH₄ solution. In contrast herewith and irrespective of the concentration of NaBH₄, the hydride generation reaction for Sb with 90% was very efficient over the whole range of concentrations of NaBH₄. For a concentration of 0.1% of NaBH₄ the efficiency of the HG reaction of $91 \pm 1\%$ increased to $95 \pm 1\%$ at the highest investigated concentration of 0.5% NaBH₄. The amount of H₂ introduced into the plasma under these conditions linearly changed from $0.6 \pm 0.1 \text{ ml min}^{-1}$ (for 0.1% NaBH₄) to $5.6 \pm 0.3 \text{ ml min}^{-1}$ (for 0.5% NaBH₄). The T_{exc} determined with Ar I lines and the n_e were found to decrease in a similar way. Apparently, the T_{exc} and the n_e

changed from 5800 to 5400 K and from 1.76 to $1.37 \cdot 10^{14} \text{ cm}^{-3}$, respectively, when the concentration of NaBH_4 increases from 0.1 to 0.5 %.

Accordingly, it can be concluded that the introduction of an increasing amount of H_2 into the Ar MSP changes the thermal processes in the plasma as a result of the higher thermal conductivity of H_2 as compared to Ar and the relatively high dissociation temperature of H_2 [167, 168]. This may result in changes of the conditions for the excitation of As and Sb through electron collisions and lead to a depletion of the n_e and a decrease of the analyte line intensities [149]. However, in the case of As, this effect might have been partly compensated for by the higher hydride generation efficiency for As and the higher introduction of analyte into the plasma.

The Ar MSP became unstable and easily extinguished when increasing the NaBH_4 concentration to 0.5 %. Therefore, a 0.4 % NaBH_4 solution was used for all further investigations. Then the Ar MSP was found to have a length of 3 to 4 mm and an intensive bright blue color. Under these conditions it is loaded with $4.2 \pm 0.2 \text{ ml min}^{-1}$ of H_2 and the efficiency of the generation of As and Sb hydrides was found to be 85 and 95 %, respectively.

3.5.1.2 Influence of the acid and its concentration

The influence of the sample acidity on the HG reaction is known to differ from one volatile hydride-forming element to the other and also the features of the HG system as well as the dynamics of the reagent mixing were found to be important [160, 169]. In the present work the use of HCl , HNO_3 and H_2SO_4 , which are commonly applied acids in different digestion or leaching procedures was studied. Their concentrations were varied from 0.5 to 4 mol l^{-1} for the case of As and from 0.1 to 4 mol l^{-1} for the case of Sb [165].

As it can be seen from the results in Fig. 32, the influence of the acid concentration on the relative net intensity of the As line was comparable for all acids used and a plateau was obtained above a concentration of 1 mol l^{-1} . Optimal reaction conditions for HG in the case of As were found to apply when the analyte solutions were acidified with HCl . The signals of As obtained with this acid were about 30-40 % higher than those obtained with HNO_3 or H_2SO_4 . In the case of Sb, the dependence of the signals on the acid concentration in the range from 1 to 4 mol l^{-1} was similar to the one for As. At these conditions, the relative net intensities for

the Sb line in the case of solutions acidified with HCl and with H₂SO₄ were comparable. When using HNO₃ the Sb signals were found to be by about 30 to 40 % lower than those obtained with HCl. For the case of HCl and H₂SO₄ the net intensities of the Sb line reached maxima at 0.2 and 0.5 mol l⁻¹, respectively. At such low acid concentrations, however, the time necessary for the achievement of a steady signal for Sb was found to be relatively high, namely 200 to 300 s (Fig. 32).

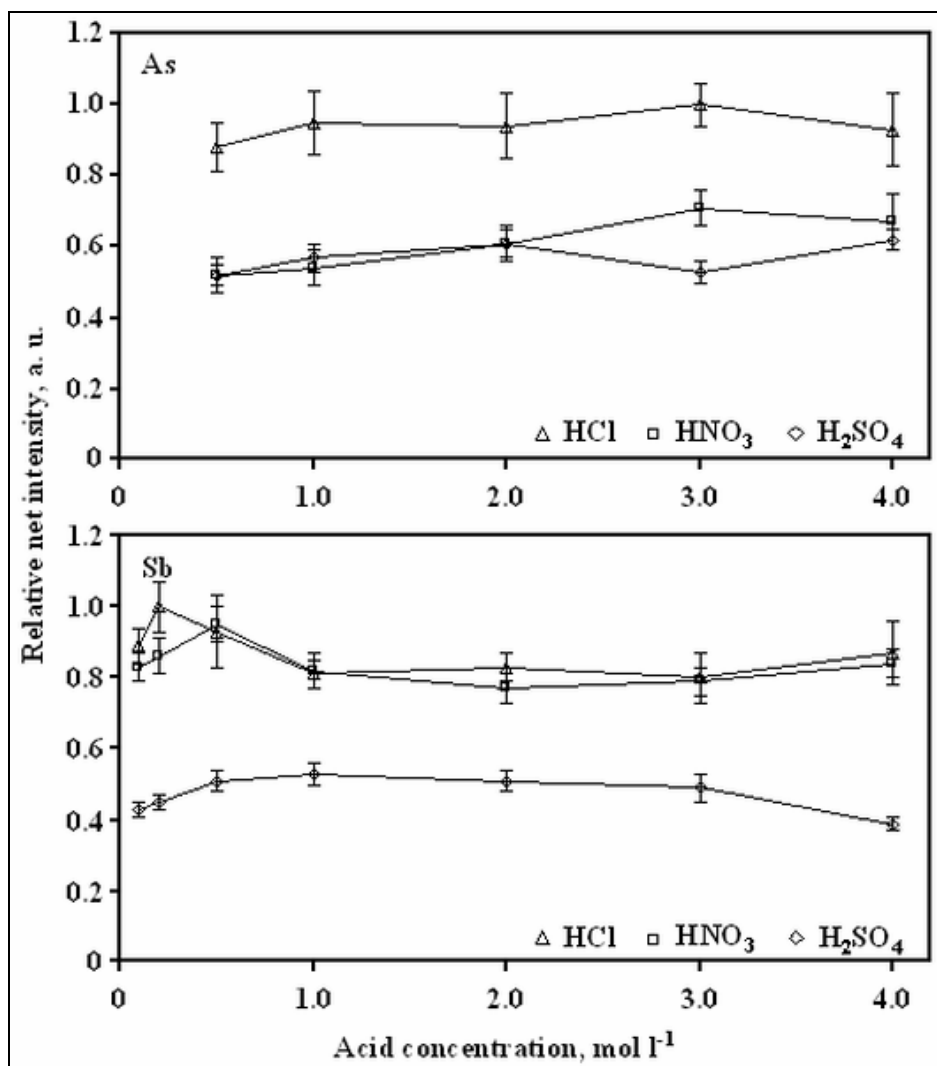


Fig. 32 Influence of the HCl, HNO₃ and HSO₄ concentrations in CHG for As and Sb.

Optimum reaction conditions for the simultaneous determination of As and Sb by CF-HG system could be realized at concentrations of 3 mol l⁻¹ of HCl. Then the time necessary for the achievement of steady signals for As and Sb typically is below 10 s. These experiences well correspond to previously reported results obtained for As and Sb when coupling CF-HG with other microwave plasma structures, such as the TE₁₀₁ cavity, the surfatron, the Okamoto

cavity and the MPT [116, 158, 160, 162, 163, 165]. Accordingly, HCl was preferred as reagent in the works cited and its optimum concentration was found to be in the range of 1 to 4 mol l⁻¹.

3.5.1.3 Influence of the Ar flow rate

The influence of the flow rate of Ar used for carrying the As and Sb hydrides and the accompanying H₂ from the GLS to the MSP as well as for sustaining the discharge was studied in the range of 6 to 82 ml min⁻¹. The changes of the relative net intensities for As and Sb lines and their SBRs within this range of the Ar flow rate are shown in Fig. 33. It was found that the highest signals for As and Sb were obtained at relatively low Ar flow rates, namely at 6 to 15 ml min⁻¹. When increasing the Ar flow rate to values beyond 15 ml min⁻¹, the relative net intensities for the As and Sb lines begin to decrease. The SBR values for these lines were found to decrease also, especially in the case of Sb. The T_{exc} as measured from Ar I lines and the n_e, however, were found to be rather constant over the whole range of the Ar flow rate investigated. The constant level of the T_{exc} values, as it was reported by Goode [170], was around 5500 K and the n_e values were found to be around 1.50·10¹⁴ cm⁻³, but the changes for both parameters were below 2 %. These results lead to the conclusion that an increase of the Ar flow rate did not result in a de-excitation through an increase of a number of radiative collisions with neutral Ar atoms, by which normally the background intensity starts to increase [157]. Here, the background intensities in the vicinity of the As and Sb emission lines also did not significantly vary under the investigated conditions. Consequently, and because of the small dimensions of the Ar MSP, a most reasonable explanation of the influence of the Ar flow rate could be the decrease of the analyte residence time in the plasma at an increase of the Ar flow rate [157, 170].

For sweeping the As and Sb hydrides into the MSP a flow rate of 15 ml min⁻¹ of Ar was finally selected for all further measurements and there the concentration of H₂ in Ar is 28 % (4.2 mL). Lower Ar flows well were found to be more favorable but then higher fluctuations of the gas flows were observed.

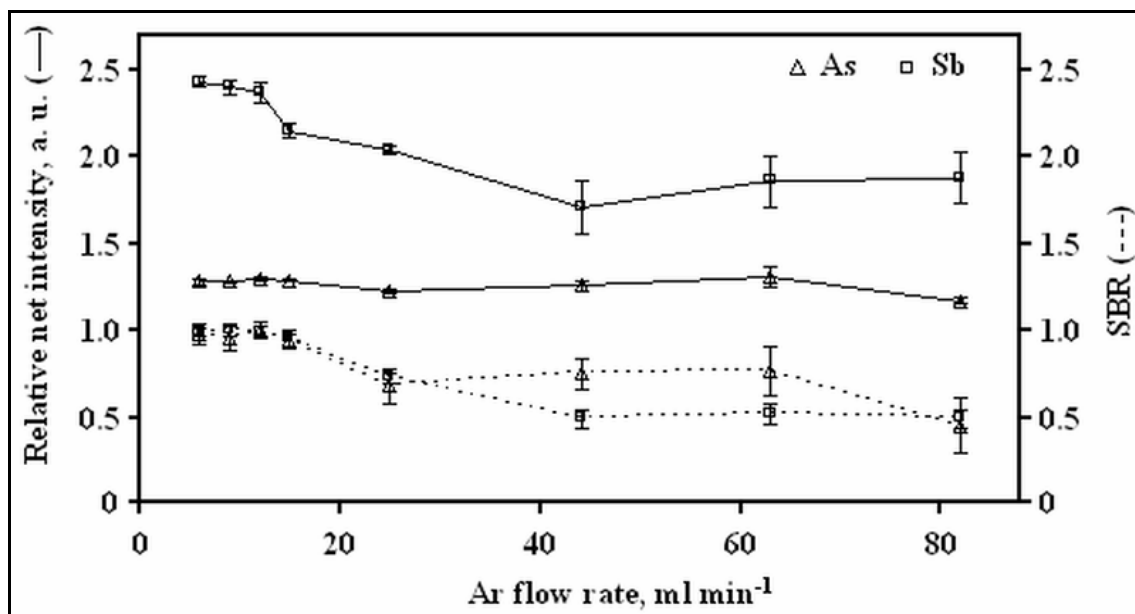


Fig. 33 Influence of the Ar flow rate on the intensities of As I 228.8 nm and Sb I 252.8 nm as well as on their SBRs

3.5.1.4 Influence of the sample and reducing agent flow rates

It is known that the flow rates of the reagents in the CF-HG manifolds influence the amount of H₂ introduced [157-159, 163, 165, 166]. Further, it is also known that at a fixed ratio of the concentrations of the acid and the NaBH₄ solutions, the amount of H₂ produced in the HG reaction increases with the flow rate of the reagents [162].

In the present study, the influence of the flow rates of the reagents at a ratio of 1:1, was studied in the range from 0.3 to 0.7 ml min⁻¹. The amount of H₂ originating from the decomposition of NaBH₄ was found to linearly increase when the sample/reductand flow rate was changed from 2.6 ± 0.1 to 5.6 ± 0.7 ml min⁻¹. From the results in Fig. 34, it can be seen that in this range there is a decrease of the intensities of the As line and its background by about 60 %. However, up to a flow rate of 0.50 ml min⁻¹, the decrease of the background intensity was found to be higher than the decrease of the intensity of the As line. At reagent flows higher than 0.55 ml min⁻¹, the background intensity and the As line intensity were found to decrease at nearly the same rate. Indeed, the SBR slightly increases up to 0.50 ml min⁻¹ and then remains almost constant at 1.30 ± 0.04 in the remaining range. The highest relative net intensities for the As line were obtained at flow rates of 0.50-0.55 ml min⁻¹. For Sb a different trend was observed. It was found that the intensities of the Sb line and its background were

increasing up to a flow rate of 0.50 ml min^{-1} , however, the background intensity enhancement was about 2 times higher than that for the line intensities. At reagent flow rates higher than 0.50 ml min^{-1} , the net intensities of the Sb line reached a plateau. Indeed, according to D'Ulivo [171], who thoroughly discussed the mechanisms involved in the decomposition of NaBH_4 and the formation of volatile hydrides, the efficiency of the HG reaction is strongly affected by the concentration of NaBH_4 , the type and the concentration of acid used as well as by the reaction medium and by the dynamics of the mixing of the reagents. The results obtained in the present study indicate that the concentration of NaBH_4 and the flow rate of the reagents have an effect on the decomposition rate of NaBH_4 as well as on the amount of H_2 liberated in the reaction. Indeed, the amount of H_2 measured using the method described above was different from that calculated on the basis of a complete decay of NaBH_4 following the hypothesis of "nascent hydrogen" [99]. It was especially evident when lower NaBH_4 concentrations and lower flow rates of the reagents were used and indicated that the reaction path is rather complicated and that probably different intermediates may take part in the reaction. For further experiments reagent flow rates of 0.50 ml min^{-1} were used.

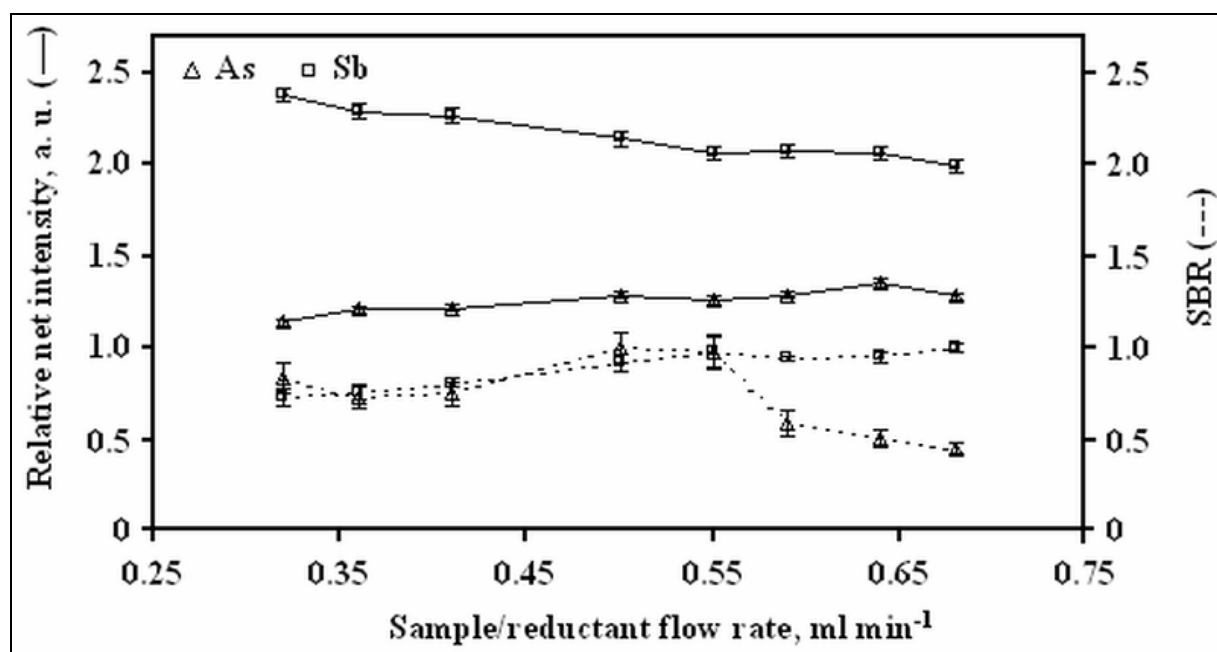


Fig. 34 Influence of the sample/reductant flow rate on the intensities of the As I 228.8 nm and Sb I 252.8 nm lines and on their SBRs.

3.5.1.5 Influence of the residual liquid volume in the gas-liquid phase separator

The volume of the reaction mixture in the GLS was kept at a constant level of 0.5 ml in all the experiments performed. This prevented from fluctuations in the pressure inside the system. The performance at lower (0.2 ml) and higher (1.0 and 1.5 ml) liquid volumes inside the GLS was also studied. It was found for As that at a change of the volume from 0.2 to 1.5 ml the relative net intensity of the As line increased from 0.74 ± 0.04 to 1.00 ± 0.05 . In contrast, the relative net intensity of the Sb line then decreased from 1.00 ± 0.02 to 0.83 ± 0.04 . In general, higher volumes of liquid inside the GLS like 1.5 and 1.0 ml, were found to require higher washing times (180 and 240 s, respectively) as compared to those with 0.2 or 0.5 ml of liquid volume inside the separator (80 and 120 s, respectively). Accordingly, a residual liquid volume of 0.5 ml in the GLS was found to be optimum and was used in all further measurements.

3.5.2. Chemical interferences caused by transition metal ions

The chemical interferences caused by the presence of transition metals such as Cd(II), Co(II), Cr(III), Cu(II), Fe(III), Mn(II), Ni(II), Pb(II) and Zn(II) in the determination of $2 \mu\text{g ml}^{-1}$ of As and Sb in 3 mol l^{-1} HCl with the described HG system at the conditions mentioned were measured. The interferences by each metal under consideration were studied individually. Therefore, at analyte solutions containing 2, 5, 10 and $20 \mu\text{g ml}^{-1}$ of the potential interferent, the net intensities of the As and Sb lines were measured and their ratios with the respective net intensities for a solution without interferent expressed as the relative net intensities.

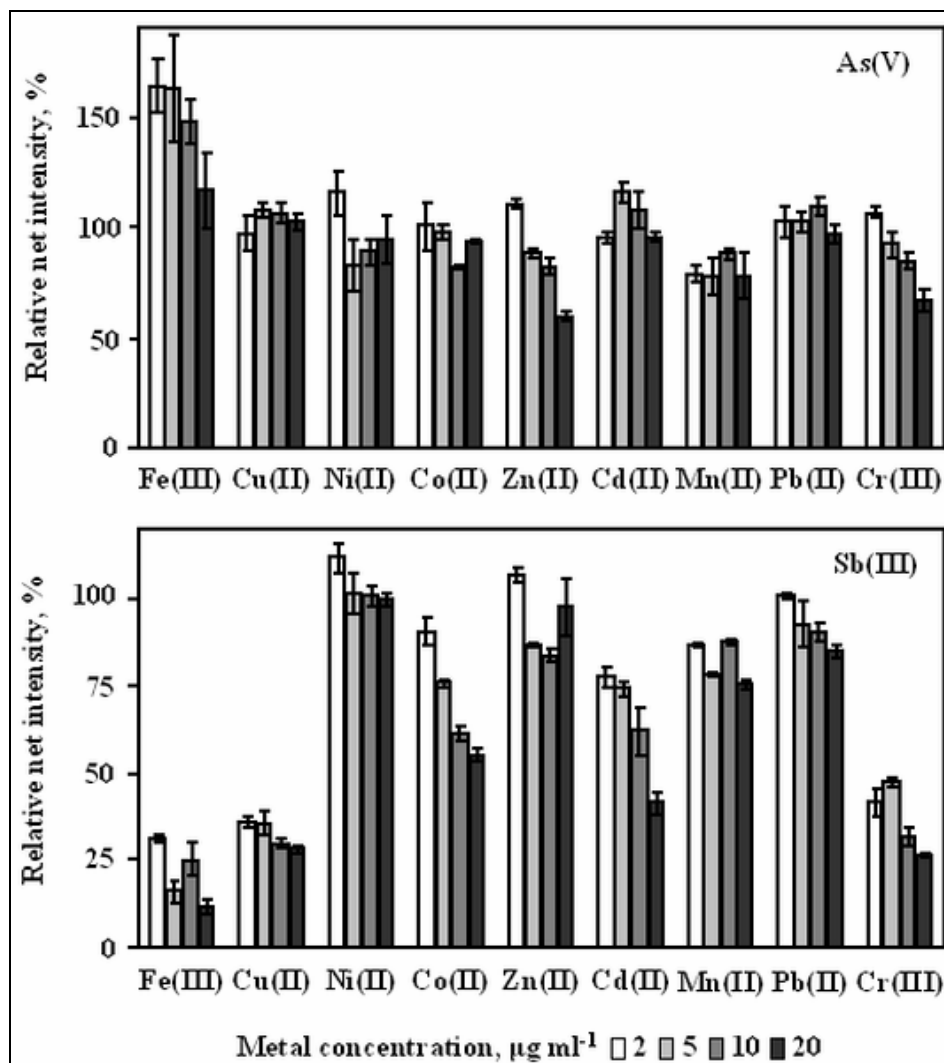
It should be mentioned that under the conditions used volatile species such as Cd are not likely to be formed. Indeed, for the generation of volatile species of Cd in the reaction with NaBH_4 in an acidic medium a relatively low acid concentration is required. For example, when HCl is used for sample acidification, its concentration in the solution for a maximum response for Cd should be close to 0.5 mol l^{-1} [172]. The sample solutions containing As and transition metals, including Cd, had an HCl concentration of 3.0 mol l^{-1} . Under these conditions, a spectral interference between As I 228.8 nm line and Cd I 228.8 nm line is not likely as in addition the Cd I 226.5 nm line was not observed.

From the results in Fig. 35, it can be seen that the presence of Fe at concentrations ranging from 2 to 20 $\mu\text{g ml}^{-1}$ resulted in an enhancement of the As signals by about 20 to 60 %, respectively. Metals such as Cd, Cu and Pb are known as severe interferents in the determinations of As by HG (see Ref. [173]). It was found that they did not affect the response for As in the interferent concentration range investigated. In the presence of Cr and Zn at the highest concentration, however, a high suppression of the analyte signals for As (up to 40 %) was found. At concentrations higher than 5 and 2 $\mu\text{g ml}^{-1}$, respectively, Co and Ni also were found to suppress the As signals by about 10 %. Mn was found to interfere in the whole investigated range and to cause a depression of around 20%.

In contrast to the HG for As, the HG for Sb was prone to chemical interferences by most of the transition metals (Cd, Co, Cu, Cr and Fe). At the lowest interferent concentrations investigated (2 and 5 $\mu\text{g ml}^{-1}$) a decrease of the Sb response from about 10 % for Co to 60 % for Cu and Cr and around 80 % in the case of Fe was found. The interference was found to increase with the concentration of the transition metals mentioned. Pb and Zn were found to cause less interferences. In the presence of these metals the signals for Sb decreased only by about 10 %. Surprisingly, Ni, known as one of the strongest interferents for all volatile hydride-forming elements [174], did not cause any interference in the case of Sb. Finally with Mn, a suppression of the signal for Sb by about 20 % over the whole investigated concentration range was found.

3.5.3 Effect of masking agents

The effect of the known masking agents, NaI, KCN, L-ascorbic acid and L-cysteine, at a concentration of 1 % (m/v) was investigated for a solution of 2 $\mu\text{g ml}^{-1}$ of As and Sb containing also Cr (1 $\mu\text{g ml}^{-1}$), Cu (0.6 1 $\mu\text{g ml}^{-1}$), Fe (56 $\mu\text{g ml}^{-1}$), Mn (0.9 $\mu\text{g ml}^{-1}$), Ni (0.6 $\mu\text{g ml}^{-1}$), Pb (0.4 $\mu\text{g ml}^{-1}$) and Zn (1 $\mu\text{g ml}^{-1}$). These concentrations of the transition metals are similar to their concentrations in a solution of the NIST coal fly ash standard reference material SRM 1633a. The masking agents were added to the sample solution or to the NaBH_4 solution and the results are given in Fig. 36. The interferences are expressed as the percent ratios of the net intensities for the As and Sb lines measured for the analyte solutions with the metals in the presence of masking agents and the net intensities measured for the analytes in the presence of the masking agents only.

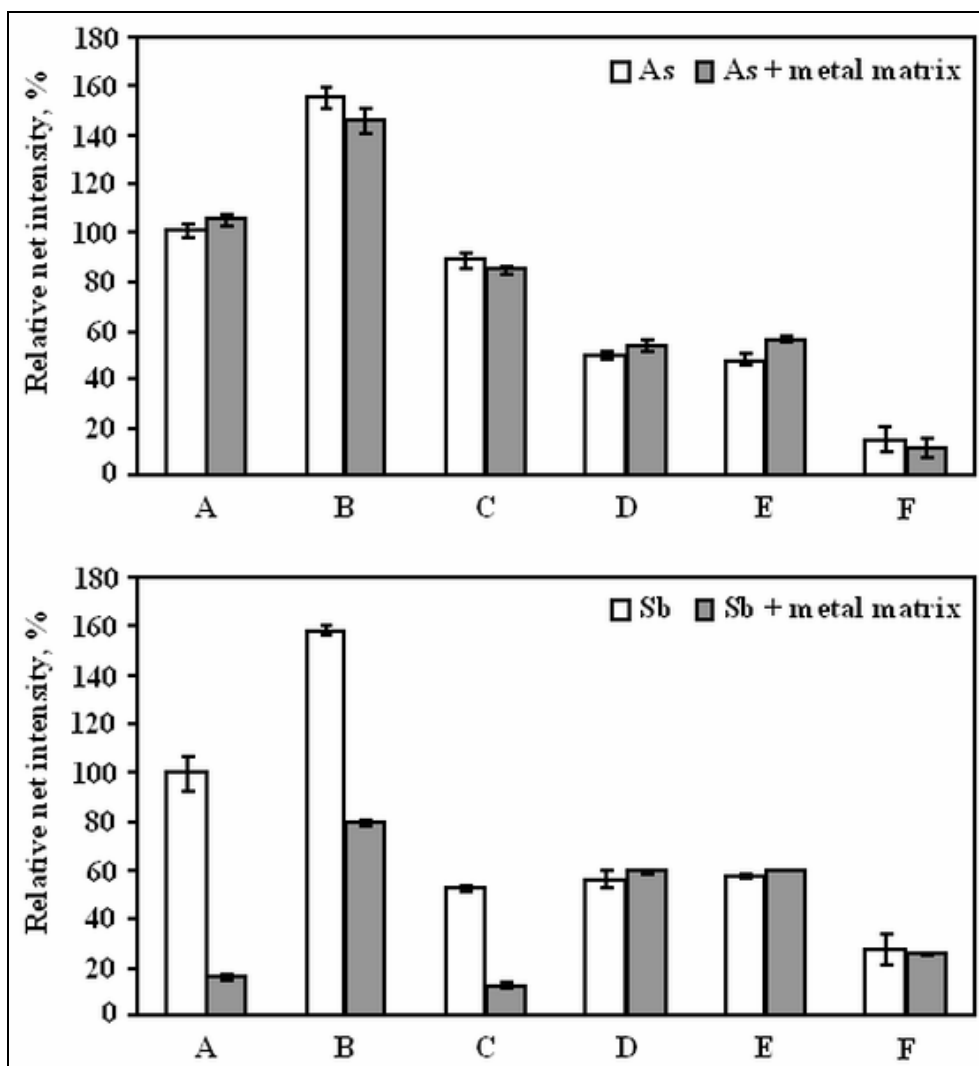


Average of three measurements and error bars corresponding to the average \pm the standard deviation

Fig. 35 Interferences of transition metals in CHG-MSP-OES for As I 228.8 nm and Sb I 252.8 nm.

It can be seen that the metal mixture added hardly had any effect on the signals for As. Indeed, Cd, Co, Cu, Ni and Pb, which are known to be serious interferences in the determination of As by means of the HG technique, were found to have only a slight effect on the signals for As or no effect at all. This could be due to the relatively low concentration of NaBH_4 used for the HG reaction as compared to the concentrations of this reducing agent used in other studies. However, the different masking agents differently affected the response for As. Apparently, an addition of NaI to the solution of NaBH_4 caused an increase of the As signal by about 50 % as compared to that obtained for a solution of As without the metals. This could be due to a reduction of As(V) to As(III), which is known to be very effective when I⁻ anions are in the NaBH_4 solution [175, 176]. The presence of other masking agents

was found to result in a suppression of the As signal from about 10 % in the case of KCN added to the NaBH₄ solution to about 90 % in the case of an addition of NaI to the sample solution. The reduction of the As signal could be related to the introduction of I₂ formed by the oxidation of I⁻ by dissolved O₂ or Fe³⁺ present in the acidified solution [177] into the plasma.



Average of three measurements and error bars corresponding to the average \pm the standard deviation

Fig. 36 Influence of masking agents added to the sample and reductand solution. Without masking agent (A), NaI in reductand (B), KCN in reductand (C), L-ascorbic acid in sample (D), L-cysteine in sample (E), and NaI in sample (F).

In the case of Sb, the metals mentioned were found to cause a reduction of the analyte signal by over 80 %. The highest interference was found for Fe(III). However, the interferences in the case of a mixture of Cr, Cu, Fe, Mn, Ni, Pb and Zn studied could be eliminated by the addition of L-cysteine, which is known as one of the most effective masking agents in HG [178, 179], or of L-ascorbic acid.

3.5.4 Figures of merit and analytical application

Under the optimized conditions, the linear dynamic ranges, the precision and the detection limits defined according to the 3σ criterion for the determination of As and Sb by CF-HG-MSP-OES were determined. The detection limits (Table 5) were found to be higher than those mentioned in the literature for conventional MIPs [157-160, 162, 163, 166] and the linearity of the calibration both for As and Sb extends to $5 \mu\text{g ml}^{-1}$. Further, the precision was evaluated for three replicate measurements of standard solutions of As and Sb at concentrations of $1 \mu\text{g ml}^{-1}$. Indeed, the detection limits found in the present study for As and Sb using the system described in Fig. 19 are not so impressive as those reported in the literature. A reason could be the much lower optical resolution of the miniaturized spectrometer applied here as compared to the spectrometers used in the cited works. The linearity ranges of the calibration curves (more than 2 orders of magnitude) and the precision are comparable to those found in the cited literature.

Table 5. Precision and limits of detection obtained for the determination of As and Sb

Element	RSD ^a , %	LoD, ng ml^{-1}	
As	3.0	18 ^b	0.7 – 65 ^c
Sb	1.6	31 ^b	0.59 – 18.8 ^c

^aAs and Sb concentrations: $1 \mu\text{g ml}^{-1}$.

^bThis work ($3\sigma_{\text{blank}}$)

^cLiterature [157-160, 162, 163, 166] ($3\sigma_{\text{blank}}$)

3.5.5 Analysis of real samples and NIST SRM 1663a

The procedure developed could be successfully used for the determination of Sb and As in a galvanic bath solution containing about 2.5 % (m/v) of NiSO_4 . The sample was spiked with As up to a concentration of $45 \mu\text{g ml}^{-1}$. The concentration of Sb found in the galvanic sample was $6.41 \pm 0.85 \mu\text{g ml}^{-1}$. This well agreed with the concentration of $6.89 \pm 0.18 \mu\text{g ml}^{-1}$ found by ICP-OES using the SPECTRO CirosCCD. For the As added, a recovery of $97.1 \pm 9.1 \%$ was obtained.

The developed HG system could also be successfully used for the determination of As in a coal fly ash NIST SRM 1663a with a certified As value of $145 \pm 15 \mu\text{g g}^{-1}$. In the

investigations on interferences, a mixture of Cr, Cu, Fe, Mn, Ni, Pb and Zn at concentrations similar to those in the solution of the NIST coal fly ash standard reference material obtained after its digestion (0.25 g in 50 ml) was not found to affect the signals for As. However, here the calibration was done by standard addition without adding L-cysteine. The concentration of As determined in the standard reference material by HG-MSP-OES with a value of $144 \pm 4 \mu\text{g g}^{-1}$ was in very good agreement with the certified value for this material ($145 \pm 15 \mu\text{g g}^{-1}$).

3.6 Comparison of the cold vapour generation using NaBH_4 and SnCl_2 as reducing agents for the determination of Hg with a microstrip microwave induced Ar plasma exiting from the wafer (type B)

A comparison of two cold vapour generation techniques using SnCl_2 and NaBH_4 as reductants, respectively, coupled to an MSP exiting the wafer (type B)-OES, using the system described in Fig. 20 for the determination of Hg is given in the present section. A univariant approach was used to investigate the influence of the parameters such as the concentration of reductant agents, the concentration of the stabilizing substances, the sample acidification, the Ar flow rate, the reagents flow rates and the dead volume in the GLS. Further the areas of stability for the source were determined. Initial conditions at 40 W for the optimization process were an Ar flow rate of 15 mL min^{-1} , Hg solutions of $0.2 \mu\text{g mL}^{-1}$ acidified with HCl up to a concentration of 2 and 0.5 mol L^{-1} , respectively, and a reagent flow rate of 0.5 mL min^{-1} . The influence of the concentration of NaBH_4 in the range of 0.05-0.6 % and of SnCl_2 in the range of 1 to 6 % on the relative net intensities of Hg I 253.6 nm line and its SBR is investigated. Chemical interferences from NaCl, transition metals and hydride forming elements were studied as well. Finally, analyses of real water samples and of a domestic sludge NIST reference material have been performed.

3.6.1 Optimization

3.6.1.1 Influence of the concentrations of the reducing agents

As it was described for the simultaneous determination of As and Sb with a plasma exiting the wafer, the concentration of NaBH_4 is critical for the analytical performance. When increasing its concentration above 0.1 %, both the net intensity of the Hg line and the SBR strongly decrease. This is a result of the introduction of the increasing amounts of H_2 into the plasma.

Indeed, the amount of H_2 was found to change from $0.3 \pm 0.1 \text{ mL min}^{-1}$ at a concentration of 0.05 % NaBH_4 to $5.6 \pm 0.3 \text{ mL min}^{-1}$ at a concentration of 0.6 % NaBH_4 . It was also found that then the T_{exc} measured with Ar I lines and the n_e changed from 6100 to 5500 K and from 1.6 to $2.0 \cdot 10^{14} \text{ cm}^{-3}$, respectively. As even at low NaBH_4 concentrations the efficiency of the CV generation for Hg can be assumed to be rather high [180], the deterioration of the response for Hg found here might be due to changes of the excitation conditions in the MSP as a result of the higher thermal conductivity and the temperature required for a dissociation of H_2 [167]. In compliance with the radiative-recombination excitation mechanism proposed for atmospheric pressure MIPs in gas mixtures containing H_2 [170], it could be expected that although the overall n_e in the MSP loaded with H_2 increases, the high energy electrons may be involved in the dissociation and the excitation of H_2 and therefore the excitation conditions for Hg may become less favorable.

Despite the fact that with a 0.05 % NaBH_4 solution the relative net intensity for the Hg line and the SBR are about 20 % higher than in the case of a 0.1 % NaBH_4 solution, the repeatability of the analytical signal in this case was poorer. Therefore a 0.1 % solution of NaBH_4 was considered to be optimal.

When performing the CV generation with SnCl_2 , which is known to be a milder reducing agent than NaBH_4 [105, 146], higher concentrations of the reductant were required so as to get a reaction. When increasing the concentration of SnCl_2 up to 4 %, the relative net intensity for the Hg line was found to steadily increase up to this concentration. At higher concentrations of SnCl_2 , a slight decrease of the response of Hg was observed. The SBR was also found to strongly depend on the concentration of SnCl_2 . The T_{exc} and n_e , however, practically remained unchanged at changing concentrations of SnCl_2 and were 6200 K and $2.0 \cdot 10^{14} \text{ cm}^{-3}$, respectively. Their variation was below 5 % within the whole concentration range of SnCl_2 investigated. A solution containing 4 % of SnCl_2 was chosen as optimal for further investigation.

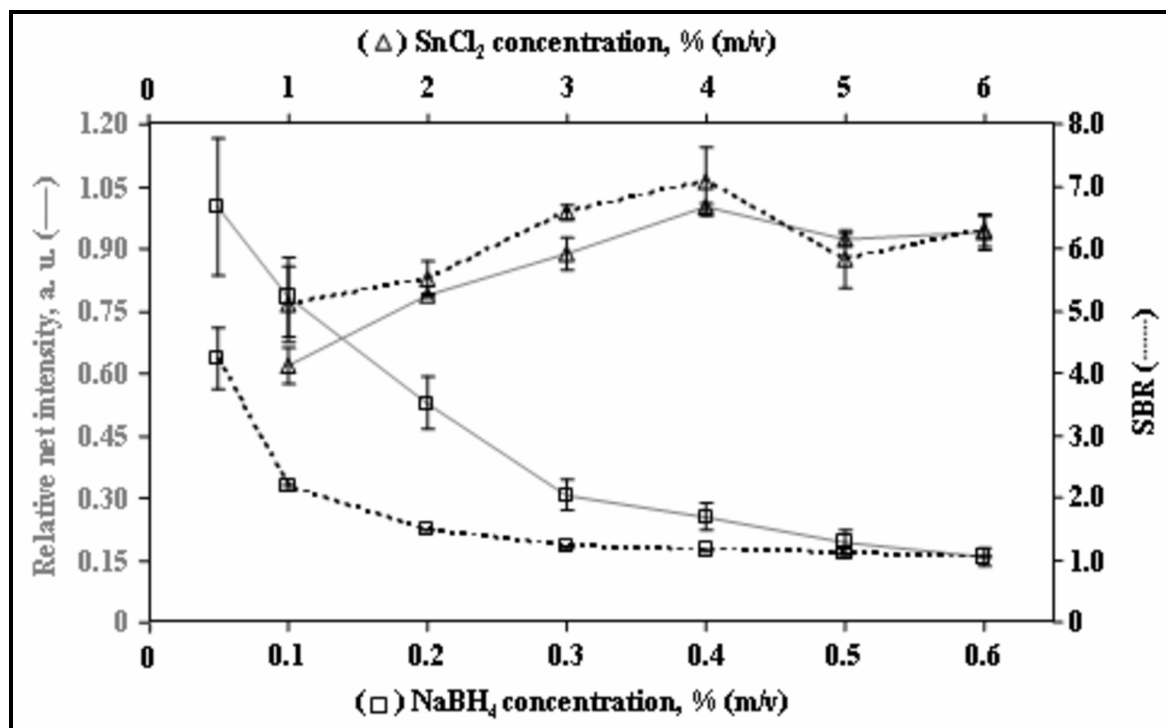


Fig. 37 Influence of the concentration of the reducing agents on the intensity of the Hg I 253.6 nm line and on its SBR

3.6.1.2 Influence of the concentrations of substances stabilizing the reducing agent solutions

NaBH₄ is known to readily decompose in acidic aqueous solutions and therefore alkaline solutions are normally required so as to keep this reductant stable. SnCl₂ tends to undergo hydrolysis in aqueous solutions and to form Sn(OH)Cl precipitate [181]. Accordingly, the solutions of SnCl₂ are usually acidified with HCl at moderate concentrations. However, the presence of both substances used for stabilization, namely NaOH and HCl, is also important with respect to the performance of the CV generation reaction and their concentrations were optimized in this study. The influence of the concentration of NaOH used for a stabilization of the 0.1 % NaBH₄ solution on the response for Hg was investigated in the range of 0.01 to 0.08 mol L⁻¹. In the case of HCl added to the 4 % solution of SnCl₂, its concentration was varied from 0.1 to 1 mol L⁻¹. All other experimental conditions used were as mentioned when describing the influence of the concentrations of the reducing agents.

When changing the concentration of NaOH in the 0.1 % NaBH₄ solution from 0.01 to 0.04 mol L⁻¹ the relative net intensity of the Hg I 253.6 nm line was found to increase from 0.8 to 1.0. At a concentration of 0.08 mol L⁻¹ of NaOH in the NaBH₄ solution the relative net intensity for the Hg line was found to be about 0.9.

In the case of the 4 % SnCl₂ solutions, the highest response for Hg was found when using a concentration of 0.5 mol L⁻¹ of HCl in the reducing agent solution. Above that concentration the relative net intensity for the Hg line decreases and it is by 25 % lower when the solution of SnCl₂ contains 1 mol L⁻¹ of HCl. Concentrations of HCl in the SnCl₂ solution, which are higher than 1 mol L⁻¹, were found to be still less favourable. Then an oxidation of SnCl₂ to SnCl₄ becomes likely, which is accompanied by a precipitation of Sn(OH)Cl. These observations were well consistent with the results reported in literature, where the molar concentration of HCl is usually 2 to 5 times higher than the one for SnCl₂ [78, 146, 180, 181].

3.6.1.3 Influence of the concentration of HCl in the sample

The concentration of HCl in the sample solution also may influence the signal for Hg in the CV generation using NaBH₄ and SnCl₂. In Fig. 3 the results on the influence of the acid for 0.1 % NaBH₄ in 0.04 mol L⁻¹ NaOH and 4 % SnCl₂ in 0.5 mol L⁻¹ HCl solutions are given, when all other operating parameters were kept as in the study on the influence of the concentrations of the reducing agents.

In the case of the CV generation reaction with NaBH₄ it was found that the concentration of HCl in the sample solution over a wide range of acid concentration, namely from 0.05 to 4 mol L⁻¹, does not affect the relative net intensity for the Hg line. This was also found to be the case for the SBR for that line, which has a value of 2.1 with a variation below 2.5 % over the whole range investigated. In all further experiments, in which the reaction with NaBH₄ was used for the CV generation of Hg, the samples were acidified with HCl at the concentration of 2 mol L⁻¹.

When using SnCl₂ in the CV generation technique, it was found that only at relatively low concentrations of HCl in the sample, namely between 0.2 and 0.5 mol L⁻¹, a high net intensity for the Hg I 253.6 nm line and a high SBR were obtained. With a further increase of the concentration of HCl the analytical signal for Hg was found to gradually decrease. This may

be understood from a lower efficiency of the reduction by SnCl_2 , which most probably is a result of its oxidation by O_2 under these conditions. Consequently, the concentrations of HCl recommended in the literature [146, 148, 182, 183] for the CV generation of Hg under the use of SnCl_2 are close to 0.2 mol L^{-1} and a such concentration was also used in the optimization process.

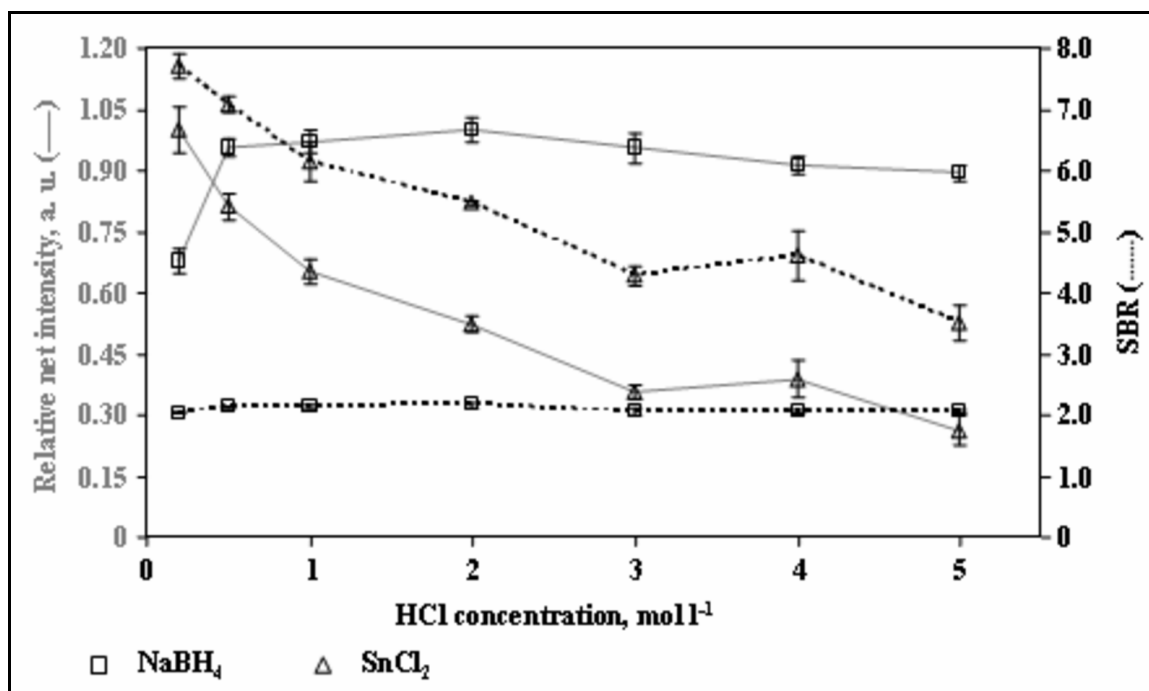


Fig. 38 Influence of the concentration of the HCl on the intensity of the $\text{Hg I } 253.6 \text{ nm}$ line and on its SBR

3.6.1.4 Influence of the Ar flow rate

As Ar serves to transport the released Hg vapours from the GLS to the discharge and also as plasma gas, it is expected that the flow rate of Ar also largely will influence the performance of the MSP exiting from the wafer. In the experiments on the influence of the Ar flow rate on the performance of the MSP the latter was operated at the power of 40 W and at a reagent flow rate of 0.5 mL min^{-1} . In the CV generation reaction with NaBH_4 a 0.1 % solution of the reducing agent in 0.04 mol L^{-1} NaOH and a sample solution containing $0.2 \text{ } \mu\text{g mL}^{-1}$ of Hg in 2 mol L^{-1} HCl were used. In the CV generation with SnCl_2 a 4 % solution of the reductant in 0.5 mol L^{-1} HCl and a solution of $0.2 \text{ } \mu\text{g mL}^{-1}$ of Hg acidified with 0.2 mol L^{-1} HCl were

used. In addition, the T_{exc} as determined with Ar I lines and the n_e were evaluated under these conditions so as to understand the changes in the analytical performance of the Ar MSP.

As it can be seen from the results in Fig. 39, the relative net intensities for the Hg I 253.6 nm line at an increase of the flow rate of Ar from 6 to 63 mL min⁻¹ gradually decreased for a CV generation performed with NaBH₄ and SnCl₂ by ca. 50 and 70 %, respectively. In a similar way, the SBR in the case of the Hg I 253.6 nm line for the CV generation reaction with NaBH₄ and SnCl₂ also decreased over the whole range of the Ar flow rate investigated from 2.3 to 2.0 and from 13 to 6.0, respectively. It was found, however, that the T_{exc} as measured from Ar I lines did not change substantially. Indeed, at changes in the Ar flow rate from 6 to 63 mL min⁻¹, the T_{exc} varied from 6100 to 6200 K and from 6000 to 6300 K in the case of the CV generation under the use of NaBH₄ and SnCl₂, respectively. However, there was not a specific trend and n_e was found to change with the Ar flow rate by about 20 and 10 % on the whole for the CV generation with NaBH₄ and SnCl₂, respectively.

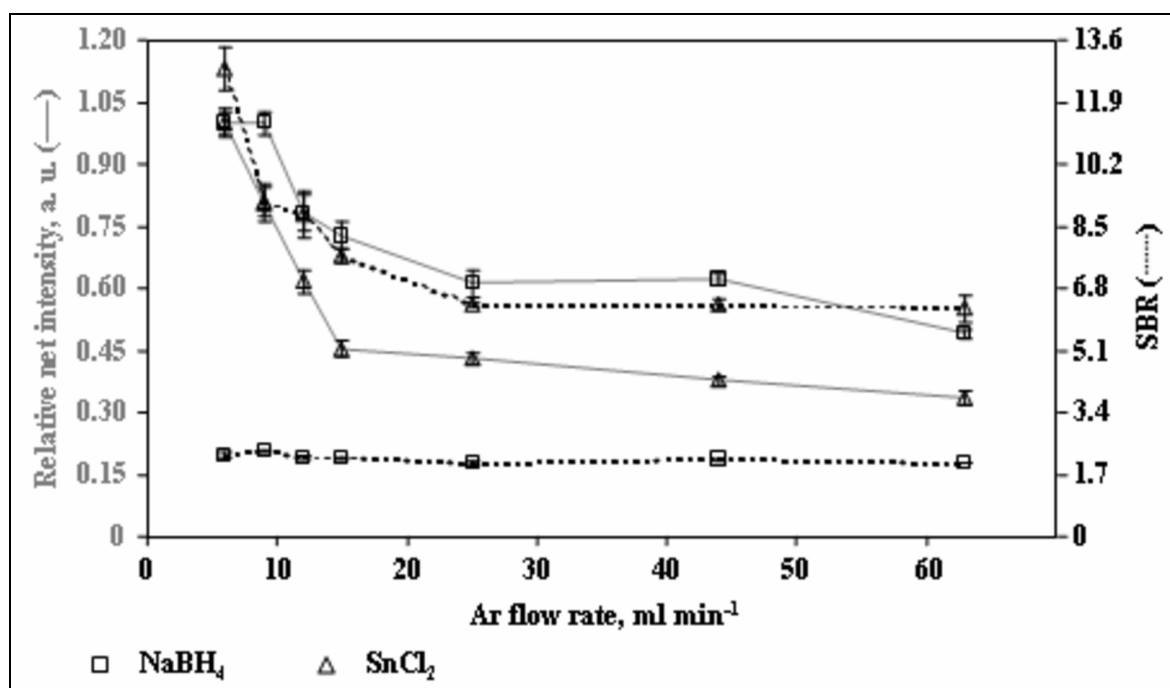


Fig. 39 Influence of the Ar flow rate on the intensity of the Hg I 253.6 nm line and on its SBR.

Considering the low change of the T_{exc} and the n_e with the Ar flow rate, it was assumed that a deterioration of the response for Hg with the increase of the flow of Ar for the studied MSP does not result from de-excitation through an increase of a number of radiative collisions with

neutral Ar atoms, as it could be expected for bulky MIP radiation sources [74, 182]. Most probably, this effect is a consequence of the lower residence time of Hg in the plasma. A very similar behavior has recently been observed for the Ar MSP coupled to CV generation when the plasma is fully sustained inside the gas channel of the sapphire wafer. In all further experiments, a flow rate for Ar of 9 mL min^{-1} was used.

3.6.1.5 Influence of the flow rate of the reagents

The flow rate of the reagents was expected to influence the reaction rate. Additionally, in the case of the CV generation with NaBH_4 the amount of H_2 produced and introduced into the MSP may change with the reagents flow rates [184]. Therefore, the influence of this parameter on the response for Hg in the CV generation with the aid of NaBH_4 and SnCl_2 was studied.

Indeed, it was found that with an increase of the flow rate of the reagents from 0.27 to 1.0 mL min^{-1} the amount of H_2 produced in the reaction changed from 2.6 ± 0.1 to $7.6 \pm 0.7 \text{ mL min}^{-1}$. When the reagent flow rate changes from 0.27 to 0.50 mL min^{-1} , as it can be seen from Fig. 40, the relative net intensity for the Hg line obtained for the CV generation with NaBH_4 was found to increase from 0.8 to 1 . Up to the flow rate of 0.59 mL min^{-1} the relative net intensity for the Hg line was found to be constant and a further increase of the flow rate of the reagents was found to result in a slight decrease of the response for Hg. These changes also were found to apply for the SBR for the Hg line. Indeed, when using flow rates above 0.59 mL min^{-1} the SBR decreased. A flow rate of 0.55 mL min^{-1} was finally found to be optimum.

In the case of the CV generation with SnCl_2 , a steady increase of the relative net intensity for the Hg line and its SBR with the flow rate of the reagents was observed in the range of 0.36 to 1.0 mL min^{-1} . Almost a 3- and a 2-fold increase of the relative net intensity for the Hg line and the SBR was found to occur in this range. A flow rate of the reagents of 1.0 mL min^{-1} was found to be optimum.

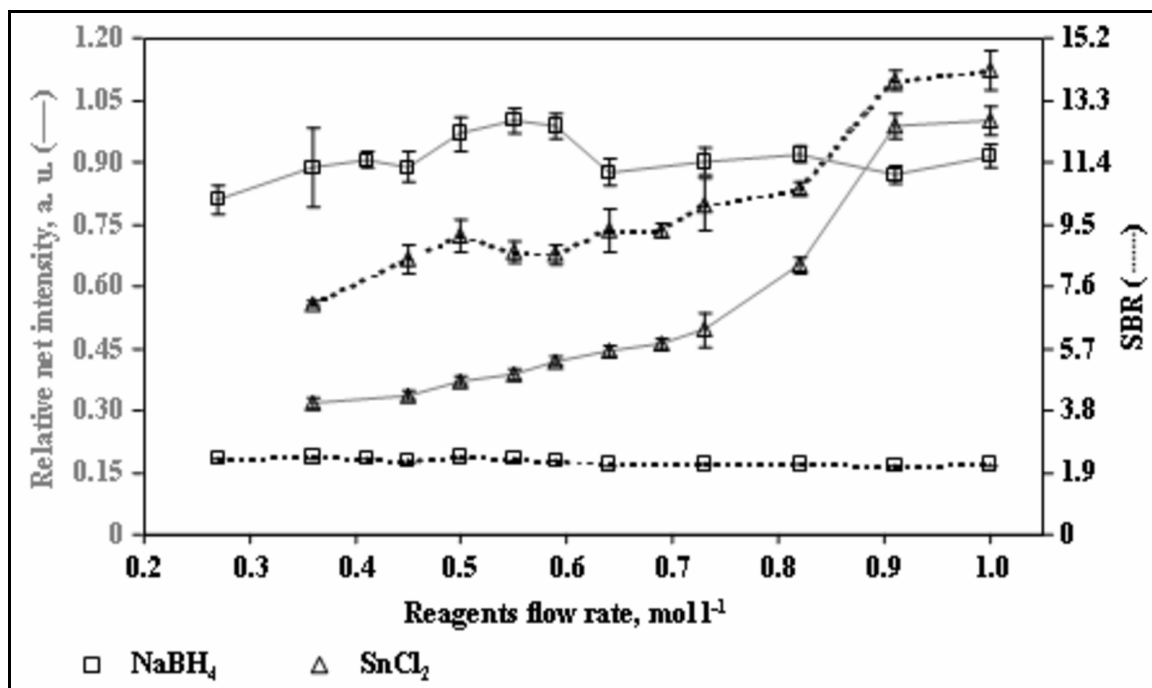


Fig. 40 Influence of the reagent flow rates on the intensity of the Hg I 253.6 nm and on its SBR.

3.6.1.6 Influence of the volume in the gas liquid separator

In all measurements reported, the volume of the liquid in the GLS was kept at a constant level of 0.5 mL. In this way, the pressure inside the low-volume GLS was constant. However, the use of other volumes, namely 0.2, 1 and 1.5 mL, also was tested. It was found that the volume of liquid in the GLS only had a slight influence on the Hg signal for both CV generation reactions. In the case of the CV generation with NaBH₄, the relative net intensity for the Hg line in the case of 0.5, 1 and 1.5 mL was close to 1, whereas for a volume of 0.2 mL a value of 0.9 was found. In the case of the CV generation with SnCl₂, the relative net intensities for the Hg line with all volumes tested were comparable, however, for volumes of 1 and 1.5 mL higher washing times were required. Therefore, a volume of liquid of 0.5 mL inside the GLS was considered as optimum and used for all further measurements.

3.6.2 Areas of stability

The stability areas for MSPs in Ar loaded with Hg vapours, as obtained with the CV generation reactions using NaBH₄ and SnCl₂, respectively, were found to be comparable. At an Ar flow rate of 9 mL min⁻¹, the MSP was found to be stable at a power between 33 and 40

W under the conditions for optimum CV generation. At lower powers the Ar MSP becomes unstable and extinguishes. When increasing the Ar flow rate up to 63 mL min^{-1} , the power range within which the Ar MSP was stable was reduced to about 35 W.

When operating the Ar MSP at a flow rate of 9 mL min^{-1} but at a power below 40 W, it was also found that the relative net intensity for the Hg line decreases. Indeed, when the power was decreased to 37 W, the signals for Hg in the case of the CV generation using NaBH_4 or SnCl_2 decreased by about 50 and 30 %, respectively. However, the SBR values under these conditions were found to change less than 2-3 %. The T_{exc} as measured from Ar I lines did not change and was 6000 and 6100 K for the CV generation using NaBH_4 and SnCl_2 , respectively. The respective n_e therefore was found to decrease from 1.6 to $1.4 \cdot 10^{14} \text{ cm}^{-3}$ and from 1.8 to $1.5 \cdot 10^{14} \text{ cm}^{-3}$, respectively.

3.6.3 Chemical interferences

Under the optimized experimental conditions, the chemical interferences in the determination of Hg by CV generation using NaBH_4 and SnCl_2 as reducing agents were investigated. The most commonly known potential interferences were studied and included transition metal ions such as Cd(II), Co(II), Cu(II), Fe(III), Ni(II) and Zn(II) as well as the volatile hydride forming elements As(V), Bi(III), Sb(III) and Se(IV). For the experiments a concentration of Hg of $0.2 \text{ } \mu\text{g mL}^{-1}$ was used, while the concentrations of interferences in the solutions were 5, 10, 20 and $50 \text{ } \mu\text{g mL}^{-1}$. The effects of the presence of transition metals on the response found for Hg in the CV generation using NaBH_4 and SnCl_2 are shown in Fig. 41. In Table 6 the results for hydride forming elements are given. In both cases the relative intensities were calculated by dividing the net intensities for the Hg line measured in the case of the solutions containing Hg and the potential interferences by those obtained for the solutions containing Hg only.

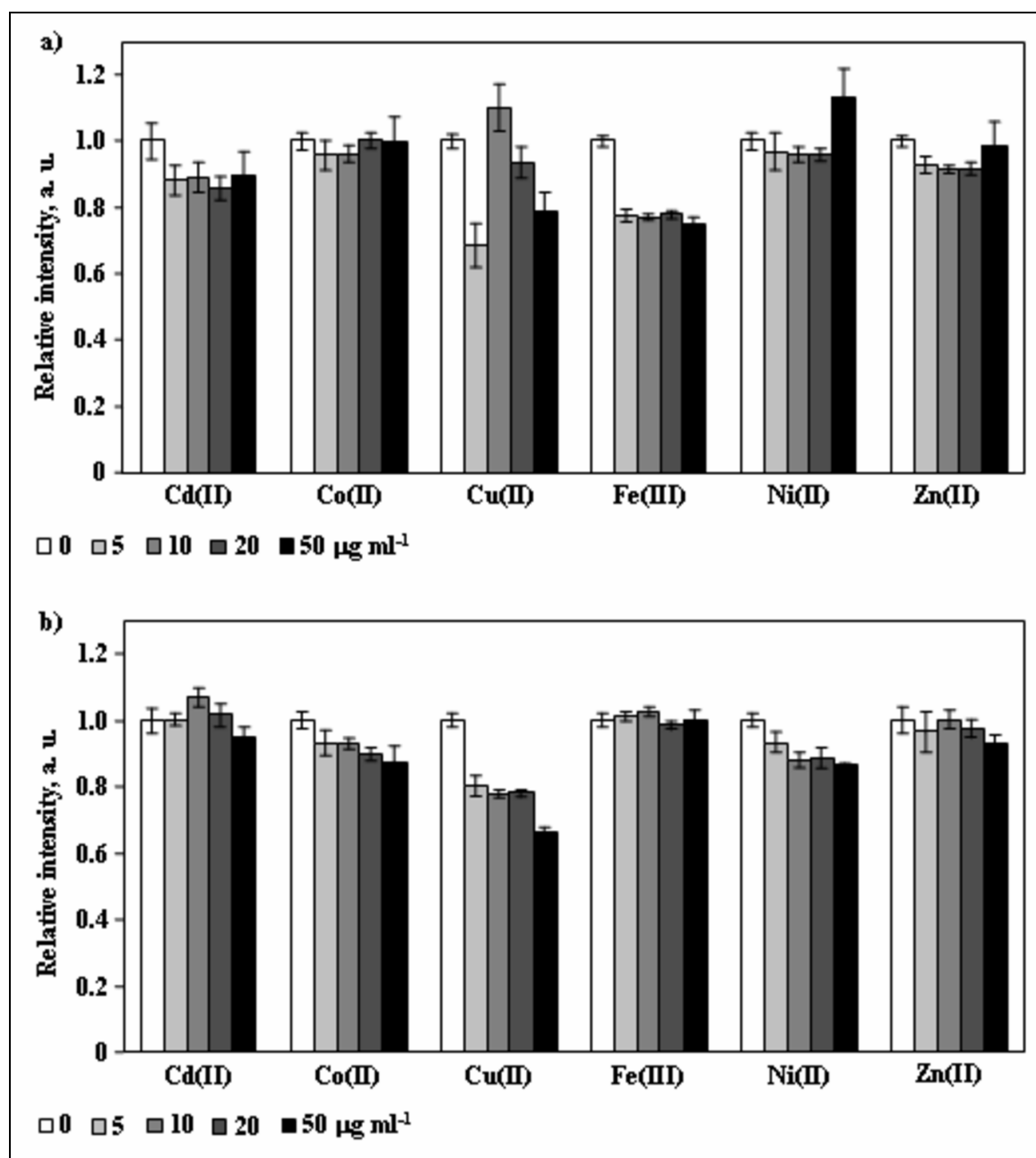


Fig. 41 Chemical interference of transition metals in the determination of Hg by the cold vapour generation technique when using NaBH_4 (a) and SnCl_2 (b)

Table 6. Influence of As, Bi, Sb and Se on the relative intensities for Hg when using the CV-MSP-OES procedure under optimized conditions.

	Interferent concentration, $\mu\text{g mL}^{-1}$			
	0	5	10	20
CV generation with NaBH_4				
As(V)	1.00 ± 0.02	1.02 ± 0.02	0.98 ± 0.03	1.00 ± 0.02
Bi(III)	1.00 ± 0.03	0.96 ± 0.05	0.96 ± 0.03	1.00 ± 0.02
Sb(III)	1.00 ± 0.04	1.04 ± 0.03	NM	NM
Se(IV)	1.00 ± 0.01	0.09 ± 0.01	0.16 ± 0.05	0.11 ± 0.02
CV generation with SnCl_2				
As(V)	1.00 ± 0.02	0.74 ± 0.02	0.74 ± 0.03	0.72 ± 0.01
Bi(III)	1.00 ± 0.02	0.86 ± 0.07	0.76 ± 0.07	0.70 ± 0.02
Sb(III)	1.00 ± 0.02	0.94 ± 0.01	0.96 ± 0.02	0.84 ± 0.04
Se(IV)	1.00 ± 0.02	0.95 ± 0.05	0.78 ± 0.03	0.68 ± 0.01

NM: Not measured.

Concentration of Hg: $0.2 \mu\text{g mL}^{-1}$. Average (n=3) \pm standard deviation

In the case of the CV generation using NaBH_4 , concentrations of $50 \mu\text{g mL}^{-1}$ of Co, Ni and Zn as well as As and Bi were found to cause no interferences in the determination of Hg. The interferent concentrations herewith can be 250 times higher than the concentration of Hg ($0.2 \mu\text{g mL}^{-1}$). This could be due to the relatively low concentration of reductant used for the CV generation reaction. For concentrations of 5 to $50 \mu\text{g mL}^{-1}$ of Cd and Fe a suppression of the signals for Hg by about 10 and 20 %, respectively, was found. This was not as strong as the effect reported for these metals by Krata *et al.* [185]. The effect of Cu was found to be more complex. At a concentration of $5 \mu\text{g mL}^{-1}$, the signal for Hg was depressed, which is most likely caused by an adsorption of the analyte on the reduced Cu [63]. Indeed, a brown deposit was found to cover the T-pieces. At a concentration of $10 \mu\text{g mL}^{-1}$ of Cu the signal for Hg was found to have increased, which is presumably due to some surface-mediated reactions of Hg hydroboron intermediates with reduced Cu deposited on the surface of the reaction system, as it was reported by Feng and co-workers [83, 186]. A very strong suppression of the signal for Hg was observed in the presence of Se even at the lowest concentration of this element investigated ($5 \mu\text{g mL}^{-1}$). This effect could be attributed to a formation of HgSe [185]. However, also a competition of the reaction of Se(IV) with NaBH_4 forming SeH_2 and the reaction of NaBH_4 with Hg(II) could be a reason [63, 180, 185]. In the case of Sb, a very intensive Sb I 252.8 nm line was observed as a consequence of the introduction of the SbH_3

produced by the reaction of Sb with NaBH_4 into the MSP. As a result of the occurrence of this line the background intensity in the vicinity of the Hg I 253.6 nm line changed, which complicated the measurement of the Hg line intensity.

When using SnCl_2 for the CV generation of Hg, the investigated metals did not cause any interferences except for Cu and Ni (Fig. 41). Their presence at a concentration of $50 \mu\text{g mL}^{-1}$ results in a reduction of the signal for Hg by about 30 and 10 %, respectively. The presence of As, Bi, and Se up to a concentration of $20 \mu\text{g mL}^{-1}$ was found to cause a decrease of the response for Hg by maximally 30 % and the presence of $20 \mu\text{g mL}^{-1}$ of Sb leads to a depression by 20 %. It could be expected that the interferences in the CV generation reaction using SnCl_2 are due to the formation of different intermetallic compounds with Hg [188].

CV-MSP-OES under the use of SnCl_2 as reducing agent was used for the determination of Hg in synthetic water samples containing $0.2 \mu\text{g mL}^{-1}$ of Hg and different amounts of NaCl as concomitant [146]. Under calibration with standard solutions containing Hg only, the recoveries for Hg at concentrations of NaCl of 1, 2 and 4 % (m/v) were 93 ± 3 , 90 ± 4 and 90 ± 4 %, respectively.

3.6.4 Figures of merit and analytical application

Under the optimized conditions the analytical performance of the cold vapour technique and MSP-OES for the determination of Hg was studied. In the case of the CV generation using NaBH_4 , the calibration curve for Hg was found to be linear up to $2 \mu\text{g mL}^{-1}$ with a correlation coefficient (R^2) of 0.999. The limit of detection for Hg, calculated according to the 3σ was found to be 9 ng mL^{-1} . This is better than the one reported in the literature for CV-MIP-OES using analyte preconcentration in a cryogenic trap [63]. The detection limit for Hg can be further improved, as it has been shown in the literature for CV-MIP-OES, by preconcentrating Hg by amalgamation [184] or by removing H_2 with a special membrane [189] after the reaction with NaBH_4 . The precision, in terms of the RSD for replicate measurements, was 0.5 and 5 % at concentrations of Hg of 2 and $0.1 \mu\text{g mL}^{-1}$, respectively.

The analytical performance under the use of SnCl_2 as reducing agent is better than in the case of NaBH_4 even after a careful optimization. The sensitivity is almost 12 times higher than the sensitivity obtained with NaBH_4 as reducing agent. The dynamic range, however, was shorter,

namely up to $1 \mu\text{g mL}^{-1}$, but the limit of detection for Hg was as low as 0.11 ng mL^{-1} . This is considerably lower than the detection limits of 0.64 and 1.1 ng mL^{-1} showed above for the CV generation with SnCl_2 in the case of Ar and He MSPs, respectively, which were fully sustained inside the gas channel of the microstrip wafer, or than the detection limit for Hg obtained in the case of an atmospheric pressure MIP realized in an MPT or a Beenakker cavity coupled with the CV generation under the use of SnCl_2 [182]. RSDs of 0.7 to 5 % at concentrations of 1 and $0.05 \mu\text{g mL}^{-1}$, respectively, were obtained.

3.6.5 Analysis of NIST SRM 2781

Cold vapour generation using SnCl_2 as reducing agent coupled to an MSP type B for OES was used for the determination of Hg in a domestic sludge NIST SRM 2781 at the optimal conditions mentioned above. Prior to chemical analysis, the SRM 2781 was digested following the procedure described by Sarawasti [147]. Under a calibration with standard addition a concentration of $3.55 \pm 0.41 \mu\text{g g}^{-1}$ for Hg was obtained, which is in good agreement with the certified value of $3.64 \pm 0.25 \mu\text{g g}^{-1}$.

3.7 Comparison of chemical and electrochemical hydride generation for the optical emission spectrometric determination of As and Sb using a miniaturized microwave induced Ar plasma exiting the microstrip wafer

The present study describes the comparison of CHG with ECHG for the determination of As and Sb by using an Ar MSP exiting the wafer as radiation source for OES. For the HG and MSP-OES systems the operating conditions were thoroughly optimized with respect to a maximum relative intensity of the background-corrected signal and a maximum signal-to-background ratio (SBR) of the used atomic emission lines for As (228.8 nm) and Sb (252.8 nm). Therefore, the concentrations of the reductant NaBH_4 and of HCl in the case of CHG as well as the electrolysis voltage and the concentrations of H_2SO_4 in the anolyte and catholyte for ECHG were subjected to a univariant optimization. Additionally, the effects of different reagents and the Ar carrier gas flow rates on the relative net intensities and the SBR values achieved by both HG-MSP-OES techniques were included in the optimization procedure. Further, the susceptibility of CHG and ECHG for the determination of As and Sb to interferences from transition metal ions and other volatile-hydride forming elements was studied. The data presented throughout this study are average values with standard deviations

based on 3 replicate measurements. The procedures further were applied to real sample analyses.

3.7.1 Optimization of CHG

3.7.1.1 Influence of the NaBH₄ concentration

With respect to the generation efficiency of volatile hydrides and the amount of H₂ co-produced in the reaction, the concentration of NaBH₄ is very critical. However, it also influences the performance of the total HG-MIP-OES procedure, especially in the case of low power atmospheric pressure MIP discharges [59, 163]. Hence, it is very important to carefully optimize this parameter to avoid plasma instability and to achieve optimum excitation conditions [160].

In this study, the influence of the concentration of NaBH₄ was investigated in the range from 0.05 to 0.4 % (m/v), based on results obtained for the optimization of a similar Ar MSP operated inside the wafer with a relatively low tolerance to the introduction of H₂ at volume flows higher than 5 mL min⁻¹. The HCl concentration of the sample was kept at 2 mol L⁻¹ and the reducing agent and sample solutions flow rates were set to 0.5 mL min⁻¹, while the Ar flow rate was adjusted to 9 mL min⁻¹.

An increase of the NaBH₄ concentration from 0.05 to 0.4 % leads to an improvement of the relative As signal from 0.15 ± 0.02 to 1.00 ± 0.01 and to an increase of the SBR from 1.37 ± 0.02 to 2.45 ± 0.02 . Contrary, the relative net intensity as well as the SBRs for the Sb line were found to decrease in the investigated NaBH₄ concentration range from 1.00 ± 0.12 to 0.77 ± 0.07 and from 3.31 ± 0.08 to 2.81 ± 0.09 , respectively. These observations well correspond with the results recently obtained for CHG coupled to an Ar MSP which is fully sustained inside the microstrip structure. It can be concluded that the described effect is related to strong changes in the AsH₃ and SbH₃ generation efficiency and in the plasma excitation characteristics. The CHG reaction for Sb was found to be very efficient even when low concentration of NaBH₄ are used, while the efficiency of the AsH₃ generation rather increases with an increasing NaBH₄ concentration. Furthermore, an increase of the H₂ volume flow from 0.4 ± 0.1 mL min⁻¹ to 4.7 ± 0.1 mL min⁻¹ within the investigated concentration

range of NaBH_4 was found to lead to a deterioration of the Sb signals, while in the case of As the corresponding effect is probably compensated for by a more efficient HG.

For further experiments a NaBH_4 concentration of 0.3 % was selected as a compromise for the determination of As and Sb and it results in a H_2 volume flow of $3.6 \pm 0.2 \text{ mL min}^{-1}$. The HG efficiencies then were found to be $94.9 \pm 0.3 \%$ for As and $95.4 \pm 0.6 \%$ for Sb. Under these conditions relative net intensities of 90 % were obtained for As and Sb, based on a 100 % signal intensity at the optimum conditions for As and Sb, respectively.

3.7.1.2 Influence of the sample and the reducing agent flow rates

To investigate the influence of the flow rates of the sample and the NaBH_4 solution on the signal intensities and the hydride and H_2 production rates, the reagents were delivered at equal rates between 0.30 and 0.80 mL min^{-1} using the same peristaltic pump, while NaBH_4 and HCl concentrations of 0.3 % and 2 mol L^{-1} , respectively, and an Ar flow rate of 9 mL min^{-1} were used.

In Fig. 42 the results of this optimization are shown by the corresponding relative net intensities for As and Sb normalized to the maximum achievable signal intensity. The relative net intensities of the As and Sb lines reach a maximum at a flow rate of 0.60 mL min^{-1} . The SBR shows a similar trend. Its values increase by about 20 % (As) and 10 % (Sb) at reagent flow rates of 0.30 and 0.60 mL min^{-1} , respectively. The amount of H_2 generated under these conditions increases from 1.9 ± 0.1 to $5.2 \pm 0.1 \text{ mL min}^{-1}$.

The highest relative net intensities for both As and Sb lines were found at reagent flow rates of 0.60 and 0.65 mL min^{-1} , respectively. For further experiments an optimum flow rate of 0.65 mL min^{-1} was selected, resulting in the production of $4.6 \pm 0.1 \text{ mL min}^{-1}$ of H_2 and generation efficiencies of 96 % for AsH_3 and SbH_3 .

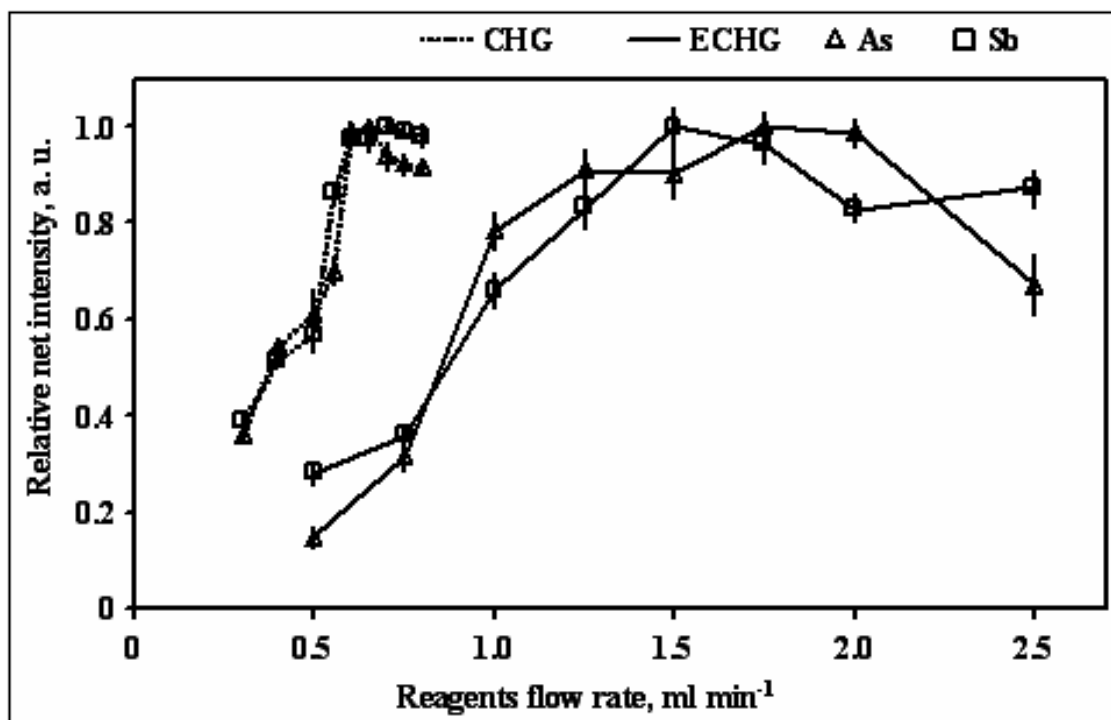


Fig. 42 Influence of the reagents flow rates on the intensities of the As I 228.8 nm and Sb I 252.8 nm lines as well as on their SBRs.

3.7.1.3 Influence of the concentration of HCl in the sample solution

The concentration of HCl used for sample acidification also seemed to be critical for the analytical performance of the CHG-MSP-OES procedure. Therefore, its influence on the analyte signals and on the hydride and H₂ generation rates was investigated in the range from 0.1 to 4 mol L⁻¹, while a NaBH₄ concentration of 0.3 % and reagents and Ar flow rates of 0.65 mL min⁻¹ and 9 mL min⁻¹, respectively, were used.

The influence of the HCl concentration on the response for As and Sb is shown in Fig. 43, and it is similar to the results reported for As and Sb in the case of CF-CHG combined with various types of MIPs [63, 157-159, 162, 163]. A concentration of HCl below 0.5 mol L⁻¹ leads to inefficient CHG, as the relative net intensities for both As and Sb lines are lower than 0.4 and 0.6, respectively, while signal maxima for both elements are reached at a concentration of 1 mol L⁻¹ of HCl.

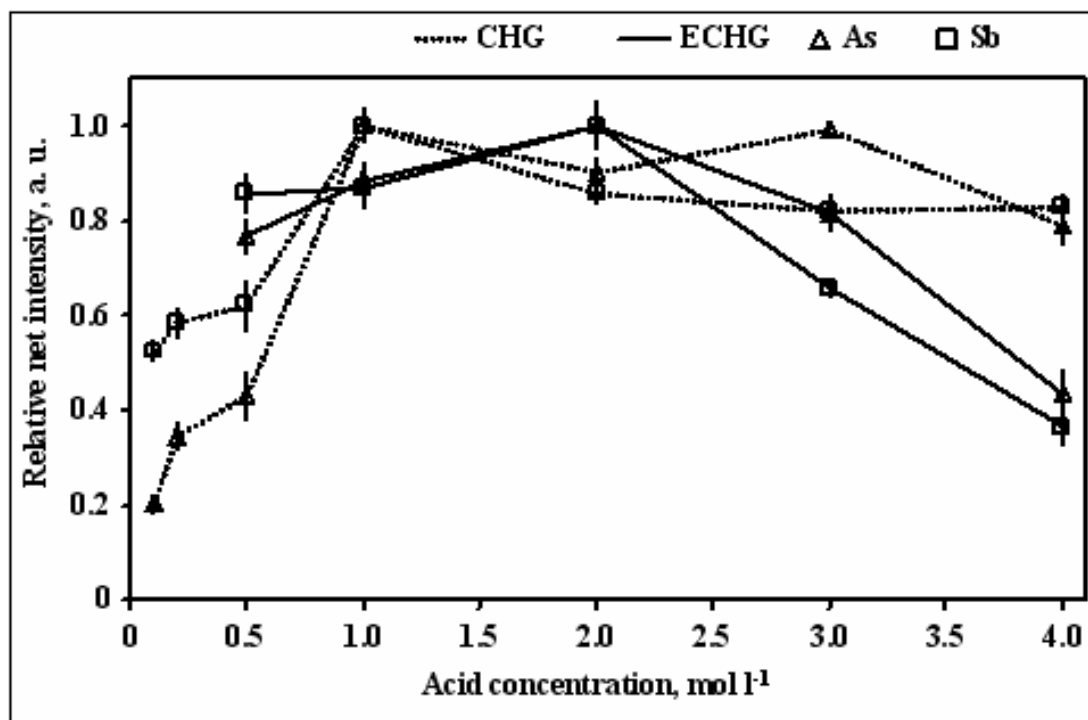


Fig. 43 Influence of the concentration of HCl on the intensities of the As I 228.8 nm and Sb I 252.8 nm lines and their SBRs

Interestingly, the volume of generated H_2 remains almost unaffected and is about 4.6 ± 0.2 mL min^{-1} at HCl concentrations in the range from 0.2 to 4 mol L^{-1} . In this case no significant changes of the spectral background signals could be observed. Therefore, the variations in the response for As and Sb can be attributed to changes in the CHG reaction efficiency only. Since the acid used for sample acidification causes a stepwise decomposition of NaBH_4 and a direct transfer of H atoms from NaBH_4 to the analytes [190, 191], of which the latter process is apparently slower at low HCl concentrations, one obtains a lower generation efficiency for AsH_3 and SbH_3 .

3.7.1.4 Influence of the Ar flow rate

The effect of the flow rate of Ar, used to sustain the MSP and to sweep the volatile hydrides and other CHG reaction by-products via the GLS to the plasma, on the analytical performance of the developed procedure was studied in the range from 6 to 36 mL min^{-1} , while NaBH_4 and HCl concentrations of 0.3 % and 1 mol L^{-1} , respectively, and reagent flow rates of 0.65 mL min^{-1} were used.

As it can be seen from the results given in Fig. 44, the highest relative net intensities for both As and Sb lines were found at Ar flow rates of 6 mL min^{-1} . When increasing the Ar flow rate above 9 mL min^{-1} the relative net intensities rapidly deteriorate. Also the SBR values decrease from 2.48 ± 0.04 to 2.02 ± 0.05 (As) and from 2.29 ± 0.05 to 1.87 ± 0.05 (Sb), when the Ar flow rate is increased from 6 to 36 mL min^{-1} . As the analytical line intensities were found to decrease twice as much as the background signals, it can be assumed that an increasing flow rate does not significantly lead to a collision-based de-excitation neutral Ar atoms in the case of the Ar MSP investigated, which would lead to a general increase of the background level [157]. Especially the lower residence time of the analyte hydrides in the plasma could be a reason for the observed signal drop, especially when considering the small dimensions of the MSP channel resulting in gas velocities of 0.3 to 2 m s^{-1} . An Ar flow rate of 9 mL min^{-1} was selected as optimum for all further measurements. Under the optimized conditions the volume flow of H_2 produced in CHG is 4.6 mL min^{-1} , leading to a H_2 concentration in the plasma working gas of 51 % (v/v). This high tolerance to H_2 is an outstanding advantage of the MSP exiting the wafer, as compared to other bulk MIP sources, such as a surfatron [163] or a microwave plasma torch [166]. This could be associated with the high electrical field density inside the plasma capillary channel as a result of its small diameter combined with the vicinity of the antenna.

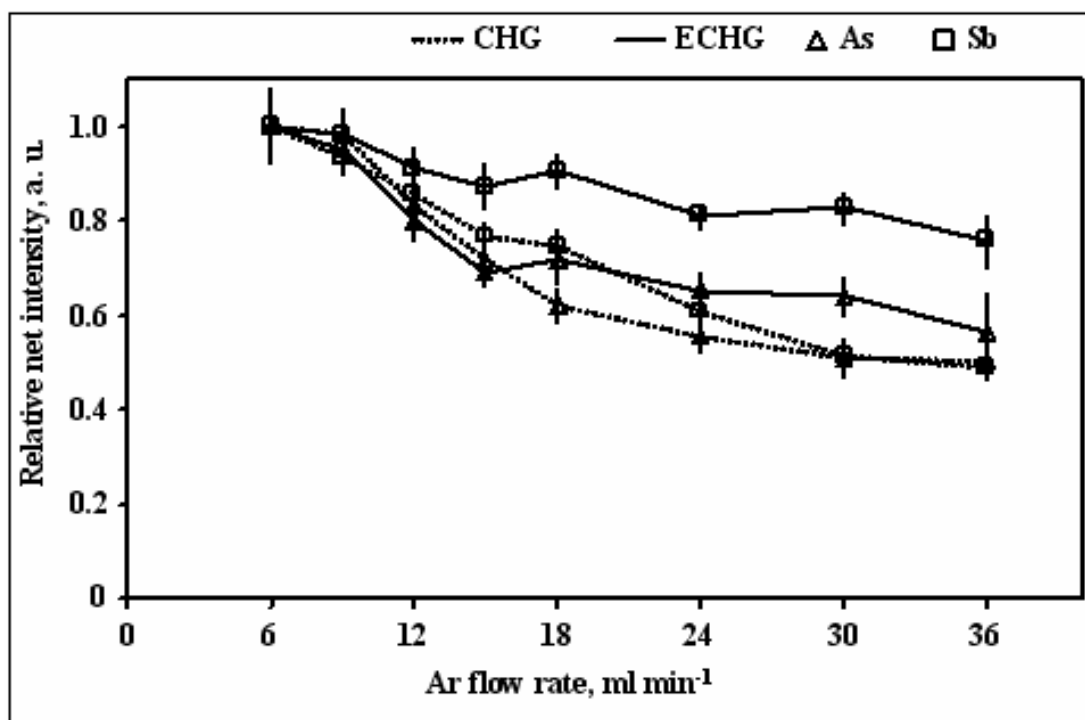


Fig. 44 Influence of the Ar flow rate on the line intensities for As and Sb in the CHG and ECHG.

3.7.2 Optimization of ECHG

3.7.2.1 Influence of the electrolysis voltage

The electrical current, which depends on the voltage applied to the electrodes and which therefore has to be selected according to the electrochemical potentials of the analytes, is one of the most important parameters to be optimized in ECHG. Indeed, it determines both the efficiency of the hydride formation and the amount of H₂ co-generated in this process [79, 147, 166]. In the present study, a three dimensional cathode made of a carbon fiber bundle was used and the electrolysis voltage was optimized in the range from 6 to 12 V, which led to electrolysis currents between 0.16 and 0.46 A. A concentration of 2 mol L⁻¹ H₂SO₄ in the anolyte and the catholyte, electrolyte flow rates of 2 mL min⁻¹ and an Ar flow rate of 9 mL min⁻¹ were used for the investigation.

When changing the potential from 6 to 10 V, it was found that the relative net intensities for the As and Sb lines increase from 0.42 ± 0.07 to 1.00 ± 0.06 (As) and from 0.36 ± 0.05 to 1.00 ± 0.08 (Sb), respectively. A further increase of the voltage to 12 V leads to a signal drop by about 20 % (As) and 10 % (Sb), respectively, as compared to the maximum signals at 10 V. The corresponding SBR values were found to linearly increase from 2.86 ± 0.09 to a maximum of 4.28 ± 0.10 at 10 V in the case of the As line and from 1.77 ± 0.10 to 2.28 ± 0.06 for the Sb line.

When increasing the electrolysis voltage, the efficiency of the electrochemical generation of AsH₃ and SbH₃ as well as of H₂ increase, which is indicated by a linear rise of the H₂ generation rate from 1.3 ± 0.1 to 3.0 ± 0.2 mL min⁻¹ within the observed interval. Apparently, up to 10 V the negative effect of the H₂ introduced into the MSP is compensated by the introduction and excitation of an increasing amount of As and Sb. This effect inverts when further increasing the applied electrolysis voltage. Finally, a potential of 10 V was chosen as an optimum value for further experiments, leading to a H₂ flow rate of 2.5 ± 0.1 mL min⁻¹ and AsH₃ and SbH₃ generation efficiencies of 40.8 ± 1.3 % and 38.9 ± 1.0 %, respectively.

3.7.2.2 Influence of the electrolyte flow rates

The anolyte provides for the transport of hydronium ions and water molecules through a membrane from the anode compartment to the cathode compartment, while the catholyte flow rate influences the residence time of the analytes inside the cell [117, 193, 194]. The effect of both flow rates was investigated within an interval of 0.50 to 2.5 mL min⁻¹, while remaining equal rates for both electrolytes. An electrolysis voltage of 10 V, a H₂SO₄ concentration of 2 mol L⁻¹ for the electrolytes and an Ar flow rate of 9 mL min⁻¹ were used for the investigation. As it can be seen in Fig. 42, a change of the flow rate of both electrolytes from 0.50 to 1.50 mL min⁻¹ leads to an increase of the relative net intensity for As and Sb as a result of the increase of the reaction efficiency in ECHG. Maximum signals were obtained at 1.50 mL min⁻¹ (As) and 1.75 mL min⁻¹ (Sb), while the sensitivity decreased at higher flow rates as a result of a too short residence time of the analytes in the cathode compartment. No specific trend was observed in the case of the SBR for both analytes, which indicates a proportional increase of the background signal, while the amount of generated H₂ remained unaffected by varying electrolyte flow rates. Correspondingly, for further experiments a compromise flow rate of the anolyte and the catholyte of 1.75 mL min⁻¹ were used.

3.7.2.3 Influence of the concentration of H₂SO₄ in the anolyte and the catholyte

Another factor influencing the efficiency of ECHG is the concentration of H₂SO₄ in the anolyte and the catholyte solutions [79, 116, 192]. In this study, different concentrations in the range between 0.5 and 4 mol L⁻¹ in both electrolytes were selected, while an electrolysis voltage of 10 V, anolyte and catholyte flow rates of 1.75 mL min⁻¹ and an Ar flow rate of 9 mL min⁻¹ were used.

It was found that the concentration of H₂SO₄ in the anolyte has no significant effect on the relative net intensities for the As and Sb lines within the investigated concentration interval, while an optimum value at 2 mol L⁻¹ was found for the case of the catholyte (Fig. 43). The signal drop at higher catholyte concentrations is probably not due to an increase of the volume of H₂, as different acid concentrations were found not to affect the H₂ generation rate. Rather a degrading diffusion of the analytes towards the cathode could be responsible, caused by the increasing density of the solutions at higher acid concentrations [193]. At lower H₂SO₄ concentrations low signals intensities were found for As and Sb, probably due to an

insufficient conductivity of the electrolyte. For further studies concentrations of H_2SO_4 of 1 mol L^{-1} (anolyte) and 2 mol L^{-1} (catholyte) were used.

3.7.2.4 Influence of the carrier gas flow rate

So as to study the influence of the Ar carrier gas flow rate on the signal intensities and the SBR values of As and Sb, optimum ECHG operating conditions were used, while the Ar flow rate was varied between 6 and 36 mL min^{-1} .

The results of this optimization are shown in Fig. 44, where the relative net intensity is plotted as a function of the carrier gas flow rate. The signals were found to clearly decrease at flow rates higher than 6 mL min^{-1} , which is most likely due to shorter residence times of the analytes within the plasma. However, the SBR for these analyte lines slightly increase with the Ar flow by about 10 and 20 %, suggesting that the analyte signal drop is slower than the respective drop of the background signal intensity. Therefore, due to a better precision, the optimum carrier gas flow rate was found to be 9 mL min^{-1} .

Under optimized conditions, the volume flow of generated H_2 is $2.5 \pm 0.1 \text{ mL min}^{-1}$, resulting in a H_2 concentration in the plasma working gas of about 28 % (v/v). The HG efficiency for As and Sb was found to be $40 \pm 1 \%$.

3.7.3 Interferences from transition metal ions and other volatile hydride-forming elements in CHG and ECHG

A wide variety of transition metal ions and other volatile hydride-forming elements are known to interfere with the generation and release of the hydrides of As and Sb in CHG as well as in ECHG, limiting the analytical applicability of both techniques [193, 195]. In this study, the susceptibility of both HG techniques combined with MSP-OES in the case of samples with $2 \mu\text{g mL}^{-1}$ of As and Sb to chemical interferences was investigated. Cd(II), Co(II), Cr(III), Cu(II), Fe(III), Ni(II), Pb(II) and Zn(II), as well as the volatile hydride-forming ions Bi(III), Hg(II), Se(IV) and Te(IV) were considered as potential interferents and their individual effects were evaluated, by ratioing the net intensities for the As and Sb lines stemming from solutions containing 5, 10, 20 and $50 \mu\text{g mL}^{-1}$ of the potential interferents with the respective net intensities obtained for solutions without interference. The resulting signals were

expressed as relative net intensities. In the case of ECHG, the effect of Pb was not investigated to avoid a precipitation of PbSO_4 , which could block the electrolysis cell.

3.7.3.1 Generation of AsH_3

As it can be seen in Fig. 45a, most significant interferences in the case of a determination of As with CHG are caused by Cd and Fe. The addition of Cd to a $2 \mu\text{g mL}^{-1}$ As solution leads to an increase of the As signal due to a spectral interference with the Cd I 228.8 nm emission line stemming from volatile Cd species generated under the used CHG conditions [197]. In contrast, the addition of $5 \mu\text{g mL}^{-1}$ of Fe already reduces the As signal by more than 70 %. Cr and Cu, as well as Co and Pb at concentrations of up to $50 \mu\text{g mL}^{-1}$ and $10 \mu\text{g mL}^{-1}$, respectively, do not significantly influence the response for As, whereas higher concentrations lead to a signal depression. While Ni, which is known to be a severe interferent in chemical AsH_3 generation [176], causes a signal suppression by 20 to 40 % when its concentration increases from 5 to $50 \mu\text{g mL}^{-1}$, the addition of up to $50 \mu\text{g mL}^{-1}$ of Zn leads to a signal drop of 15 % only.

In ECHG for the case of As, Cu was already found to cause serious interferences [193]. In this study, an addition of $5 \mu\text{g mL}^{-1}$ of Cu was found to cause a 40 % increase of the As signal, followed by a decrease of the response with an increasing amount of Cu added to the As solution to only 10 % at $50 \mu\text{g mL}^{-1}$ (Fig. 45b). Co and Ni were found to have no interfering effect on the determination of As by ECHG-MSP-OES, as it was also outlined by Ding and Sturgeon [124]. The addition of Cd as well as of Cr and Fe at concentrations higher than $10 \mu\text{g mL}^{-1}$ and $20 \mu\text{g mL}^{-1}$, respectively, was found to lead to a decrease of the analyte signal by 20-30 %.

Regarding the susceptibilities of CHG and ECHG for the determination of As to interferences more pronounced effects were caused by other volatile-hydride forming elements. The data obtained are given in Table 7 and show that, despite a significant loss of sensitivity, the determination of As by CHG is less affected by the presence of Bi, Hg, Se and Te than ECHG. In the latter case, Bi was found to cause an increase of the As signal to up to 90 %, as formerly reported for a similar electrolysis cell [192]. Se and Te were found to substantially reduce the efficiency for As in ECHG. A concentration of $10 \mu\text{g mL}^{-1}$ of these interferents

leads to a drop of the As signal by 50 % and 90 %, respectively, while the addition of small amounts of Hg results in a complete signal loss.

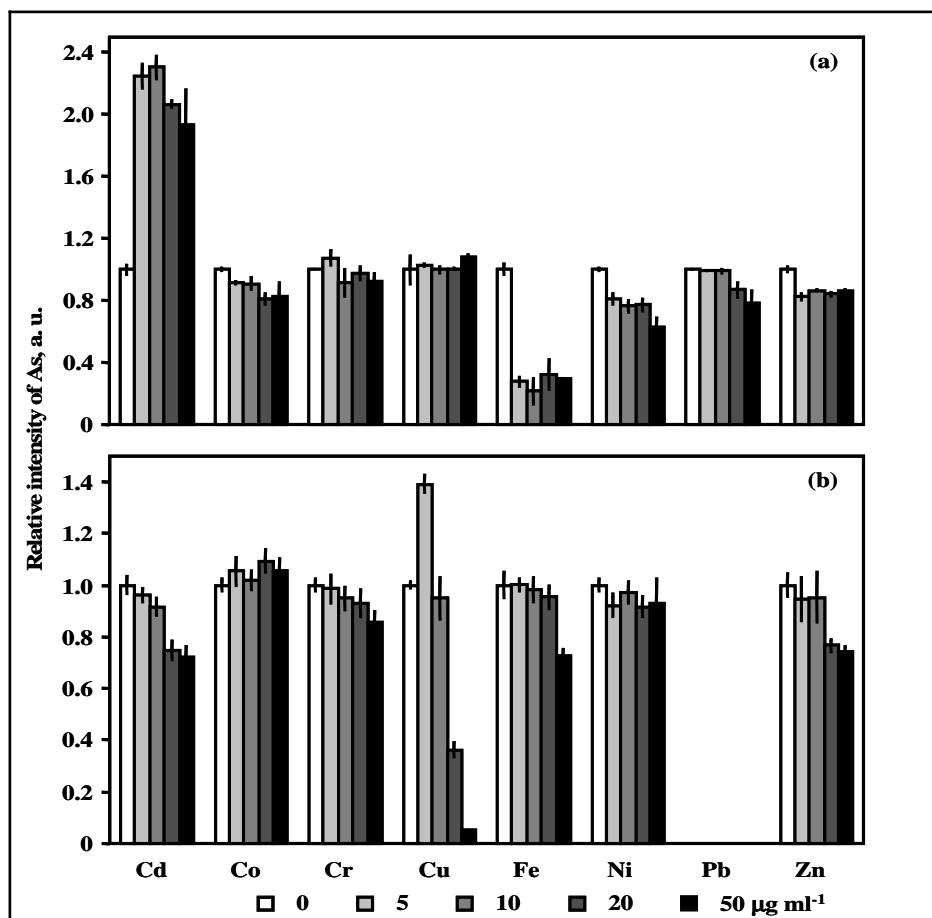


Fig. 45 Metal interferences in the determination of As by CHG (a) and ECHG (b) in MSP.

3.7.3.2 Generation of SbH_3

The efficiency of CHG for the determination of Sb was found to be strongly influenced by changes of the Fe content of the sample solutions, which for $2 \mu\text{g mL}^{-1}$ of Sb can be seen in Fig. 46a. A concentration of $5 \mu\text{g mL}^{-1}$ of Fe leads to a signal suppression of 80 %, while Co and Cr do not cause significant interferences within the investigated concentration interval of $5\text{-}50 \mu\text{g mL}^{-1}$. Cd at a concentration of $50 \mu\text{g mL}^{-1}$ leads to a drop of the Sb signal by 10 %, while $10 \mu\text{g mL}^{-1}$ of Pb cause a 20 % increase of signal. When added at a concentration of $50 \mu\text{g mL}^{-1}$ Cu and Ni, commonly known as strong interferences in CHG [174], suppress the response for Sb by 25 % and 20 %, respectively. In comparison to Ni, Cu is the stronger interferent, causing a 10 % signal drop when added in a concentration of only $5 \mu\text{g mL}^{-1}$. Zn

was found to be the weakest interferent. An addition of $50 \mu\text{g mL}^{-1}$ of Zn resulted in a signal loss of 5 % only.

In ECHG all investigated metal ions were found to seriously affect the SbH_3 generation efficiency. Cu again is the strongest interferent, since a concentration of $5 \mu\text{g mL}^{-1}$ Cu already leads for the Sb line to an intensity decrease of over 80 % and a complete signal loss at higher concentrations, as shown in Fig. 46b. Co as well as Cd and Fe were found to have a somewhat weaker influence on the Sb signal intensity. The addition of $5 \mu\text{g mL}^{-1}$ of the respective interferent leads to a decrease of the signal for the line of Sb by 20 % (Co) to 30 % (Cd, Fe). In comparison, the interferences caused by Cr, Zn and Ni were found to be significantly weaker, since $10 \mu\text{g mL}^{-1}$ (Cr, Zn) and $50 \mu\text{g mL}^{-1}$ (Ni), respectively, lead to a 20 % loss in signal.

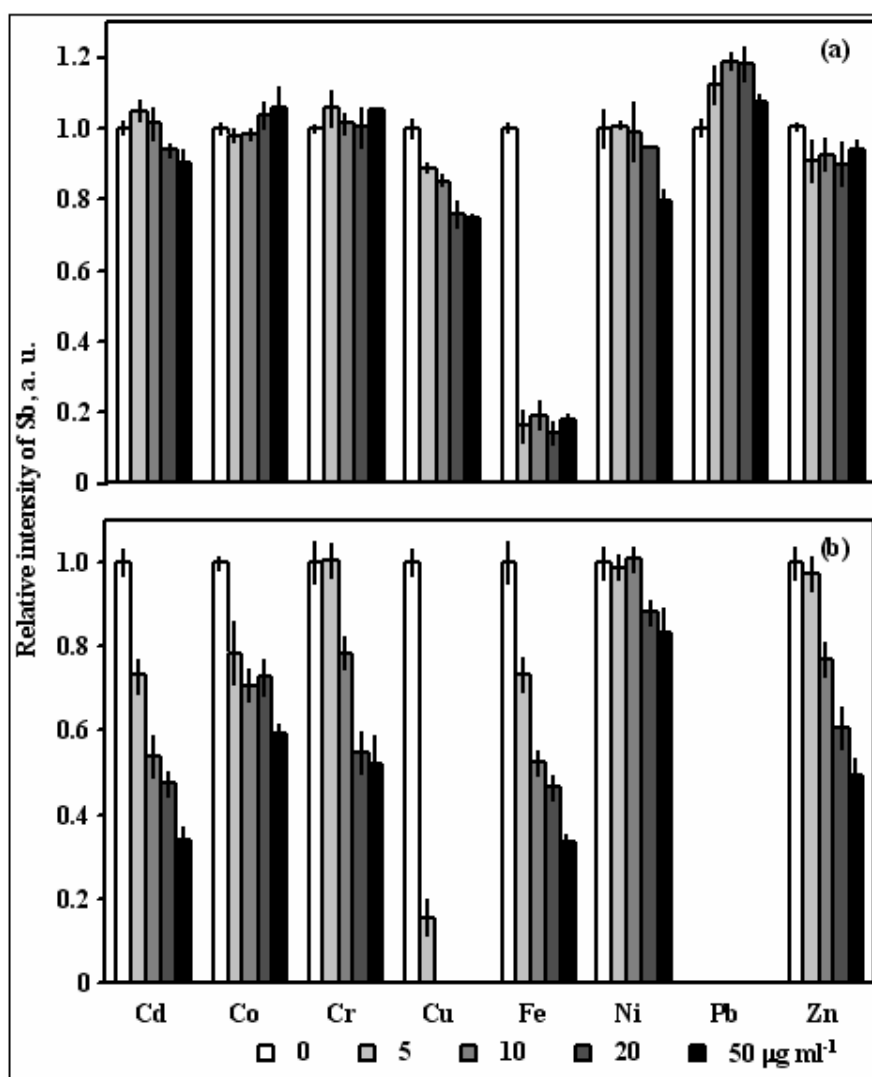


Fig. 46 Metal interference in the determination of Sb by CHG (a) and ECHG (b) and MSP-OES.

CHG and ECHG revealed significantly different susceptibilities to interferences by other volatile-hydride forming elements for the case of Sb. The data are summarized in Table 8 and indicate that CHG is mostly affected by the presence of Bi. An 80 % drop of the signal for the Sb line was found at a concentration of $20 \mu\text{g mL}^{-1}$. While Hg and Te do not significantly interfere in the case of Sb, Se leads to a maximum signal decrease of 30 %. To resume, the determination of Sb by ECHG is highly susceptible to interferences by all the examined volatile-hydride forming elements except for Bi, which at concentrations of 5 and $20 \mu\text{g mL}^{-1}$ leads to a suppression of the line intensity for Sb by 25 to 70 %, respectively.

Table 7. Influence of Bi, Hg, Se and Te on the relative intensities for the As 228.8 nm line when using CHG and ECHG coupled to MSP-OES under optimized conditions.

	Interferent concentration, $\mu\text{g mL}^{-1}$			
	0	5	10	20
CHG				
Bi(III)	1.00 ± 0.09	0.99 ± 0.01	0.88 ± 0.07	0.79 ± 0.09
Hg(II)	1.00 ± 0.02	0.97 ± 0.03	1.05 ± 0.08	0.91 ± 0.06
Se(IV)	1.00 ± 0.06	0.81 ± 0.01	0.73 ± 0.01	0.61 ± 0.01
Te(IV)	1.00 ± 0.01	0.86 ± 0.07	0.75 ± 0.10	0.70 ± 0.06
ECHG				
Bi(III)	1.00 ± 0.09	1.73 ± 0.18	1.87 ± 0.12	1.90 ± 0.13
Hg(II)	1.00 ± 0.05	ND	ND	ND
Se(IV)	1.00 ± 0.01	0.36 ± 0.04	0.13 ± 0.01	ND
Te(IV)	1.00 ± 0.03	0.70 ± 0.03	0.49 ± 0.01	0.36 ± 0.01

ND: Not detected.

Concentration of As and Sb: $2 \mu\text{g mL}^{-1}$. Average (n=3) \pm standard deviation.

Table 8. Influence of Bi, Hg, Se and Te on the relative intensities for the Sb line 252.8 nm in CHG and ECHG coupled to MSP-OES under optimized conditions.

	Interferent concentration, $\mu\text{g ml}^{-1}$			
	0	5	10	20
CHG				
Bi(III)	1.00 ± 0.02	0.56 ± 0.05	0.29 ± 0.01	0.21 ± 0.06
Hg(II)	1.00 ± 0.02	1.01 ± 0.04	1.00 ± 0.01	0.92 ± 0.04
Se(IV)	1.00 ± 0.04	0.90 ± 0.06	0.87 ± 0.02	0.69 ± 0.02
Te(IV)	1.00 ± 0.07	1.04 ± 0.10	0.99 ± 0.03	0.96 ± 0.10
ECHG				
Bi(III)	1.00 ± 0.06	0.75 ± 0.07	0.64 ± 0.08	0.33 ± 0.05
Hg(II)	1.00 ± 0.02	ND	ND	ND
Se(IV)	1.00 ± 0.08	ND	ND	ND
Te(IV)	1.00 ± 0.07	0.08 ± 0.01	ND	ND

ND: Not detected.

Concentration of As and Sb: $2 \mu\text{g ml}^{-1}$. Average ($n=3$) \pm standard deviation.

3.7.4 Analytical performance

Under the optimized conditions, the Ar MSP exiting the wafer can be combined with ECHG and CHG, but the amount of H_2 co-generated in the latter case is about 2 times higher than in ECHG. This, results in higher background intensities and lower intensities of the analyte lines, especially in the case of Sb. Therefore, the detection limits (3σ) for As and Sb were found to be 3 times lower in ECHG than in CHG. They are 6 ng mL^{-1} and 7 ng mL^{-1} for As and Sb in CHG, respectively, while the detection limits obtained in CHG-MSP-OES are 16 ng mL^{-1} for As and 22 ng mL^{-1} for Sb. Due to a better analytical performance the use of the MSP exiting the wafer is advantageous over the application of the MSP inside in the wafer and coupled with CHG. Furthermore, the detection limit obtained for As in the case of ECHG-MSP-OES is also significantly better than the previously reported values of 24 to 68 ng mL^{-1} , obtained when combining MPT-OES with different ECHG cells [192].

For the determination of As by MSP-OES, the detection limit of ECHG is more than 3 times better than in CHG, while for Sb a gain of still 25 % can be obtained. The linear dynamic ranges for As and Sb are similar for both HG techniques and span more than 2 orders of

magnitude (up to $5 \mu\text{g mL}^{-1}$). The achievable precision in CHG-MSP-OES, expressed as the relative standard deviation (RSD) of 3 consecutive measurements, using different As and Sb concentrations, is between 2 and 6 % for both analytes. This figure marginally deteriorates to 4 to 7 %, when ECHG is used instead of CHG.

3.7.5 Analysis of real samples and NIST SRM 1663a

ECHG-MSP-OES has been applied to the analysis of a galvanic bath sample, which was spiked with As to a concentration of $12 \mu\text{g mL}^{-1}$. A recovery of $99.2 \pm 5.0 \%$ was found for As and the determined Sb concentration of $6.59 \pm 0.28 \mu\text{g mL}^{-1}$ agrees well with the value of $6.89 \pm 0.18 \mu\text{g mL}^{-1}$, obtained through ICP-OES using pneumatic nebulization of the sample solution. Additionally, a tap water sampled at different locations in Hamburg was analyzed, after spiking with As and Sb to concentrations of $0.50 \mu\text{g mL}^{-1}$ each. The recoveries obtained were $101 \pm 5 \%$ for As and $98.9 \pm 2.6 \%$ for Sb.

The ECHG-MSP-OES procedure developed could also successfully be applied to the determination of As in a digested certified coal fly ash standard reference material (NIST SRM 1663a). The concentration value of $140 \pm 8 \mu\text{g g}^{-1}$ obtained agrees well with the certified value of $145 \pm 15 \mu\text{g g}^{-1}$.

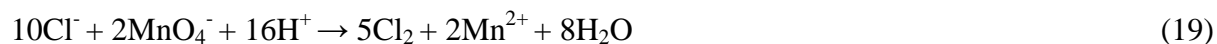
3.8 Determination of non-metals with the aid of an improved MSP exiting the wafer and optical emission spectrometry

Not only volatile-hydride forming elements but also elements which are volatile in their elemental form or which can be released under the form of other volatile compounds as a result of chemical reactions can be determined by MSP-OES. This will be shown at the hand of Cl, Br, S and C.

3.8.1 Generation of Br_2 and Cl_2

The continuous flow chemical generation of Br_2 and Cl_2 , from Br^- and Cl^- containing solutions was carried out through the addition of H_2SO_4 and KMnO_4 as oxidant. As compared to formerly reported works, in which an additional flow of a H_2SO_4 solution was used for the reaction [196-198] and KMnO_4 solutions were acidified with concentrated H_2SO_4 [197-199]

or mixed with a sample solution before the reaction [196], the procedure for Br₂ and Cl₂ generation proposed here uses a mixing an oxidizing agent solution with the sample solution containing Br⁻ and Cl⁻ after previously acidifying with H₂SO₄. The redox reactions taking place are:



The effect of the KMnO₄ concentration on the performance of the He MSP was studied in the range of 0.5-100 mmol l⁻¹. It was found that the most favorable concentrations of KMnO₄ for the oxidation of Br⁻ and Cl⁻ are completely different. In the case of Br⁻, only at very low KMnO₄ concentrations (1-5 mmol l⁻¹) high net intensities for the Br II 478.5 nm line are obtained. For the case of Cl⁻, however, the concentrations of KMnO₄ giving the maximal net intensity and SBR for the Cl I 439.0 nm line are about 10 times higher (10-30 mmol l⁻¹). Also in the H₂SO₄ concentration required for an efficient oxidation of both halides a large difference was observed. It was found that the generation of Br₂ can be carried out with H₂SO₄ solutions of a relatively low concentration. From a concentration of 4 mol l⁻¹ H₂SO₄ onwards no further increase in the signals for the Br line is observed. Contrary to the generation of Br₂, the signals for the Cl I 439.0 nm line could not be detected when the concentrations of H₂SO₄ in the solutions of Cl⁻ were lower than 5 mol l⁻¹. Indeed, the net intensity and the SBR for the Cl line were found to strongly increase when the H₂SO₄ concentration changed from 5 to 9 mol l⁻¹ and then stabilize at 10-12 mol l⁻¹. These results obtained with the introduction of Br₂ and Cl₂ into the He MSP well correspond with the findings reported in the literature for conventional MIP sources coupled to gas-phase sample introduction for Br⁻ and Cl⁻ [196-199]. Also here, milder conditions with respect to the concentrations of KMnO₄ and H₂SO₄ are required for the efficient generation of Br₂ than in the case of the oxidation of Cl⁻.

The highest net intensity and SBR for the Br II 478.5 nm line were obtained at reagent flow rates of 2-4 ml min⁻¹. Beyond or below this range, the signals for Br were found to gradually decrease. For the generation of Cl₂, a steady increase of the signal for the Cl line was observed when the flow rates of the oxidizing agent and the sample solutions increased from 1 to 9 ml min⁻¹. The flow rate of He was also found to have an important influence on the

analytical performance of the MSP, because it is relevant for the separation and the transport of gaseous Br₂ and Cl₂ from the GLS to the plasma and the stability of the MSP discharge. With our arrangement, however, no special time for stabilization was found to be required as compared for example to Ref. [199]. Steady state signals for Br and Cl could be obtained within less than 30 s. When considering the gas channel diameter (0.64 mm) and the length of the He MSP filament formed in the wafer (~ 5 mm), the plasma volume is lower than about 2 µl and the gas flow considerably affects the residence time of the analytes in the plasma. Indeed, the maximal analytical response for Br and Cl is obtained at very low He flow rates. Because Br₂ is heavier and less volatile than Cl₂ [197], it was also found that it requires a slightly higher flow rate (9 ml min⁻¹) for being transported than Cl₂ (3 ml min⁻¹).

3.8.2 Generation of H₂S

As previously reported by Nakahara *et al.* [200] for the continuous flow chemical generation of H₂S the solution containing S²⁻ can be mixed with a HCl solution, but HNO₃ and H₂SO₄ solutions could also be used:



A 2 mol l⁻¹ solution of HCl was found to be optimal for the generation of H₂S. The influence of the flow rates of the reagents and of the He on the signal of the S I 469.4 nm line was found to be considerable. Indeed, when increasing the flow rates of the reagents from 1 to 3 ml min⁻¹, the net intensity for the S line strongly increases and from 3 ml min⁻¹ reaches a plateau. The maximal net intensity and the SBR for the S line were found at a He flow of 3 ml min⁻¹. With a further increase of the He flow rate a gradual decrease of the response for S is observed.

Table 9. Optimized experimental conditions for the determination of Br⁻, Cl⁻ and S²⁻ by OES with the aid of a He MSP and gas-phase sample introduction.

	Br	Cl	S
He flow rate, ml min ⁻¹	9	3	3
Sample/reagent flow rates, ml min ⁻¹	3	9	3
Acid concentration, mol l ⁻¹	4 ^a	10 ^a	2 ^b
KMnO ₄ concentration, mmol l ⁻¹	5	20	—

^a H₂SO₄ added to sample.

^b HCl in separate stream.

3.8.3 Analytical performance

The limits of detection (LOD, 3σ) for Br^- , Cl^- and S^{2-} in the case of the He MSP coupled with a generation of gaseous halogens and hydrogen sulfide were found to be about one order of magnitude higher than those reported in the literature for conventional MIP sources combined with different gas-phase introduction systems [197-203]. Therefore, the LODs for Br^- , Cl^- and S^{2-} found in the case of the MSP are much lower than those obtained with other microplasmas, such as the CCP [204] or the DBD [205], coupled to GCs and combined with miniaturized spectrometers for atom line and/or molecular band detection.

Table 10 Figures of merit obtained for the determination of Br^- , Cl^- and S^{2-} by MSP-OES using He and gas-phase sample introduction

	Br II 478.5 nm	Cl I 439.0 nm	S I 469.4 nm
LOD, ng ml⁻¹	330	190	220
RSD^a (n=3), %	0.6 (100) – 4.3 (5)	0.9 (100) – 1.7 (5)	2.8 (500) – 3.5 (5)
Dynamic range, $\mu\text{g ml}^{-1}$	up to 100	up to 100	up to 500

^a The concentration of standard solutions (in $\mu\text{g ml}^{-1}$) are given in brackets.

3.8.4 Interferences

The effect of various metals and non-metals on the determination of Br^- , Cl^- and S^{2-} with MSP-OES using He and combined with gas-phase sample introduction was also studied. The tolerance limits for the various concomitants when generating Br_2 , Cl_2 or H_2S are given in Table 11.

As it can be seen in the case of the generation of Br_2 and Cl_2 , the examined metals and non-metal caused almost no interference up to concentrations being 100 times higher than the concentrations of Br^- and Cl^- . Only when CO_2 or HCN , respectively, are co-generated due to the presence of CO_3^{2-} and CN^- in the sample and introduced with Br_2 and Cl_2 into the He MSP, very intensive molecular bands in the wavelength region of 400-480 nm are found to complicate the intensity measurement for the Br II 478.5 nm and Cl I 439.0 lines. The same spectral interferences were observed for the S I 469.4 nm line.

In the case of the generation of H₂S, the interferences stemming from metals were not investigated due to a possible precipitation of the respective metal sulfides, however, the reaction was found to be free from interferences from anions such as Br⁻, Cl⁻, I⁻, SO₄²⁻, S₂O₃²⁻ and PO₄³⁻.

Table 11. Tolerance limits to interferences in the determination of Br⁻, Cl⁻ and S²⁻ (5 µg ml⁻¹) by MSP-OES using He and an introduction of gaseous Br₂, Cl₂ and H₂S

Ion added	Tolerance ratio		
	Br	Cl	S
Al ³⁺	10:1	100:1	— ^a
Cd ²⁺	100:1	100:1	— ^a
Co ²⁺	100:1	100:1	— ^a
Cu ²⁺	100:1	100:1	— ^a
Fe ³⁺	100:1	100:1	— ^a
Hg ²⁺	100:1	10:1	— ^a
Ni ²⁺	100:1	100:1	— ^a
Zn ²⁺	100:1	100:1	— ^a
Br ⁻	—	100:1	100:1
Cl ⁻	100:1	—	100:1
I ⁻	100:1	100:1	100:1
CN ⁻	10:1	— ^b	— ^b
NO ₃ ⁻	100:1	100:1	100:1
CO ₃ ²⁻	— ^b	— ^b	— ^b
SO ₄ ²⁻	100:1	100:1	100:1
S ₂ O ₃ ²⁻	100:1	100:1	100:1
PO ₄ ³⁻	100:1	10:1	100:1

^a Not investigated.

^b Spectral interferences.

3.8.5 Application to the determination of Br⁻, Cl⁻ and S²⁻ in tap water samples

To demonstrate the practical usefulness and the suitability of the developed procedure to the analysis of real samples, OES with a He MSP in combination with gas-phase sample

introduction was applied to the determination of Br^- , Cl^- and S^{2-} in domestic water samples. Water samples were directly taken from three different locations and due to a lack of Br^- and S^{2-} they were spiked with these anions up to concentrations of $10 \mu\text{g ml}^{-1}$. The concentrations of Cl^- found in the samples are 20.0 ± 0.3 , 20.1 ± 0.8 and $26.6 \pm 1.0 \mu\text{g ml}^{-1}$. These values are in very good agreement with the concentrations determined with ICP-OES, as shown by the results both methods which differ by less than 2%. The recoveries for the Br^- and S^{2-} added are in the range of 99.0 ± 1.7 to $102 \pm 2\%$, which demonstrate the good accuracy and the precision of the procedure.

3.8.6. Emission characteristics of the He MSP

Despite the low resolution of the USB2000 spectrometer, with which molecular bands are not resolved and spectral overlaps occur, as it has been observed for other microplasmas and microdischarges [206-210], some rotational bands of the diatomic molecules present in the He MSP can be identified, when introducing CO_3^{2-} and CN^- .

Indeed, the resolution of the USB2000 spectrometer used in this work is adequate enough for monitoring the selected atom and ion emission lines for the non-metals studied and for the identification of some rotational bands of various diatomic molecules in the He MSP, when loading it with Br_2 , Cl_2 , H_2S , CO_2 and HCN , respectively, as it is generated through the oxidation of Br^- and Cl^- and the acidification of S^{2-} , CO_3^{2-} and CN^- containing solutions.

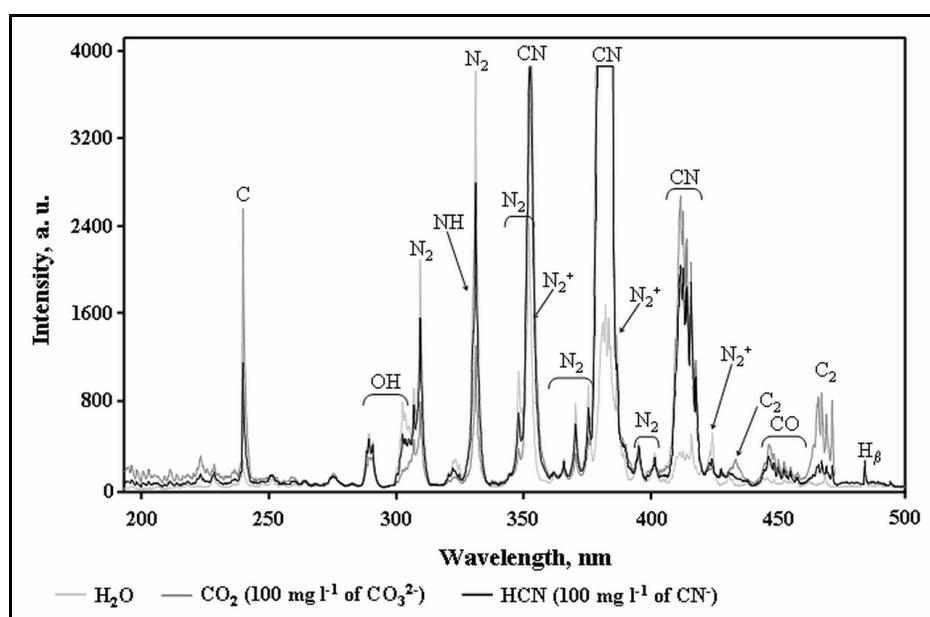


Fig. 47 Emission spectra of the He MSP.

As it can be seen from the results in Fig. 47, in the 294-301 nm and 306-320 nm wavelength regions [211] OH⁻ bands are found in the case of the He MSP when introducing H₂O into the gas-phase sample introduction system. Due to trace impurities of N₂ in He [208] an intensive head of (0-0) NH molecular band at 336.0 nm, overlapped by a very strong (0-0) N₂ band head at 337.1 nm, can be observed in the 330-340 nm wavelength region [212]. Very intensive (1-0) and (0-1) N₂ molecular bands with heads at 315.9 and 357.6 nm, respectively, can also be found. In the case of the (0-1) N₂ band, two additional rotational lines at 353.7 and 350.2 nm can also be observed. Less intensive (0-2) and (0-3) N₂ bands with heads at 380.5 and 405.9 nm, respectively, and rotational lines at 366.1, 371.0 and 375.5 nm (0-2 transition) and 399.8 nm (0-3 transition) are observed as well [212]. The band heads at 358.2 nm (1-0 transition), overlapped by the (0-1) N₂ band at 391.4 nm (0-0 transition) and at 427.8 nm (0-1 transition) can be attributed to the presence of N₂⁺ radicals [211].

When introducing the CO₂ and HCN, resulting from the acidification of CO₃²⁻ and CN⁻ containing solutions with HCl, the NH, N₂ and N₂⁺ molecular bands coincide with strong CN⁻ violet bands, of which the heads are at 359.0 nm (1-0 transition) and 388.3 nm (0-0 transition) [212]. Three other rotational lines of this CN⁻ band are found at 385.5, 386.2 and 387.1 nm. Another (0-1) CN violet band is observed in the spectral region of 412-424 nm and has its head at 421.6 nm and four additional rotational lines belonging to this band are found at 415.9, 416.7, 418.0 and 419.7 nm, respectively. Along with CN⁻ bands, rotational bands of CO in the wavelength region of 446-463 nm (Angstrom band) and C₂ in the wavelength regions of 433-440 nm and 464-477 nm (Swan bands) can also be identified [212]. In the case of the (1-0) C₂ Swan molecular band, the head is at 473.7 nm and three additional rotational lines are observed at 468.4, 469.7 and 471.5 nm, respectively. Additionally, it was found that the intensities of the NH, N₂ and N₂⁺ bands significantly decrease when C containing gases (CO₂, HCN) are introduced into the He MSP as the production of CN and C₂ radicals in the plasma obviously is more favorable under these conditions.

As working gas lines, the H I 486.3 nm line (H_β) and two He atom lines at 492.2 and 501.6 nm could be identified. When introducing CO₂ and HCN into the He MSP, a very intensive C I 247.9 nm line also appears. When Br₂, Cl₂ and H₂S are generated and introduced into the He MSP, an intensive Br II 478.5 nm line interfered by the less intensive Br I 478.0 nm line [199], a weak Cl II 481.9 nm line and two more intensive Cl atom lines, at 439.0 and 452.6 nm, respectively, [196] as well as a strong S I 469.4 nm line, interfered with two other

closely-spaced S atom lines at 469.5 and 469.6 nm, respectively, [213] are found in the He MSP spectra.

E. Conclusions and outlooks

The trend to miniaturized analytical systems with easy to be tuned and low-cost small sources corresponds to the need to perform multielemental analyses with portable equipments for in-situ use. In this context microplasmas based on microstrip technology (MSP) with microwave discharges inside and exiting a sapphire wafer coupled to different sample introduction techniques have been studied. The compact design of the MSP has been shown to allow it to form stable discharges with a low power input (40 W) at a frequency of 2.45 GHz. They can be coupled by very simple components like a sub-miniaturized connector type A (SMA) and a small antenna easy to a generator. MSPs with different gases, such as Ar and He, can be operated with low gas flow rates (3-15 ml min⁻¹) and used to determine metals and non-metals, respectively. In addition, MSP discharges were shown to have a very long term stability. Due to the small plasma discharge size (\approx 3-4 mm) sample introduction techniques, where gaseous products are produced by chemical reactions, can be coupled to MSPs in a continuous flow sample introduction mode and the MSP was shown to be resistant to a loading with dry aerosols and molecular species.

A miniaturized USB2000 Ocean Optics spectrometer with a Sony ILX511 high-performance 2048-pixel linear CCD array for optical emission spectrometry (OES) was shown to be ideally suited to resolve and measure the analyte signals by sampling radiation emitted by the plasma source through a fiber cable with a lens at the tip. An USB-port eases the connection of the spectrometer to a portable personal computer, which eliminates the need for external A/D converter. This reduces the size of the complete analytical system. Nevertheless, in a number of cases limitations arising from an insufficient resolution of the spectrometer or from a restricted wavelength coverage must be taken in account. Through the spectral range from 200 nm to 500 nm, intensive analytical lines especially for the non-metals being at wavelengths of up to 950 nm could not be detected.

The features explained above made it possible to use the MSP as analytical radiation source for element determinations, in an easy coupling with continuous flow sample introduction including different gas-liquid phase separators. It was found absolutely necessary, however, to dry the loaded Ar and He which act as analyte carrier and plasma working gas, before their entering into the microplasma source. Therefore, it was found more effective to conduct the gas stream through a 10 mL vessel filled with H₂SO₄ so as to separate the analyte from the

moisture and to avoid deterioration of the analyte signals. Other manifolds investigated suffer from short-life time and low drying efficiency, which is the case with $\text{Mg}(\text{ClO}_4)_2 \cdot x\text{H}_2\text{O}$, filled tubes or long analyte transportation lines, as it is the case with a Liebig condenser.

The MSP has some drawbacks as a result of its small size through which wet aerosols would extinguish it. Therefore dry analytes can be well excited as a result of the rather high excitation temperatures and electron number densities, which are near to those of analytical ICPs.

Therefore, Ar and He MSPs are suitable for being coupled with the Hg cold vapour generation technique using SnCl_2 as reducing agent. The MSP sustained with Ar as working gas was found to have the better analytical performance. With Ar the T_{exc} and n_e were also found to be higher than with the He plasma.

CHG has been used for the simultaneous determination of As and Sb in the present work. It was found that an MSP sustained inside the wafer could be operated with noble gases containing 28% of H_2 , being reaction by-products. The use of a small concentric gas-liquid phase separator, which keeps the liquid level at a constant volume, allows it to have short washing times and to keep the internal system pressure constant, by which fluctuations of the analytical signals are avoided. The efficiency of the HG reaction was found to be strongly affected by the concentration of NaBH_4 , the type and the concentration of acid used as well as the dynamics of the reagents mixing. In our work finally HCl was used. Analytical parameters such as the concentration of NaBH_4 and the flow rate of the reagents were found to have an effect on the decomposition rate of NaBH_4 as well as on the amount of H_2 liberated in the reaction. It was also demonstrated that some interferences only occur as a result of the catalysis of or the competition with hydride forming elements. This was the case for Cd, which has an analytical line at 226.5 nm with a tail for the As I 228.8 nm line. Some elements that have been demonstrated to give serious interferences in HG were, however, found to have no special effect on the As and Sb analytical line intensities at low reductant concentrations as used in the present work. Masking agents added to the sample solution and/or to the reductant solution in small-scale systems were found to be not very effective and their use was avoided.

It was found that the MSP exiting the wafer can be easily viewed end-on without suffering from space-angle limitations. Both reducing agents, NaBH_4 and SnCl_2 could be used for the reduction of Hg(II) in acidic solutions to its volatile elemental form. NaBH_4 is very often preferred over SnCl_2 as the reduction of both inorganic and organic Hg is more effective and faster. However, in the reaction using NaBH_4 , the vapours of Hg are accompanied by an excess of H_2 , which may considerably affect the analytical performance, when it is introduced into the radiation source. With both reductants, it was found that the MSP exiting the wafer could be stably operated with a low power and a low working gas flow. With both reductants, a reasonably fair analytical performance could be obtained. Under the optimized conditions, the detection limit for Hg of CV-MSP-OES in the case of SnCl_2 , however, was found to be lower than the one obtained with the same experimental set-up under the use of NaBH_4 as reductant. Indeed, the co-generated H_2 in the CV generation reaction was found to deteriorate the excitation of Hg in the Ar MSP, despite the plasma still tolerated the introduction of H_2 at a level of several mL min^{-1} .

CHG in the case of an MSP exiting the wafer offers favorable conditions for the excitation of As and Sb, but the water moisture and the excess of H_2 co-generated with the volatile hydrides, often lead to a deterioration of the plasma and excitation conditions. Particularly the introduction of a high amount of H_2 , which has a higher thermal conductivity than Ar and a high dissociation temperature, often results in a deterioration of the analytical performance of the CHG-MSP system with respect to achievable precision and the detection limits. Instead of using CHG with NaBH_4 as a reducing agent, which in addition is a source of sample contamination and only can be kept when prepared in alkaline solution, electrochemical hydride generation (ECHG) in a miniaturized electrolysis cell can be used as an alternative. It has been shown, that a such approach allows a better analytical performance in the case of the MSP, due to the reduced volumes of co-generated H_2 , as compared with CHG. In a miniaturized ECHG system we could use a carbon bundle fiber as cathode material because of its inertness, easy fabrication, low electrical resistance, low cost and large potential window and a platinum rod as anode material. A Nafion membrane was used to separate the anode and the cathode compartments.

From the economical point of view ECHG has many advantages as compared to CHG because expensive reagents, which must be daily prepared and kept at a high pH, are not required. In ECHG the reagent solutions partly can be recovered and recirculated through the

analytical system saving time. In our case, however, the small cell size did not make it possible to recirculate the acid solution through the anode compartment. Because of the deposition of transition metals on the cathode surface, which pollutes it irreversibly, ECHG has been shown to have interferences from transition metals and from other volatile-hydride forming elements.

The Ar-MSP exiting the sapphire wafer has been demonstrated to have better analytical performance than the MSP with the plasma sustained inside the wafer. In view of the availability of battery-powered microwave oscillators and of miniaturized and portable spectrometers, the MSP emission source in combination with CF-HG and ECHG can be an integrated part of measurement devices fulfilling the requirements of the micrototal analysis systems (μ -TAS). Further improvements of the features of CF-HG-MSP-OES may lie in the use of membranes, which enable it to better separate the by-products from the analyte generation. The by-products decrease the operation stability of the MSP. A reduction of their amounts is also a result of a decrease of the consumption of the reagents.

The last part of the study was focused on the use of a He MSP exiting from the wafer for the determination of Br^- , Cl^- and S^{2-} using a continuous gas-phase sample introduction. He was used because of its line poor spectrum between 400 and 500 nm and the possibility to excite non-metals. The limits of detection found for Br^- , Cl^- and S^{2-} are at the 100 ng ml^{-1} level and well correspond to those obtained with other miniaturized plasmas. As mentioned before in the comparison of the use of Ar and He plasmas in combination with Hg cold vapour generation, He needs a higher microwave power to adequately excite non-metals. Another point is the separation of the analyte which is liberated with the aid of the He flow sent through the gas-liquid phase separator from the bottom. This gas flow carries away moisture from the reaction solution that may deteriorate the plasma stability. High acid concentrations in the determination of Cl and Br (around 50 % of the volume of the total sample is H_2SO_4) were found to be required so that the use of a loop for the reagents mixing might be favorable.

The limit of detection obtained for C is 100 times lower than for Br^- , Cl^- and S^{2-} and much better than the one reported for miniaturized dc-glow discharge or CCP sources coupled to GC. Intensive C_2 , CN, CO, NH, N_2 and N_2^+ molecular bands, in addition to Br, Cl, S and C atom and ion lines observed in the He MSP spectrum could readily enable the detection of volatile hydrocarbons and halogenated hydrocarbons or industrial inorganic gases in GC

effluents. As compared to MIP sources operated in resonant cavities or surfatrons, the He MSP has the additional benefit of a 2-5 times lower power and a 20-170 times lower gas consumption. Therefore, this radiation source is well suitable for on-line analyses and monitoring. When using a miniaturized CCD spectrometer a substantial reduction in the size of the instrumentation is obtained additionally.

Generally, it was necessary to use standard addition to obtain the full accuracy of the developed procedures. For validation, synthetic and real samples as well as NIST SRMs were analyzed. Synthetic samples containing NaCl at concentrations of up to 6% were found to suffer from light interferences in the Hg response for both Hg cold vapour generation procedures studied. Real samples such as natural waters and a galvanic bath solution as well as a solution of the NIST SRMs 1633a domestic sludge and 2781 coal fly ash obtained with the aid of microwave-assisted digestion show good recoveries, when comparing to the certified values or results obtained with alternative methods.

For the generation of the volatile species also the use of UV-photoreactions should be considered. This is a possibility to extend the method also to a series of transition metals and further non-metals.

F. Instruments and chemicals

Instruments

- Power oscillator: Dirk Fischer Elektronik, Germany.
- Voltage regulator: type 2231.1, Statron Geratechnik, Germany.
- Mass flow-meter: type F-201C-FB-33V, Bronkhorst High-Tec B.V., Netherlands.
- Optical fiber: 600 μm diameter, FC-UV600-2SR, Avantes, USA.
- Kevlar reinforced PVC jacket: 3.8 mm outer diameter.
- Collimating lens: COL UV/VIS, 6 mm in diameter.
- USB 2000 spectrometer (Ocean Optics Inc., USA) with a build-in Sony ILX511 2048-element linear silicon CCD array detector.
- Three-dimensional miniaturized home-made electrolysis cell.
- Anode: Pt rod (1.5 mm diameter, 45 mm length).
- Cathode: bundle of fibrous carbon (45 mm length).
- Peristaltic pumps: Spetec, Germany.
- ICP-OES using pneumatic nebulization: SPECTRO CiroscCD, Spectro, Kleve, Germany.
- Zeeman 3030 AA Spectrophotometer with HG-600 furnace and AS-60 autosampler: Perkin-Elmer, Germany.

Chemicals

For the preparation and dilution of the solutions bidistilled water from a home-made distillation system was used.

- $\text{SnCl}_2 \cdot \text{H}_2\text{O}$, Merck, Germany.
- NaBH_4 , Merck, Germany.
- As (III), Merck, Germany.
- As (V), Merck, Germany.
- Sb (III), Merck, Germany.
- Hg (II), Merck, Germany.
- NaBr, Merck, Germany.

- Na_2S , Merck, Germany.
- NaCl , Merck, Germany.
- NaOH , Merck, Germany.
- HCl , Merck, Germany.
- HNO_3 , Merck, Germany.
- H_2SO_4 , Merck, Germany.
- $\text{Mg}(\text{ClO}_4)_2 \cdot \text{XH}_2\text{O}$, Merck, Germany.
- Cd- Standard Solution, Merck, Germany.
- Co- Standard Solution, Merck, Germany.
- Cr- Standard Solution, Merck, Germany.
- Cu- Standard Solution, Merck, Germany.
- Fe- Standard Solution, Merck, Germany.
- Mn- Standard Solution, Merck, Germany.
- Ni- Standard Solution, Merck, Germany.
- Pb- Standard Solution, Merck, Germany.
- Zn- Standard Solution, Merck, Germany.
- Bi- Standard Solution, Merck, Germany.
- Se- Standard Solution, Merck, Germany.
- Te- Standard Solution, Merck, Germany.
- ICP-Standard IV solution. , Merck, Germany.

Gases:

- Ar 4.8, Westfalen, Germany
- He 4.6, Westfalen, Germany

National Institute of Standards and Technology (NIST) Standard Reference Materials (SRM):

- NIST coal fly ash SRM 1633a.
- NIST domestic sludge, SRM 2781.

Samples:

- Domestic water from University of Hamburg and different sampling points in Hamburg.
- Water sample from Alster Lake and Elbe River in Hamburg.
- Galvanic bath solution, Atotech, Berlin, Germany.

G. References

- [1] M. Huang, D.S. Hanselman, Q. Jin and G. M. Hieftje, Non-thermal features of atmospheric-pressure argon and helium microwave-induced plasmas observed by laser-light Thomson scattering and Rayleigh scattering, *Spectrochim. Acta*, 45B, 1339-1352 (1990).
- [2] A. Manz, N. Graber and H.M. Widmer, Miniaturized total chemical analysis systems: a novel concept for chemical sensing, *Sens. Actuators, B* 1, 244-248 (1990).
- [3] J.P. Kutter and O. Geschkes, in: O. Geschkes, H. Klank and P. Telleman (Editors), *Microsystems engineering of lab-on-a-chip devices*, Wiley-VCH, Weinheim, Germany (2004).
- [4] P.A. Greenwood and G.M. Greenway, Sample manipulation in micro total analytical systems, *Trends Anal. Chem.*, 21, 726-740 (2002).
- [5] B.H. Weigl, R.L. Bardell and C.R. Cabrera, "Lab-on-a-chip for drug development," *Adv. Drug Delivery Rev.*, 55, 349-377 (2003).
- [6] O. Geschke, H. Klank and P. Telleman (Editors), *Microsystems engineering of lab-on-a-chip devices*, Wiley-VCH, Weinheim, Germany (2004).
- [7] T. Vilknær, D. Janásek and A. Manz, Micro total analysis systems. Recent developments, *Anal. Chem.*, 76, 3373-3386 (2004).
- [8] J.A.C. Broekaert, *Analytical atomic spectrometry with flames and plasmas*, Wiley-VCH, Weinheim, Germany (2001).
- [9] R. Kellner, J. M. Mermet, M. Otto and H. M. Widmer, *Analytical chemistry*, Wiley-VCH, Weinheim, Germany (1998).
- [10] A. Montaser and D.W. Golightly, *Inductively atomic plasma in analytical atomic chemistry*, VCH Publishers, New York, U.S.A. (1987).
- [11] D. A. Skoog and J.J. Leary, *Instrumental analysis*, Springer, Berlin, Germany (1996).
- [12] G.W. Johnson, H.E. Taylor and R.K. Skogerboe, Evaluation of solute vaporization interference effects in a direct current plasma, *Anal. Chem.*, 51, 2403-2405 (1979).
- [13] M. Margoshes and B.F. Scribner, The plasma jet as spectroscopic source, *Spectrochim. Acta*, 15B, 138-145 (1959).
- [14] T.B. Reed, Induction coupled plasma torch, *J. Appl. Phys.* 32, 821-824 (1961).

- [15] S. Greenfield, I.L.W. Jones and C.T. Berry, High-pressure plasmas as spectrometric emission source, *Analyst*, 89, 713-720 (1964).
- [16] R.H. Wendt and V.A. Fassel, Induction coupled plasma spectrometric excitation source, *Anal. Chem.*, 37, 920-922 (1965).
- [17] M. Huang, S.A. Lehn, E.J. Andrews and G.M. Hieftje, Comparison of electron concentrations, electron temperatures, gas kinetic temperatures and excitation temperatures in Ar ICP operated at 27 and 40 MHz, *Spectrochim. Acta*, 52B, 1173-1193 (1997).
- [18] L. Edbon, A. Fisher and S.J. Hill, *An introduction to analytical atomic spectrometry*, John Wiley and Sons, New York, U.S.A. (1998).
- [19] D.J. Kalnicky, R.N. Kniseley and V.A. Fassel, Inductively coupled plasma-optical emission spectrometry. Excitation temperatures by analyte species, *Spectrochim. Acta*, 30B, 511-525 (1975).
- [20] B. Raeymaekers, J.A.C. Broekaert and F. Leis, Radially resolved rotation temperatures in nitrogen-argon and argon inductively coupled plasmas, *Spectrochim. Acta*, 43B, 941-949 (1988).
- [21] J.D. Cobine and D.A. Wilber, The electronic torch and related high frequency phenomena, *J. Appl. Phys.*, 22, 835 (1951).
- [22] W. Schmidt, Der mikrowellen-plasmabrenner, *Elektron. Rundschau*, 11, 404-406, (1959).
- [23] R. Mavrodineanu and R.C. Hughes, Excitation in radio-frequency discharges, *Spectrochim. Acta*, 19B, 1309-1317 (1963).
- [24] H.P. Broida and J.W. Meyer, Spectroscopic analysis of deuterium in hydrogen-deuterium mixtures, *J. Opt. Soc. Am.*, 42, 37-41 (1952).
- [25] H. Feuerbacher, A new CMP excitation source for optical emission spectroscopy, *ICP Inf. Newsl.*, 6, 571-575 (1981).
- [26] W. Tappe and J. Van Calker, Quantitative specktrochemische Untersuchungen mit hochfrequenten Plasmaflammen, *Fresenius'Z. Anal. Chem.*, 198, 13-20, (1963).
- [27] C.I.M. Beenakker, A cavity for microwave-induced plasmas operated in helium and argon at atmospheric pressure, *Spectrochim. Acta*, 31B, 483-487 (1976).
- [28] B.D. Quimby, P.C. Uden and R.M. Barnes, Atmospheric pressure helium microwave detection system for gas chromatography, *Anal. Chem.*, 50, 2112-2118 (1978).

- [29] C.B. Motley, M. Ashraft-Khorassani and G.L. Long, Microwave-Induced plasma as an elemental detector for packed-column supercritical fluid chromatography, *Appl. Spectrosc.*, 43, 737-741 (1989).
- [30] D.J. Douglas and J.B. French, Elemental analysis with a microwave-induced plasma/quadrupole mass spectrometer system, *Anal. Chem.*, 53, 37-41 (1981).
- [31] M. Moisan, C. Beautry and P. LePrince, Small microwave plasma source for long time column production without magnetic field, *IEEE Trans. Plasma. Sci.*, 3, 55-59 (1975).
- [32] J. Hubert, M. Moisan and A Ricard, A new microwave plasma at atmospheric pressure, *Spectrochim. Acta*, 33B, 1-10 (1984)
- [33] T. Hanai, S. Coulombe, M. Moisan and J. Hubert, In R.M. Barnes (Ed), *Developments in Atomic Plasma Spectrochemical Analysis*, Wiley, Chichester, 337-344 (1981).
- [34] D.R. Luffer, L.J. Galante, P.A. David, M. Novotny and G.M. Hieftje, Evaluation of a supercritical fluid chromatograph coupled to a surface-wave-sustained microwave-induced-plasma detector, *Anal. Chem.*, 60, 1365-1369 (1988)
- [35] I.J. Galante, M. Selby, D.R. Buffer, G.M. Hieftje and M. Novotny, Characterization of microwave-induced plasma as a detector for supercritical fluid chromatography, *Anal. Chem.*, 60, 1370-1376 (1988)
- [36] D. Boudreau and J. Hubert, Atmospheric-pressure argon surface-wave plasma (SWP) as an ion source in elemental mass spectrometry, *Appl Spectrosc.*, 47, 609-614 (1993).
- [37] Q. Jin, G. Yang, A Yu, J. Liu, H. Zang and Y. Ben, Abstract book of Pittcon '85, abstract N° 1171 (1985).
- [38] E.A.H. Timmermans, Temperatures in atmospheric microwave induced plasmas at different frequencies, University of Technology, Eindhoven, internal report.
- [39] M. Huang, Comparison between ICPs and MIPs in terms of excitation mechanism and deviation from LTE, *Microchem. J.*, 53, 79-87 (1996).
- [40] G.W. Hansen, F.A. Huf and H.J. De Jong, Low-power microwave plasma source for chromatography detection, *Spectrochim Acta*, 40B, 307-316 (1985).
- [41] B.D. Quimby, V. Giarrocco, J.J. Sullivan and K.A. McCleary, Fast analysis of oxygen and sulfur compounds in gasoline by GC-AED, *J High Resolut. Chromatogr.*, 15, 705-709 (1992).

- [42] J.J. Selley, Y. Zeng and P.C. Uden. Pyrolysis–gas chromatographic atomic emission detection for sediments, coals and other petrochemical precursors, *J. Anal. At. Spectrom.*, 7, 979-985 (1992).
- [43] S. Maruyama, H. Matsumo and M. Yamamoto, Excitation of solutions in a 2450 MHz discharge, *Spectrochim. Acta*, 23B, 513-514 (1968).
- [44] S.Y. Laio, *Microwave devices and circuits*, Prentice Hall, Englewood Cliff, New Jersey, U.S.A. (1980).
- [45] N.H. Bings, M. Olschewski and J.A.C. Broekaert, Two-dimensional spatially resolved excitation and rotational temperatures as well electron number density measurements in capacitively coupled microwave plasma using argon, nitrogen and air as working gases by spectroscopic methods, *Spectrochim. Acta*, 52B, 1965-1981 (1997).
- [46] N.H. Bings and J.A.C. Broekaert, The use of different plasma gases (Ar, N₂ and air) for CMP-OES: figures of merit and temperature measurements, *Fresenius' J. Anal. Chem.*, 355, 242-243 (1996).
- [47] B. Kirsch, S. Hamamura and J.D. Winefordner, Diagnostical measurements in a single electrode, atmospheric pressure, microwave plasma, *Spectrochim. Acta*, 39B, 955-963 (1984).
- [48] B.M. Spencer, B.W. Smith and J.D. Winefordner, Diagnostics in a high-flow-rate (>6 L min⁻¹) helium capacitively coupled microwave plasma: aqueous versus organic solution, *Appl Spectrosc.*, 48, 289-296 (1994).
- [49] W.R.L. Masamba, A.H. Ali and J.D. Winefordner, Temperature and electron density measurements in a helium/hydrogen capacitively coupled microwave plasma, *Spectrochim. Acta*, 47B, 481-491 (1992).
- [50] H. Uchida, P.A. Johnson and J.D. Winefordner, Evaluation of the capacitively coupled helium microwave plasma as an excitation source for the determination of inorganic and organic tin, *J. Anal. Atom. Spectrom.*, 5, 81-85 (1990).
- [51] H. Uchida, A. Berthod and J.D. Winefordner, Determination of non-metallic elements by capacitively coupled helium microwave plasma atomic emission spectrometry with capillary gas chromatography, *Analyst*, 115, 933-937 (1990).
- [52] D. Huang and M.W. Blades, Evaluation of a 13.56 MHz capacitively coupled plasma as a detector for gas chromatographic determination of organotin compounds, *J. Anal. Atom. Spectrom.*, 6, 215-219 (1991).
- [53] M.W. Wensing, D.H. Liu, B.W. Smith and J.D. Winefordner, Determination of lead in whole blood using a capacitively coupled microwave plasma atomic emission spectrometer, *Anal. Chim. Acta*, 299, 1-7 (1994).

- [54] M.W. Smith, B.W. Smith and J.D. Winefordner, Capacitively coupled microwave plasma atomic emission spectrometer for the determination of lead in whole blood, *Anal. Chem.*, 66, 531-535 (1994).
- [55] A.D. Besteman, N. Lau, D.Y. Liu, B.W. Smith and J.D. Winefordner, Determination of lead in whole blood by capacitively coupled microwave plasma atomic emission spectrometry, *J. Anal. Atom. Spectrom.*, 11, 479-481 (1996).
- [56] S. Hanamura, W. Wang and J. D. Winefordner, Determination of hydrogen and oxygen in metals with the aid of a helium single electrode microwave plasma emission technique, *Canad. J. Spectrosc.*, 30 46-51 (1985).
- [57] D. Kollotzek, P. Tschöpel and G. Tölg, Lösungsemissionspektrometrie mit mikrowelleninduzierten Mehrfaden- und Hohlzylinderplasmen: die radiale Verteilung von Signal und Untergrundintensitäten, *Spectrochim. Acta*, 37B, 91-96 (1982).
- [58] G. Heltai, J.A.C. Broekaert, F. Leis and G. Tölg, Study of a toroidal argon and a cylindrical helium microwave induced plasma for analytical atomic emission spectrometry- I. Configurations and spectroscopic properties, *Spectrochim. Acta*, 45B, 301-311 (1990).
- [59] E. Bulska, P. Tschöpel, J.A.C. Broekaert and G. Tölg, Different sample introduction systems for simultaneous determination of As, Sb and Se by microwave induced plasma atomic emission spectrometry, *Anal. Chim. Acta*. 27, 171-181 (1993).
- [60] E.I. Brooks and K.J. Timmins, Sample introduction device for use with a microwave-induced plasma, *Analyst*, 110, 557-558 (1991).
- [61] B.D. Quimby and J.J. Sullivan, Evaluation of a microwave cavity, discharge tube, and gas flow system for combined gas chromatography-atomic emission detection, *Anal. Chem.*, 62, 1027-1034 (1990).
- [62] H. Matusiewicz, R.E. Sturgeon and S.S. Berman, In situ hydride generation pre-concentration of arsenic in a graphite furnace with sample vaporization into a microwave induce plasma for emission spectrometry, *Spectrochim. Acta*, 45B, 209-214 (1990).
- [63] C. Dietz, Y. Madrid, C. Cámara and P. Quevauviller, Simultaneous determination of As, Hg, Se and Sb by hydride generation-microwave induced plasma atomic emission spectrometry after preconcentration in a cryogenic trap. *J. Anal. Atom. Spectrom.*, 14, 1349-1355 (1999).
- [64] K.J. Mulligan, M.H. Hahn, J.A. Caruso and F.L. Fricke, Comparison of several microwave cavities for simultaneous determination of arsenic, germanium, antimony and tin by plasma emission spectrometry, *Anal. Chem.*, 51, 1935-1938 (1979).

- [65] N.W. Barnett, L.S. Chen and G.F. Kirkbright, The rapid determination of arsenic by optical emission spectrometry using microwave induced plasma source and a miniature hydride generation device, *Spectrochim Acta*, 39B, 1141-1147 (1984).
- [66] E.H. Evans, J.A. Caruso and R.D. Satzger, Evaluation of a tantalum tip electrothermal vaporization sample introduction device for microwave-induced plasma mass spectrometry and atomic emission spectrometry, *Appl. Spectrosc.*, 45, 1478-1484 (1991).
- [67] B. Rosenkranz and J. Bettmer, Microwave induced plasma-optical emission spectrometry- fundamental aspects and applications in metal speciation analysis, *Trends Anal. Chem.*, 19, 138-156 (2000).
- [68] E. Bulska, J.A.C. Broekaert, P. Tschöpel and G. Tölg, Comparative study of argon and helium plasmas in a TM₀₁₀ cavity and a surfatron and their use for hydride generation microwave-induced plasma atomic emission spectrometry, *Anal. Chim. Acta*, 276, 377-384 (1993).
- [69] M. Moisan, A. Shivarova and A.W. Trievepiece, Experimental investigation of the propagation of the surface waves along the plasma column, *Plasma Phys.*, 24, 1331-1400 (1982).
- [70] M. Selby and G.M. Hieftje, Taming the surfatron, *Spectrochim. Acta*, 42B, 285-298 (1987).
- [71] B. Rosenkranz, W. Buscher, J. Bettmet, R Lobinski, I. Rodriguez Pereiro, A. Wasik, F.C. Adams and S. Slaets, Presentation on: The First International Conference on Trace Element Speciation in Biomedical, Nutricional and Enviromental Sciences, München, Germany (1988).
- [72] J.M. Costa Fernández, F. Lunzer, R. Pereiro-García and A. Sanz Medel, N. Bordel García, Direct coupling of high-performance liquid chromatography to microwave-induced plasma atomic emission spectrometry *via* volatile-species generation and its application to mercury and arsenic speciation, *J. Anal. Atom. Spectrom.*, 10, 1019 (1995).
- [73] F.Liang, PhD Thesis, Jilin University, Changchun, China, 1997.
- [74] J.F. Camuna-Aguilar, R. Pereiro, J.E. Sanchez Uria and A. Sanz Medel, A comparative study of three microwave induced plasma sources for atomic emission spectrometry-I. Excitation of mercury and its determination after on-line continuous cold vapour generation, *Spectrochim. Acta*, 49B, 475-489 (1994).
- [75] Q. Jin, H. Zang, W. Yang, Q. Jin Jr. and Y. Shi, Determination of trace Ag, Au, Ge, Pb, Sn and Te by microwave plasma torch atomic emission spectrometry coupled with an electrothermal vaporization sample introduction system, *Talanta*, 44, 1605-1614 (1993)

- [76] Q. Jin, F. Wang, C Zhu, D.M. Chambers and G.M. Hieftje, Atomic emission detector for gas chromatography and supercritical fluid chromatography, *J. Anal. At. Spectrom.*, 5, 487-494 (1990).
- [77] A.M. Bilgic, E. Voges, U. Engel and J.A.C. Broekaert, A low-power 2.45 GHz microwave induced helium plasma source at atmospheric pressure based on microstrip technology, *J. Anal. At. Spectrom.*, 15, 579-580 (2000).
- [78] U. Engel, A.M. Bilgic, O. Haase, E. Voges and J.A.C. Broekaert, A microwave-induced plasma based on microstrip technology and its use for the atomic emission spectrometric determination of mercury with the aid of the cold-vapor technique, *Anal. Chem.*, 72, 193-197 (2000).
- [79] S. Schermer, N.H. Bings, A.M. Bilgic, R. Stonies, E. Voges and J.A.C. Broekaert, An improved microstrip plasma for optical emission spectrometry of gaseous species, *Spectrochim. Acta*, 58B, 1585-1596 (2003).
- [80] G.L. Gouy. Photometric research on colored flames, *Ann. Chim. Phys.*, 18, 5-101 (1879).
- [81] C.C. Wohlers, Comparison of nebulizers for the inductively coupled plasma, *ICP Inf. Newsl.* 3: 37-51(1977).
- [82] J.L. Todoli, I.V. Hernandis, A. Canals and J.M. Mermet, Comparison of characteristics and limits of detection of pneumatic micronebulizers and a conventional nebulizer operating at low uptake rates in ICP-AES, *J. Anal. At. Spectrom.*, 14, 1289-1295 (1999).
- [83] Y.L. Feng, R.E. Sturgeon and J.W. Lan, Generation of atomic and molecular cadmium species from aqueous media, *Anal. Chem.*, 75, 635-640 (2003).
- [84] J. Li, T. Umemura, T. Odake, K. Tsunoda, A high-efficiency cross-flow micronebulizer for inductively coupled plasma mass spectrometry, *Anal. Chem.*, 73, 1416-1424 (2001).
- [85] R.S. Babington, Method of atomizing liquid in a mono-dispersed spray, U.S. Patent 3,421,692 (1969).
- [86] L. Ebdon and M. R. Cave, A study of pneumatic nebulization systems for ICP emission spectrometry, *Analyst*, 107, 172-178 (1982).
- [87] W. Holak, Gas-sampling technique for arsenic determination by atomic absorption spectrophotometry, *Anal. Chem.*, 41, 1712-1713 (1969).
- [88] R.E. Madsen, Atomic absorption determination subsequent to arsine reaction with 0.01N silver nitrate, *At. Absorpt. Newsl.*, 10, 57-58 (1971).

- [89] E.F. Dalton and A. J. Malonoski, Atomic absorption analysis of copper and lead in meat and meat products, *J. Ass. Offic. Anal. Chem.* **52** 1035 (1969).
- [90] J. F. Fernandez and D.C. Manning, Determination of arsenic at submicrogram levels by atomic absorption spectrophotometry, *At. Absorpt. Newsl.*, 10, 86-88 (1971).
- [91] E.N. Pollock and S.J. West, Generation and determination of covalent hydrides by atomic absorption, *At. Absorpt. Newsl.*, 11, 104-106 (1971).
- [92] L.S. Braman, L.L. Justen and Forkeback, Direct volatilization-spectral emission type detection system for nanogram amounts of arsenic and antimony, *Anal. Chem.*, 44, 2195-2199 (1972).
- [93] F.J. Schmidt and J.L. Royer, Microgram determination of arsenic, selenium, antimony, and bismuth by atomic absorption utilizing sodium borohydride reduction, *Anal. Letters*, 6, 17-21 (1973).
- [94] K.C. Thompson and D.R. Tommerson, Atomic-absorption studies on the determination of antimony, arsenic, bismuth, germanium, lead, selenium, tellurium and tin by utilizing the generation of covalent hydrides, *Analyst*, 99, 595-600 (1974).
- [95] RE Sturgeon and Z. Mester, Analytical Application of Volatile Metal Derivatives, *Appl. Spectrosc.*, 56, 8, 202A-213A (2002).
- [96] D. C. Manning, A high sensitivity arsenic, selenium sampling system for atomic absorption spectroscopy, *At. Absorpt. Newsl.*, 10: 123-128 (1971).
- [97] M. Thompson, B. Pahlavanpour, S.J. Walton and G.F. Kirkbright, Simultaneous determination of trace concentrations of arsenic, antimony, bismuth, selenium and tellurium in aqueous solution by introduction of the gaseous hydrides into an ICP source for emission spectrometry, *Analyst*, 103, 568-579 (1978).
- [98] J.A.C. Broekaert and F. Leis, Application of two different ICP hydride techniques to the determination of arsenic, *Fresenius' Z Anal Chem* 300, 22-27 (1980).
- [99] J. Dedina, Flow methods in gas-liquid separators in A. Sanz Medel (ed.) *Flow analysis in atomic spectrometric detection*, 1989, Elsevier, Amsterdam, The Netherlands, 237-273 (1989).
- [100] W.B. Robbins and J.A. Caruso, Development of hydride generation methods for atomic spectroscopic analysis, *Anal. Chem.*, 51, 889A-899A (1979).

- [101] F. Laborda, E. Bolea, M.T. Barangan and J.R. Castillo, Hydride generation in analytical chemistry and nascent hydrogen: when is it going to be over?, *Spectrochim. Acta*, 57B, 797-802 (2002).
- [102] A. D'Ulivo, C. Baiocchi, E. Pitzalis, M. Onor and R. Zamboni, Chemical vapor generation for atomic spectrometry. A contribution to the comprehension of reaction mechanisms in the generation of volatile hydrides using borane complexes, *Spectrochim. Acta*, 59B, 471-486 (2004).
- [103] D.R. Qiu, C. Vandecasteele, K. Vermeiren and R. Dams, Continuous hydride generation inductively coupled plasma atomic emission spectrometry for tin: optimization of working parameters and an approach to clarifying the mechanism of stannane generation, *Spectrochim. Acta*, 57B, 439-451 (1990).
- [104] C. S. Stringer and M. Attrep Jr., Comparison of digestion methods for determination of organoarsenicals in wastewater, *Anal. Chem.* 51, 731-734 (1979).
- [105] B. Welz, M. Melcher, H.W. Sinemus and D. Maier, Picotrace determination of mercury using the amalgamation technique, *At. Spectrosc.*, 5, 37-42 (1984)
- [106] H.J.E. Sand and J.E. Hackford, Electrolytic estimation of minute quantities of arsenic, *J. Chem. Soc.*, 85, 1018-1027 (1904).
- [107] E. Tommlinson, Electrolytic stibine formation, *J. Electrochem. Soc.*, 111, 592-596 (1964).
- [108] V. I. Rigin and G. N. Verkhoturov, Atomic absorption determination of arsenic using prior electrochemical reduction., *Zh. Anal. Khim.*, 32, 1965-1968 (1977).
- [109] V. I. Rigin, AA determination of Sn in water and biological materials using electrolytic separation and atomization in the gas phase, *Zh. Anal. Khim.*, 34, 1569-1573 (1979).
- [110] V. I. Rigin and G. N. Verkhoturov, Dispersionless atomic fluorescence of arsenic in biological materials, *Zh. Anal. Khim.*, 33, 1966-1971(1977).
- [111] Y. Lin, X. Wang, D. Yuan, P. Yang, B. Huang and Z. Zhuang, Flow injection electrochemical hydride generation technique for atomic absorption spectrometry *J. Anal. At. Spectrom.*, 7, 287-291 (1992).
- [112] Y. Lin, Z. Zhuang, X. Wang, W. Ding and B. Huang, Proceedings of 3rd Beijing Conference and Exhibition on Instrumental Analysis, Peking University, 1989, C119.
- [113] Y. Lin, Z. Zhuang, X. Wang and B. Huang, Proceedings of 1990 Changchun International Symposium on Analytical Chemistry, Jilin University press, Changchun, 1990, p. 221.

- [114] Y. Lin, PhD Thesis, Xiamen University, China (1991).
- [115] L. F. R. Machado, A. O. Jacintho, A. A. Menegario, E. A. G. Zagatto and M. F. Giné, Electrochemical and chemical processes for hydride generation in flow injection ICP-MS: determination of arsenic in natural waters, *J. Anal. At. Spectrom.*, 13, 1343-1346 (1998).
- [116] C. Schickling, J. Yang and J.A.C. Broekaert, Optimization of the electrochemical hydride generation coupled to microwave-induced plasma atomic emission spectrometry for the determination of arsenic and its use for the analysis of biological tissue samples, *J. Anal. At. Spectrom.*, 11, 739-745 (1996).
- [117] W.-W. Ding and R. E. Sturgeon, Evaluation electrochemical hydride generation for determination of total antimony in natural waters by electrothermal atomic absorption spectrometry with in-situ concentration, *J. Anal. At. Spectrom.*, 11, 225-230 (1996).
- [118] W.-W. Ding and R. E. Sturgeon, Evaluation of electrochemical hydride generation for the determination of arsenic and selenium in sea waters by graphite furnace atomic absorption with in-situ concentration, *Spectrochim. Acta*, 51B, 1325-1334 (1996).
- [119] U. Pyell, A. Dworschak, F. Nitschke and B. Neidhart, Flow injection electrochemical hydride generation atomic absorption spectrometry (FI-EHG-AAS) as a simple device for the speciation of inorganic arsenic and selenium, *Fresenius' J. Anal. Chem.*, 363, 495-498 (1999).
- [120] J. Sima, P. Rychlovsky and J. Dedina, Proceedings of XIVth Seminar on Atomic Spectrochemistry, High Tatras, Podbanske, September 1998, p. 243.
- [121] D.M. Hueber and D.J. Winefordner, A flowing electrolytic hydride generator for continuous sample introduction in atomic spectrometry, *Anal. Chim. Acta*, 316, 129-144 (1995).
- [122] L.F.R. Machado, A.O. Jacinto, A.A. Menegario, E.A.G. Zgatto and M.F. Giné, Electrochemical and chemical process for hydride generation in flow injection ICP-MS: determination of arsenic in natural waters, *J. Anal. Atom. Spectrom.*, 13, 1343-1346 (1998).
- [123] D. Schaumlöffel and B. Neidhart, A FIA-system for As (III)/As(V)-determination with electrochemical hydride generation and AAS detection, *Fresenius' J. Anal. Chem.*, 354, 866-869 (1996).
- [124] W.W. Ding and R.E. Sturgeon, Interference of copper and nickel on electrochemical hydride generation, Interference of copper and nickel on electrochemical hydride generation, *J. Anal. Atom. Spectrom.*, 11, 421-425 (1996).

- [125] E. Denkhaus, A. Golloch, X.-M Guo and B. Huang, Electrolytic hydride generation (EC-HG)- a sample introduction system with some special features, *J. Anal. At. Spectrom.*, 16, 870-878 (2001).
- [126] X.M. Guo, R.E. Sturgeon, Z. Mester and G.J. Gardner, UV light-mediated alkylation of inorganic selenium, *Appl. Organomet. Chem.*, 17, 575–579 (2003).
- [127] X.M. Guo, R.E. Sturgeon, Z. Mester and G.J. Gardner, Photochemical alkylation of inorganic selenium in the presence of low molecular weight organic acids, *Environ. Sci. Technol.*, 37, 5645–5650, (2003).
- [128] X.M. Guo, R.E. Sturgeon, Z. Mester and G.J. Gardner, UV Vapor generation for determination of selenium by heated quartz tube atomic absorption spectrometry, *Anal. Chem.*, 75, 2092–2099 (2003).
- [129] X.M. Guo, R.E. Sturgeon, Z. Mester and G.J. Gardner, UV photosynthesis of nickel carbonyl, *Appl. Organomet. Chem.*, 18, 205–211 (2004).
- [130] X.M. Guo, R.E. Sturgeon, Z. Mester and G.J. Gardner, Vapor generation by UV irradiation for sample introduction with atomic spectrometry, *Anal. Chem.*, 76, 2401–2405 (2004).
- [131] X. Guo, R.E. Sturgeon, Z. Mester and G.J. Gardner, Photochemical alkylation of inorganic arsenic Part 1. Identification of volatile arsenic species, *J. Anal. At. Spectrom.*, 20, 702–708 (2005).
- [132] C. Zheng, Y. Li, Y. He, Q. Ma and X. Hou, Photo-induced chemical vapor generation with formic acid for ultrasensitive atomic fluorescence spectrometric determination of mercury: potential application to mercury speciation in water, *J. Anal. At. Spectrom.*, 20, 746–750 (2005).
- [133] R. F. Bendl, J. T. Madden, A. L. Regan and N. Fitzgerald, Mercury determination by cold vapor atomic absorption spectrometry utilizing UV photoreduction, *Talanta*, 68, 1366–1370 (2006).
- [134] S. McSheehy, X. Guo, R.E. Sturgeon and Z. Mester, Photochemical alkylation of inorganic arsenic Part 2. Identification of aqueous phase organoarsenic species using multidimensional liquid chromatography and electrospray mass spectrometry, *J. Anal. At. Spectrom.*, 20, 709–716 (2005).
- [135] R. Figueroa, M. Garcia, I. Lavilla and C. Bendicho, Photoassisted vapor generation in the presence of organic acids for ultrasensitive determination of Se by electrothermal-atomic absorption spectrometry following headspace single-drop microextraction, *Spectrochim. Acta*, 60B, 1556–1563 (2005).

- [136] S. Fragueiro, I. Lavilla and C. Bendicho, Hydride generation-headspace single-drop microextraction-electrothermal atomic absorption spectrometry method for determination of selenium in waters after photo-assisted pre-reduction, *Talanta*, 68, 1096-1101 (2006).
- [137] D. L. Tsalev, M. Sperling and B. Welz, Speciation determination of arsenic in urine by high-performance liquid chromatography-hydride generation atomic absorption spectrometry with on-line ultraviolet photooxidation, *Analyst*, 123, 1703-1710 (1998).
- [138] X. Wei, C. A. Brockhoff-Schwegel and T.J. Creed, A comparison of urinary arsenic speciation *via* direct nebulization and on-line photo-oxidation-hydride generation with IC separation and ICP-MS detection, *J. Anal. At. Spectrom.*, 16, 12-19 (2001).
- [139] D. Mazej, I. Falnoga, M. Veber and V. Stibilj, Determination of selenium species in plant leaves by HPLC-UV-HG-AFS, *Talanta*, 68, 558-568 (2006).
- [140] A.K. Knighta, R.P. Sperline, G.M. Hieftje, E. Young, C.J. Barinaga, D.W. Koppenaal and M.B. Denton, The development of a micro-Faraday array for ion detection, *International Journal of Mass Spectrometry* 215 131-139 (2002).
- [141] J.S. Becker, *Inorganic Mass Spectrometry: Principles and Applications*, John Wiley and Sons, Ltd., Chichester (2007).
- [142] T.W. Burgoyne, G.M. Hieftje, and R.A. Hites, Space Charge Evaluation in a Plasma-Source Mass Spectrograph, *Anal. Chem.*, 69, 485-489 (1997).
- [143] J.M. Costa Fernandez, R. Pereiro Garcia, A. Sanz Medel and N Bordel García, Effect of plasma pressure on the determination of mercury by microwave-induced plasma atomic emission spectrometry, *J Anal At Spectrom* 10, 649-654 (1995).
- [144] J.C. Wuilloud, R.G. Wuilloud, J.A. Salonia, R.A. Olsina and L.D. Martinez, Modified gas-liquid separator for the determination of mercury with cold vapor flow injection-inductively coupled plasma optical emission spectrometry, *J. Anal. Chem.* 57, 799-801 (2002).
- [145] H. Bings, Z. Stefanka and S. Rodríguez Mallada, Flow injection electrochemical hydride generation inductively coupled plasma time-of-flight mass spectrometry for the simultaneous determination of hydride forming elements and its application to the analysis of fresh water samples, *Anal. Chim. Acta*, 479, 203-214 (2003).
- [146] O. Haase, M. Klare, K. Krenzel-Rothensee and J.A.C. Broekaert, Evaluation of the determination of mercury at the trace and ultratrace element in the presence of high concentration of NaCl by flow-cold vapour atomic absorption spectrometry using SnCl₂ and NaBH₄, *Analyst*, 123, 1219-1222 (1998).
- [147] R. Saraswati, T.W. Vetter and R.L. Watters, Comparison of reflux and microwave oven digestion for the determination of arsenic and selenium in sludge reference material using

flow injection hydride generation and atomic absorption spectrometry, *Analyst*, 120, 95-99 (1995).

[148] K. Tanabe, H. Haraguchi and K. Fuwa, Some spatial characteristics of an atmospheric pressure helium microwave-induced plasma, *Spectrochim. Acta*, 38B, 49-60 (1983).

[149] J. Cotrino, M. Saez, M.C. Quintero, A. Menendez, J.E. Sanchez Uria and A. Sanz Medel, Spectroscopic determination of fundamental parameters in an argon microwave-induced plasma (surfatron) at atmospheric pressure, *Spectrochim. Acta*, 47B, 425-435 (1992).

[150] W.L. Wiese and G.A. Martin, Wavelengths and transition probabilities of atoms and atomic ions, US Department of Commerce, National Bureau of Standards, Washington (1980).

[151] W.L. Wiese, M.W. Smith and B.M. Miles, Wavelengths and atomic transition probabilities for atoms and atomic ions, US Government Printing Office, Washington (1969).

[152] H.R. Griem, Spectral line broadening by plasmas, Academic, New York (1974).

[153] M.M. Abdillahi and R.D. Snook, Determination of bromide using a helium microwave induced plasma with bromine generation and electrothermal vaporisation for sample introduction, *Analyst*, 111, 265-267 (1986).

[154] P.M. Houpt, Physical phenomena and analytical applications of helium microwave discharges, *Anal Chim Acta*, 86, 129-138 (1976).

[155] K. Tanabe, K. Chiba, H. Haraguchi and K. Fuwa, Determination of mercury at the ultratrace level by atmospheric pressure helium microwave-induced plasma emission spectrometry. *Anal. Chem.*, 53, 1450-1453 (1981).

[156] P.G. Brandl and J.W. Carnahan, Charge transfer in analytical helium plasmas, *Spectrochim. Acta*, 49B, 105-115 (1994).

[157] F. Lunzer, R. Pereiro Garcia, N. Bordel Garcia and A Sanz Medel, Continuous hydride generation low-pressure microwave-induced plasma atomic emission spectrometry for the determination of arsenic, antimony and selenium, *J. Anal. At. Spectrom.*, 10, 311-315 (1995).

[158] M. Wlodarczyk and W. Zyrnicki, Spectroscopic characterization of low power argon microwave induced plasma with gaseous species produced from ethanol-water solutions in continuous hydride generation process, *Spectrochim. Acta*, 58B, 511-522 (2003).

[159] P. Liang and A. Li, Determination of arsenic by continuous hydride generation with direct introduction into an O₂-argon microwave plasma torch atomic emission spectrometer, *Fresenius' J. Anal. Chem.*, 368, 418-420 (2000).

- [160] P. Pohl, Hydride generation: recent advances in atomic emission spectrometry, *Trends Anal. Chem.*, 23, 87-101 (2004).
- [161] D.M. Hueber, W.R.L. Masamba, B.M. Spencer and J.D. Winefordner, Application of hydride generation to the determination of trace concentrations of arsenic by capacitively coupled microwave plasma, *Anal. Chim. Acta*, 278, 279-285 (1993).
- [162] Z. Gong, W. F. Chan, X. Wang and F.S.C. Lee, Determination of arsenic and antimony by microwave plasma atomic emission spectrometry coupled with hydride generation and a PTFE membrane separator, *Anal. Chim. Acta*, 450, 207-214 (2001).
- [163] J. Yang, C. Schickling, J.A.C. Broekaert, P. Tschoepel and G. Tölg, Evaluation of continuous hydride generation combined with helium and argon microwave induced plasmas using a surfatron for atomic emission spectrometric determination of arsenic, antimony and selenium, *Spectrochim. Acta*, 50B, 1351-1363 (1995).
- [164] S. Luge and J.A.C. Broekaert, The use of optical emission spectrometry with microwave induced plasma (MIP) discharge in a surfatron combined to different types of hydride generation for the determination of arsenic, *Microchim. Acta*, 113, 277-286 (1994).
- [165] T. Nakahara and Y. Li, Determination of trace amounts of antimony in pure copper by high-power nitrogen microwave induced plasma atomic emission spectrometry with hydride generation, *J. Anal. Atom. Spectrom.*, 13, 401-405 (1998)
- [166] R. Pereiro, M. Wu, J.A.C. Broekaert and G.M. Hieftje, Direct coupling of continuous hydride generation with microwave plasma torch atomic emission spectrometry for the determination of arsenic, antimony and tin, *Spectrochim. Acta*, 49B, 59-73 (1994).
- [167] I. Novotny, J.C. Farinas, W. Jia-liang, E. Poussel and J.M. Mermet, Effect of power and carrier gas flow rate on the tolerance to water loading in inductively coupled plasma atomic emission spectrometry, *Spectrochim. Acta*, 51B, 1517-1526 (1996).
- [168] B. Pateyron, M.F. Elchinger, G. Delluc and P. Fauchais, Thermodynamic and transport properties of Ar-H₂ and Ar-He plasma gases used for spraying at atmospheric pressure. I: Properties of the mixtures, *Plasma Chem. Plasma Process*, 12, 421-448 (1992).
- [169] T. Nakahara, Hydride generation techniques and their applications in inductively coupled plasma-atomic emission spectrometry, *Spectrochim. Acta Rev.* 14, 95-109 (1991).
- [170]] S.R. Goode, N.P. Buddin, B. Chambers, K.W. Baughman and J.P. Deavor, Influence of pressure on the properties of a microwave-induced plasma, *Spectrochim. Acta*, 40B, 317-328 (1985).
- [171] A. D'Ulivo, Chemical vapor generation by tetrahydroborate(III) and other borane complexes in aqueous media: A critical discussion of fundamental processes and mechanisms

involved in reagent decomposition and hydride formation, *Spectrochim. Acta*, 59B, 793-825 (2004).

[172] H. Matusiewicz, M. Kopras and R.E. Sturgeon, Determination of cadmium in environmental samples by hydride generation with in situ concentration and atomic absorption detection, *Analyst*, 122, 331-336 (1997).

[173] H. Uggerud and W. Lund, Use of thiourea in the determination of arsenic, antimony, bismuth, selenium and tellurium by hydride generation inductively coupled plasma atomic emission spectrometry, *J. Anal. At. Spectrom.*, 10, 405-408 (1995).

[174] P. Pohl and W. Zyrnicki, Study of chemical and spectral interferences in the simultaneous determination of As, Bi, Sb, Se and Sn by hydride generation inductively coupled plasma atomic emission spectrometry, *Anal. Chim. Acta*, 468, 71-79 (2002).

[175] A. Risnes and W. Lund, Comparison of systems for eliminating interferences in the determination of arsenic and antimony by hydride generation inductively coupled plasma atomic emission spectrometry, *J. Anal. At. Spectrom.*, 11, 943-948 (1996).

[176] P. Schramel and L.-Q. Xu, Determination of arsenic, antimony, bismuth, selenium and tin in biological and environmental samples by continuous flow hydride generation ICP-AES without gas-liquid separator, *Fresenius' J. Anal. Chem.*, 340, 41-47 (1991).

[177] H. Chen, I.D. Brindle and X.C. Le, Prereduction of arsenic(V) to arsenic(III), enhancement of the signal, and reduction of interferences by L-Cysteine in the determination of arsenic by hydride generation, *Anal. Chem.*, 64, 667-672 (1992).

[178] T. Zoltan, Z. Benzo, M. Murillo, E. Marcano, C. Gomez, J. Salas and M. Quintal, Performance of a new nebulizer system for simultaneous determination of Sb, Sn (hydride generation), V, and Zn by ICP-OES, *Anal. Bioanal. Chem.*, 382, 1419-1430 (2005).

[179] A. Matsumoto, T. Shiozaki and T. Nakahara, Simultaneous determination of bismuth and tellurium in steels by high power nitrogen microwave induced plasma atomic emission spectrometry coupled with the hydride generation technique, *Anal. Bioanal. Chem.*, 379, 90-95 (2004).

[180] Y.W. Chen, J. Tong, A. D'Ulivo and N. Belzile, Determination of mercury by continuous flow cold vapor atomic fluorescence spectrometry using micromolar concentration of sodium tetrahydroborate as reductant solution, *Analyst*, 127, 1541-1546 (2002).

[181] G. Graf, Tin, tin alloys, and tin compounds, Wiley-VCH Verlag, Weinheim, Germany (2005).

[182] J.C. de Andrade and M.I.M.S. Bueno, A continuous flow cold vapour procedure for mercury determination by atomic emission using the reverse flow injection approach. *Spectrochim. Acta*, 49B, 787-795 (1994).

[183] E. Bulska, W. Kandler, P. Paslawski and A. Hulanicki, Atomic absorption spectrometric determination of mercury in soil standard reference material following microwave sample pre-treatment, *Microchim. Acta*, 119, 137-146 (1995).

[184] M. Murillo, N. Carrion, J. Chirinos, A. Gammiero and E. Fassano, Optimization of experimental parameters for the determination of mercury by MIP/AES, *Talanta*, 54: 389-395 (2001).

[185] A. Krata, K. Pyrzynska and E. Bulska, Use of solid-phase extraction to eliminate interferences in the determination of mercury by flow-injection CV AAS, *Anal. Bioanal. Chem.*, 377, 735-739 (2003).

[186] Y.L. Feng, R.E. Sturgeon, J.W. Lam and A. D'Ulivo, Insights into the mechanism of chemical vapor generation of transition and noble metals, *J. Anal. At. Spectrom.*, 20, 255-265 (2005).

[187] J.C. de Andrade, C. Pasquini, N. Baccan and J.C. van Loon, Cold vapor atomic absorption determination of mercury by flow injection analysis using a teflon membrane phase separator coupled to the absorption cell, *Spectrochim. Acta*, 38B, 1329-1338 (1983).

[188] N. Amini, T.J. Cordwell, R.W. Catrall, R.J.S. Morrison and S.D. Kolev On-line determination of mercury(II) by membrane separation flow injection analysis, *Talanta*, 63, 1069-1075 (2004).

[189] H. Tao and A. Miyazaki, Determination of germanium, arsenic, antimony, tin and mercury at trace levels by continuous hydride generation-helium microwave-induced plasma atomic emission spectrometry, *Anal. Sci.*, 7, 55-59 (1991).

[190] A. D'Ulivo, M. Onor and E. Pitzalis, Role of hydroboron intermediates in the mechanism of chemical vapor generation in strongly acidic media, *Anal. Chem.*, 76, 6342-6352 (2004).

[191] A. D'Ulivo, Z. Mester and R.E. Sturgeon, The mechanism of formation of volatile hydrides by tetrahydroborate(III) derivatization: A mass spectrometric study performed with deuterium labeled reagents, *Spectrochim. Acta*, 60B, 423-438 (2005).

[192] B. Özmen, F.M. Matysik, N.H. Bings and J.A.C. Broekaert, Optimization and evaluation of different chemical and electrochemical hydride generation systems for the determination of arsenic by microwave plasma torch optical emission spectrometry, *Spectrochim. Acta*, 59B, 941-950 (2004).

[193] F. Laborda, E. Bolea and J.R. Castillo, Electrochemical hydride generation as a sample-introduction technique in atomic spectrometry: fundamentals, interferences and applications, *Anal. Bioanal. Chem.*, 388, 743-751 (2007).

- [194] E. Bolea, F. Laborda, J.R. Castillo and R.E. Sturgeon, Electrochemical hydride generation for the simultaneous determination of hydride forming elements by inductively coupled plasma-atomic emission spectrometry, *Spectrochim. Acta*, 59B, 505-513 (2004).
- [195] L. Lampugnani, C. Solvetti and D.L. Tsalev, Hydride generation atomic absorption spectrometry with different flow systems and in-atomizer trapping for determination of cadmium in water and urine—overview of existing data on cadmium vapour generation and evaluation of critical parameters, *Talanta*, 61, 683-698 (2003).
- [196] T. Nakahara and T. Nishida, Analyte volatilization for the determination of low concentrations of chlorine by atmospheric-pressure helium microwave-induced plasma atomic emission spectrometry, *Spectrochim. Acta*, 53B, 1209-1220 (1998).
- [197] J.F. Camuña, M. Montes, R. Pereiro, A. Sanz Medel, C. Katschthaler, R. Gross and G. Knapp, Determination of halides by microwave induced plasma and stabilized capacitive plasma atomic emission spectrometry after on-line continuous halogen generation, *Talanta*, 44, 535-544 (1997).
- [198]] F. Camuña, J.E. Sanchez Uria and A. Sanz Medel, Continuous flow and flow injection halogen generation for chloride, bromide and iodide determination by microwave induced plasma atomic emission spectroscopy, *Spectrochim. Acta*, 48B, 1115-1125 (1993).
- [199] T. Nakahara, S. Morimoto and T. Wasa, Analyte volatilization procedure for continuous-flow determination of bromine by atmospheric pressure helium microwave-induced plasma atomic emission spectrometry, *J. Anal. At. Spectrom.*, 7, 211-217 (1992).
- [200] T. Nakahara, T. Mori, S. Morimoto and H. Ishikawa, Continuous-flow determination of aqueous sulfur by atmospheric-pressure helium microwave-induced plasma atomic emission spectrometry with gas-phase sample introduction, *Spectrochim. Acta*, 50B, 393-403 (1995).
- [201] N.W. Barnett, Improvements in the chemical generation of chlorine, bromine and their respective hydrides as a means of sample introduction into an atmospheric pressure helium microwave-induced plasma, *J. Anal. At. Spectrom.*, 3, 969-972(1988).
- [202] M.D. Calzada, M.C. Quintero, A. Gamero and M. Gallego, Chemical generation of chlorine, bromine and iodine for sample introduction into a surfatron-generated argon microwave-induced plasma, *Anal. Chem.*, 64, 1374-1378 (1992).
- [203] .D. Calzada, M.C. Quintero, A. Gamero and J. Cotrino, Determination of bromide by low power surfatron microwave induced plasma after bromine continuous generation, *Talanta*, 39, 341-347 (1992).
- [204] R. Guchardi and P.C. Hauser, Capacitively coupled microplasma for on-column detection of chromatographically separated inorganic gases by optical emission spectrometry, *J. Chrom. A*, 1033, 333-338 (2004).

- [205] K. Kunze, M. Miclea, J. Franzke and K. Niemax, The detection barrier discharge as a detector for gas chromatography, *Spectrochim. Acta*, 58B, 1435-1443 (2003).
- [206] J.C.T. Eijkel, H. Stoeri and A. Manz, An atmospheric pressure dc glow discharge on a microchip and its application as a molecular emission detector, *J. Anal. At. Spectrom.*, 15, 297-300 (2000).
- [207] J.C.T. Eijkel, H. Stoeri and A. Manz, A dc microplasma on a chip employed as an optical emission detector for gas chromatography, *Anal. Chem.*, 72, 2547-2552 (2000).
- [208] A. Bass, C. Chevalier and M.W. Blades, A capacitively coupled microplasma (CC μ P) formed in a channel in a quartz wafer, *J. Anal. At. Spectrom.*, 16, 919-921 (2001).
- [209] J.A.C. Broekaert, V. Siemens and N.H. Bings, Microstrip microwave induced plasma on a chip for atomic emission spectral analysis, *IEEE Trans. Plasma Sci.*, 33, 560-561 (2005).
- [210] A. Michels, S. Tombrink, W. Vautz, M. Miclea and J. Franzke, Spectroscopic characterization of a microplasma used as ionization source for ion mobility spectrometry, *Spectrochim. Acta Part B*, 62B, 1208-1215 (2007).
- [211] P.W.J.M. Boumans, *Inductively Coupled Plasma Emission Spectroscopy. Part 1: Methodology, Instrumentation and Performance*, Wiley, New York, U.S.A. (1987).
- [212] G. Herzberg, *Molecular Spectra and Molecular Structure I: Spectra of Diatomic Molecules*, Van Nostrand Co., New York, USA (1950).
- [213] O.B. Minayeva and J.A. Hopwood, Emission spectroscopy using a microfabricated inductively coupled plasma-on-a-chip, *J. Anal. At. Spectrom.*, 17, 1103-1107 (2002).

H. Lebenslauf**Persönliche Daten**

Name	Andrés Israel Humberto Jiménez Zapata
Geburtsdatum	14.09.1978
Geburtsort	Lima
Familienstand	verheiratet
Staatgehörigkeit	peruanisch

Schulbildung

04/1990-12/1995	Salesian High School, Lima, Perú
-----------------	----------------------------------

Studium

04/1997-07/2002	“Bachelor in Science, Chemistry” “Universidad Nacional Mayor de San Marcos, Lima, Perú”
11/2003	“Diploma in science, Chemistry” Tutor: Prof. Dr. Jorge Reynaldo Angulo Cornejo Thesis: “Synthesis and characterization of N, N-1, 1-alquilalcanthioureas and their. Ni, Cu and Co complexes.”
Seit 10/2005	Promotion am Institut für Anorganische and Angewandte Chemie der Universität Hamburg bei Prof. Dr. José Broekaert Thesis: “Optical emission spectrometry with microwave induced plasmas in structures based on microstrip technology for the determination of Hg, As, Sb, Cl, Br and S with the aid of cold vapour generation techniques.”

Beruflicher Werdegang

08/2003-11/2003	“Analyst Assistant” J. Ramón del Perú
08/2004-11/2004	“Analyst Assistent” Ecolab Perú
02-2005-05/2005	“Analyst” CIMM Perú

Stipendien

12/2002-2003	Austauschpraktikum an der Universität Leipzig gefördert durch DAAD
01/2004-03/2004	Austauschpraktikum an der Universität Hamburg gefördert durch DAAD
Seit 10/2005	DAAD Stipendium zur Durchführung der Promotion an der Universität Hamburg

Publikationen

Analytical & Bioanalytical Chemistry	Evaluation and application of argon and helium microstrip plasma for the determination of mercury by the cold vapour
--------------------------------------	--

- technique and optical emission spectrometry
- Spectrochimica Acta, Part B Optical emission spectrometric determination of arsenic and antimony by continuous flow chemical hydride generation and a miniaturized microwave microstrip argon plasma operated inside a capillary channel in a sapphire wafer
- Microchimica Acta Comparison of the cold vapor generation using NaBH_4 and SnCl_2 as reducing agents and atomic emission spectrometry for the determination of Hg with a microstrip microwave induced argon plasma exiting from the wafer
- Analytica Chimica Acta Optimization and comparison of chemical and electrochemical hydride generation for optical emission spectrometric determination of arsenic and antimony using a novel miniaturized microwave induced argon plasma exiting the microstrip wafer
- Spectrochimica Acta, Part B Characterization of a microwave microstrip helium plasma with gas-phase sample introduction for the optical emission spectrometric determination of bromine, chlorine, sulfur and carbon using a miniaturized optical fiber spectrometer